



**RV AKADEMIK M. A. LAVRENTYEV CRUISE 27  
CRUISE REPORT**

**GREGORY**

**GERMAN RUSSIAN EXPEDITION  
FOR GEOLOGICAL / GEOPHYSICAL  
OKHOTSK SEA RESEARCH**

**Vladivostok - Pusan - Okhotsk Sea - Pusan - Vladivostok  
September 7 - October 12, 1996**

**Edited by**

**Dirk Nürnberg, Boris V. Baranov, and Boris Ya. Karp**

**The GREGORY marine expedition was initialized on responsibility of  
the Pacific Oceanological Institute (Vladivostok)  
the P. P. Shirshov Institute of Oceanology (Moscow)  
and the  
GEOMAR Research Center for Marine Geosciences (Kiel)**

**GEOMAR**  
Forschungszentrum  
für marine Geowissenschaften  
der Christian-Albrechts-Universität  
zu Kiel

**Kiel 1997**

**GEOMAR REPORT 60**

**GEOMAR**  
Research Center  
for Marine Geosciences  
Christian Albrechts University  
in Kiel

Redaktion der Serie:  
Umschlag:

Gerhard Haass  
Kerstin Kreis, Harald Gross,  
GEOMAR Technologie GmbH

Managing Editor:  
Cover:

Gerhard Haass  
Kerstin Kreis, Harald Gross,  
GEOMAR Technologie GmbH

**GEOMAR REPORT**  
ISSN 0936 - 5788

**GEOMAR REPORT**  
ISSN 0936 - 5788

**GEOMAR**  
Forschungszentrum  
für marine Geowissenschaften  
D-24148 Kiel  
Wischhofstr. 1-3  
Telefon (0431) 600-2555, 600-2505

**GEOMAR**  
Research Center  
for Marine Geosciences  
D-24148 Kiel / Germany  
Wischhofstr. 1-3  
Telephone (49) 431 / 600-2555, 600-2505

---

## Contents:

1. Preface	1
2. List of participants	3
3. Scientific background and objectives	4
3.1 Tectonics	4
3.2 Petrology	7
3.3 Paleoceanography	7
3.4 Gas geochemistry	9
4. Methods and instruments	10
4.1 Geophysical methods	10
4.1.1 Gravity	10
4.1.2 Magnetic intensity	10
4.1.3 Seismic	10
4.1.4 Bathymetry	11
4.2 Geological and geochemical methods	11
4.2.1 Recovery of deep-sea sediments	11
4.2.1.1 Multicorer	11
4.2.1.2 Gravity corer	11
4.2.1.3 Dredging	12
4.2.2 Sediment sampling and processing aboard the ship	13
4.2.2.1 GEOMAR approach	13
4.2.2.2 POI approach	14
4.2.3 Gas sampling	14
4.2.4 Mechanical properties of the sediments	14
4.2.5 Magnetic susceptibility	15
4.2.6 Micropaleontology	15
4.3 Hydrographical methods	16
4.3.1 Plankton net	16
4.3.2 Water sampling	17
5. Results	18
5.1 Marine geophysics	18
5.1.1 Bathymetry	18
5.1.2 Seismic	21
5.1.3 Gravity and magnetics	26
5.2 Marine geology and geochemistry	29
5.2.1 Bedrocks	29
5.2.2 Sediment stratigraphy	31
5.2.3 Mineralogy	32
5.2.4 Morphometric analysis of terrigenous quartz	34
5.2.5 Mechanical properties of sediments	36
5.2.6 Magnetic susceptibility	38
5.2.7 Radiolarians in the Okhotsk Sea sediments	39
5.2.8 Sedimentation at the northeastern slope of Sakhalin	41
5.2.9 Marine geology of the central Okhotsk Sea	43
5.2.10 Gas geochemistry	48
5.3 Plankton investigations	52
5.4 Conclusions	53
6. Tectonic structure of the northern Kurile Basin slope: Implication to the Okhotsk Sea geodynamics	54
7. Conclusions and perspectives	64

8. References

66

Appendix I. Research vessel "Akademik M.A. Lavrentyev"

Appendix II. Station coordinates

Appendix III. Track coordinates

Appendix IV. Tables

Appendix V. Sediment core description

Appendix VI. Magnetic susceptibility and humidity of all sites

## 1. Preface

(B.Ya. Karp, D. Nürnberg, and B.V. Baranov)

The Okhotsk Sea belongs to the NW-Pacific marginal sea system. To the northwest and to the north, it is bound by the Asian continent. To the east and southeast, the NE-SW trending Kurile-Kamchatka Island Arc separates the Okhotsk Sea from the Bering Sea and the Pacific Ocean. The Okhotsk Basin is separated from the Japan Sea and the Asian continent by the N-S trending Hokkaido and Sakhalin mountain systems, which lie approximately  $45^\circ$  to the strike of the Kurile-Kamchatka Island Arc. With respect to geodynamical and environmental problems, each of the marginal seas of the NW-Pacific marginal sea system represents a unique object for research. The Okhotsk Sea is the most interesting among them due to certain peculiar features of its tectonic structure, distinctly manifested seasonal character of the climate and hydrology, and the high level of the primary production. The investigations of tectonics, environment and ecology of the Okhotsk Sea and surrounding areas is, thus, suggested to be of highest priority.

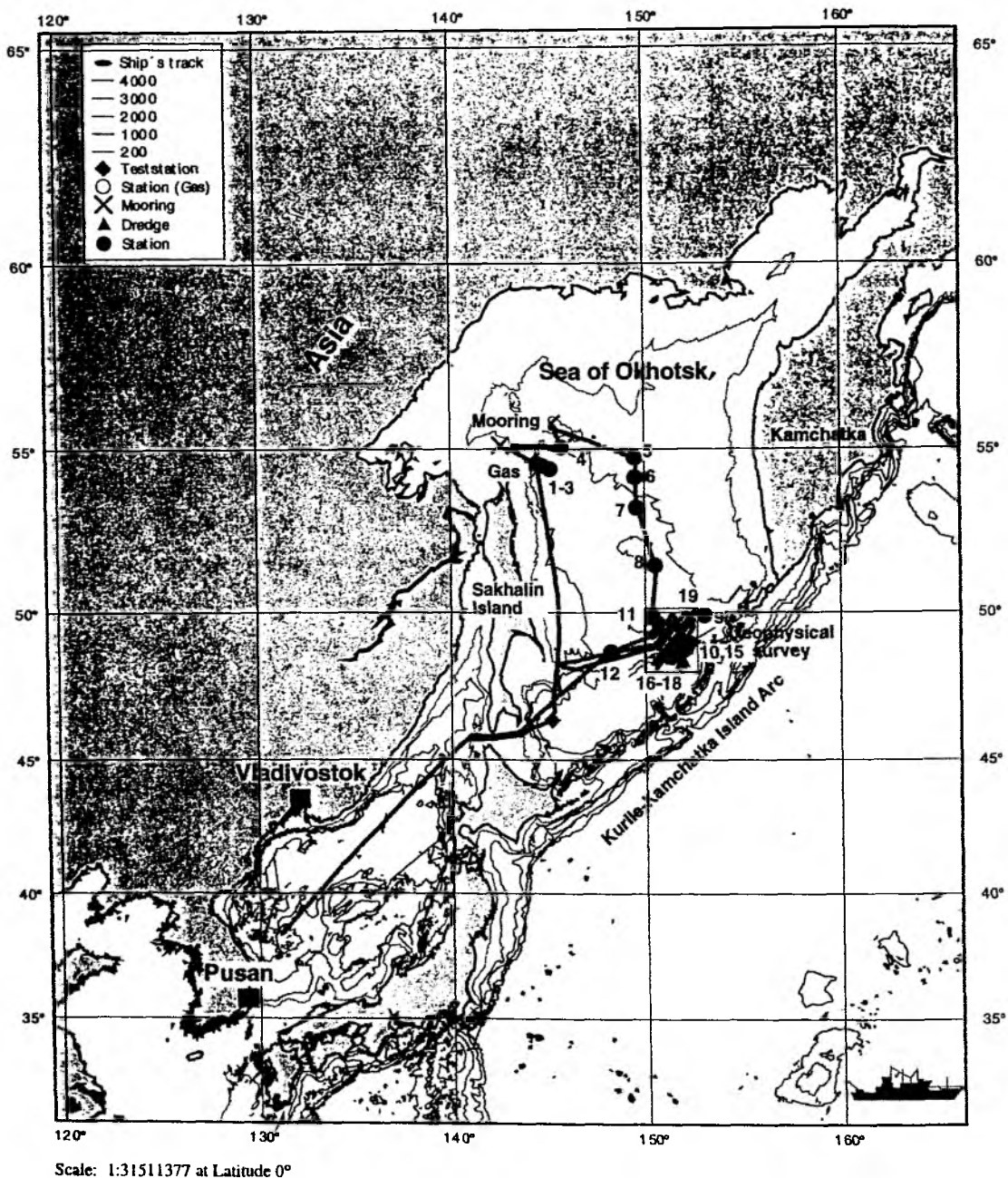
The joint German/Russian KOMEX Project (Kurile - Okhotsk - Marine Expedition), a Russian-German cooperation planned for 1997-1999 - suggests three major topics of research:

1. environmental parameters, fluxes, paleoceanographical proxies;
2. crustal structure, tectonics and geodynamics;
3. volcanic volatiles and petrogenesis.

Within the framework of the multidisciplinary KOMEX project the 27th cruise of RV Akademik Lavrentyev was jointly organized by the Pacific Oceanological Institute, Far East Branch of the Russian Academy of Sciences (POI, Vladivostok), the Institute of Oceanology of the Russian Academy of Sciences (IORAS, Moscow), and GEOMAR, Research Center for Marine Geosciences at Kiel University, and was intended to be a pre-KOMEX activity. The cruise was sponsored by the Ministry of Science and Technology (BMBF, Germany) and the Russian Academy of Sciences.

Initially, it was planned to conduct several ship expeditions during KOMEX to focus on each of these research topics separately. However, the pre-KOMEX RV Akademik Lavrentyev cruise combines both the tectonic and the environmental topics, in order to allow all participating partner institutions to evaluate the area for future investigations, to estimate possibilities of the equipment available, and to coordinate their scientific interests and the scientific and logistical planning for future cooperations.

RV Akademik Lavrentyev set sail from Vladivostok on September 7th, 1996 to its first stop at Pusan, South Korea, to pick up the German scientific party and their equipment. The ship departed from Pusan on September 11th, 1996 and arrived again at Pusan on October 9th, 1996. The scientific program of the cruise included geological and geophysical investigations. The route of the expedition, geological site locations and the geophysical survey area are shown in Fig. 1.1. The geological investigations comprised the sampling of sediments and bed rocks by gravity core, multicorer and dredge. The geophysical investigations included single channel seismic reflection profiling as well as magnetic total intensity and gravity measurements. In addition, bathymetry was recorded by a wide-beam echosounder. The geophysical investigations were conducted on the northern slope of the Kurile Basin. The geological sampling was carried out in the central part of the Okhotsk Sea, near eastern Sakhalin island and within the geophysical survey area.



**Fig. 1.1:** Ship's track of R/V Akademik Lavrentyev during cruise 27 and site locations. The inserted rectangular indicates the detailed geophysical investigation.

Considering that there is a good tradition from the beginning of the joint German-Russian Okhotsk Sea investigations to name expeditions "POSETIVE" (1994) and "GERDA" (1995), we suggest to call this year's expedition "GREGORY" (abbreviation from German-Russian Expedition for Geological/Geophysical Okhotsk Sea Research).

## 2. List of participants

Karp, Boris	Co-chief scientist, seismics (POI FED RAS)
Nürnberg, Dirk	Co-chief scientist, marine Geology (GEOMAR)
Baranov, Boris	Scientific leader, tectonics (IO RAS)
Nikolaev, Sergey	Deputy of chief scientist, gravity (POI FED RAS)
Lelikov, Evgeniy	Deputy of chief scientist, petrology (POI FED RAS)
Karnaikh Victor	Scientific coordinator, Seismics (POI FED RAS)
Astakhov, Anatoliy	Lithology (POI FED RAS)
Botzul, Anatoliy	Seismics (POI FED RAS)
Dergachov, Aleksandr	Lithology (POI FED RAS)
Dozorova, Karina	Tectonics (IO RAS)
Golovan', Anatoliy	Magnetics (POI FED RAS)
Gorbarenko, Sergey	Paleoceanology (POI FED RAS)
Gruetzner, Jens	Marine geophysics (GEOMAR)
Kolpashikova, Tat'ayna	Gravity (POI FED RAS)
Krainikov, Gennadiy	Technician (POI FED RAS)
Matul, Aleksandr	Micropaleontology (IO RAS)
Neufeld, Sergej	Technician (GTG)
Obzhurov, Anatoliy	Gas geochemistry (POI FED RAS)
Prokudin, Vladimir	Seismics (POI FED RAS)
Sibekin, Victor	Seismics (POI FED RAS)
Sudakov, Anatoliy	Seismics (POI FED RAS)
Svarichevskiy, Aleksandr	Geomorphology (POI FED RAS)
Tararin, Igor	Petrology (FEGI FED RAS)
Terekhov, Evgeniy	Petrology (POI FED RAS)
Tzovbun, Nikolay	Magnetics (POI FED RAS)
Valitov, Maksim	Gravity (POI FED RAS)
Vogt, Christoph	Marine geology (GEOMAR)
Wolfsdorf, Jan-Malte	Marine geology (GEOMAR)

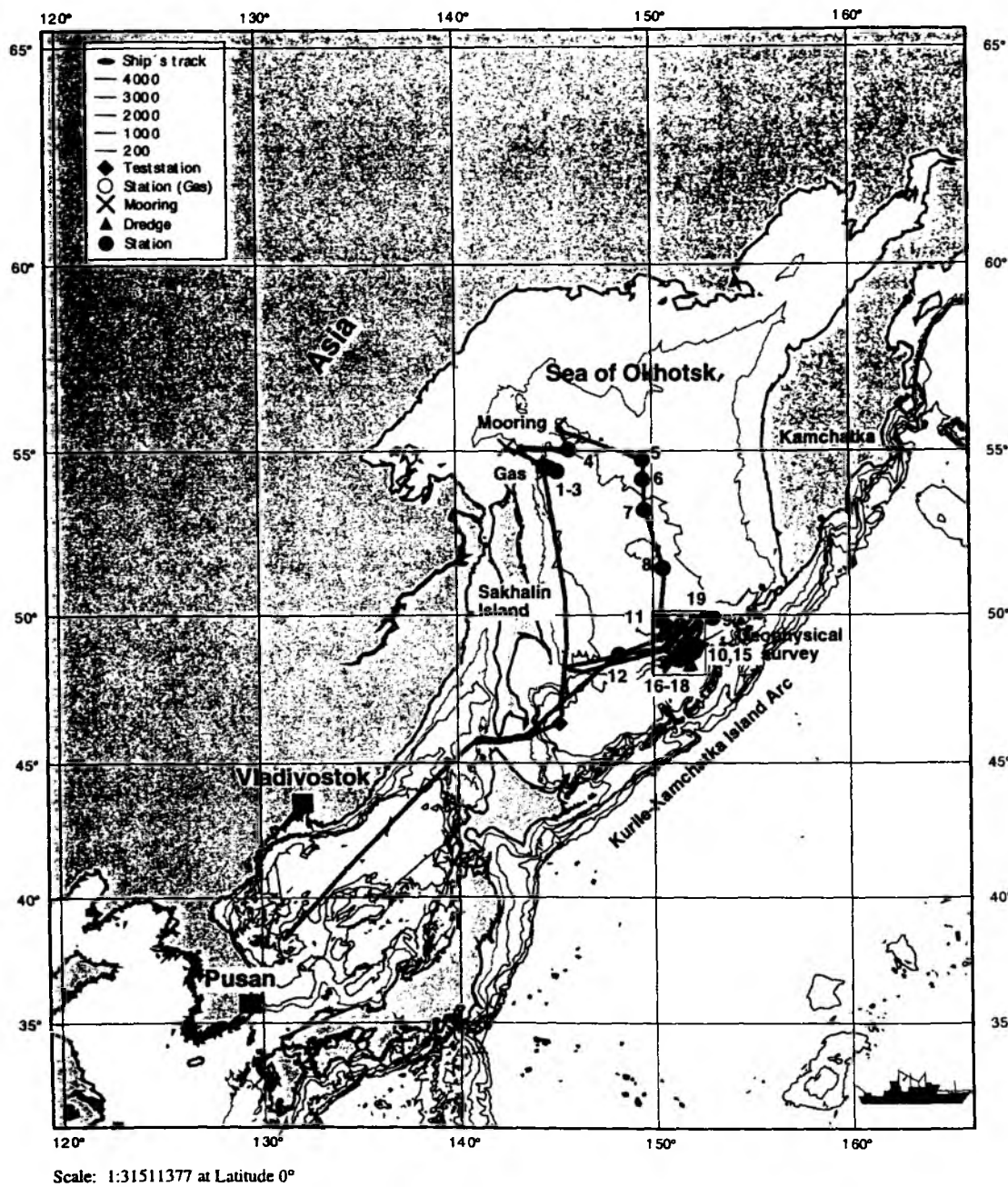
FEGI FED RAS: Far Eastern Geological Institute, Far Eastern Division of the Russian Academy of Sciences, Vladivostok.

GEOMAR: Research Center for Marine Geosciences, Christian - Albrechts - University, Kiel.

GTG: GEOMAR Technology GmbH, Kiel.

IO RAS: P.P. Shirshov Institute of Oceanology, Russian Academy of Sciences, Moscow.

POI FED RAS: Pacific Oceanological Institute, Far Eastern Division of the Russian Academy of Sciences, Vladivostok.



**Fig. 1.1:** Ship's track of R/V Akademik Lavrentyev during cruise 27 and site locations. The inserted rectangular indicates the detailed geophysical investigation.

Considering that there is a good tradition from the beginning of the joint German-Russian Okhotsk Sea investigations to name expeditions "POSETIVE" (1994) and "GERDA" (1995), we suggest to call this year's expedition "GREGORY" (abbreviation from German-Russian Expedition for Geological/Geophysical Okhotsk Sea Research).



## 2. List of participants

Karp, Boris	Co-chief scientist, seismics (POI FED RAS)
Nürnberg, Dirk	Co-chief scientist, marine Geology (GEOMAR)
Baranov, Boris	Scientific leader, tectonics (IO RAS)
Nikolaev, Sergey	Deputy of chief scientist, gravity (POI FED RAS)
Lelikov, Evgeniy	Deputy of chief scientist, petrology (POI FED RAS)
Karnaikh Victor	Scientific coordinator, Seismics (POI FED RAS)
Astakhov, Anatoliy	Lithology (POI FED RAS)
Botzul, Anatoliy	Seismics (POI FED RAS)
Dergachov, Aleksandr	Lithology (POI FED RAS)
Dozorova, Karina	Tectonics (IO RAS)
Golovan', Anatoliy	Magnetics (POI FED RAS)
Gorbarenko, Sergey	Paleoceanology (POI FED RAS)
Gruetzner, Jens	Marine geophysics (GEOMAR)
Kolpashikova, Tat'ayna	Gravity (POI FED RAS)
Krainikov, Gennadiy	Technician (POI FED RAS)
Matul, Aleksandr	Micropaleontology (IO RAS)
Neufeld, Sergej	Technician (GTG)
Obzhirov, Anatoliy	Gas geochemistry (POI FED RAS)
Prokudin, Vladimir	Seismics (POI FED RAS)
Sibekin, Victor	Seismics (POI FED RAS)
Sudakov, Anatoliy	Seismics (POI FED RAS)
Svarichevskiy, Aleksandr	Geomorphology (POI FED RAS)
Tararin, Igor	Petrology (FEGI FED RAS)
Terekhov, Evgeniy	Petrology (POI FED RAS)
Tzovbun, Nikolay	Magnetics (POI FED RAS)
Valitov, Maksim	Gravity (POI FED RAS)
Vogt, Christoph	Marine geology (GEOMAR)
Wolfsdorf, Jan-Malte	Marine geology (GEOMAR)

FEGI FED RAS: Far Eastern Geological Institute, Far Eastern Division of the Russian Academy of Sciences, Vladivostok.

GEOMAR: Research Center for Marine Geosciences, Christian - Albrechts - University, Kiel.

GTG: GEOMAR Technology GmbH, Kiel.

IO RAS: P.P. Shirshov Institute of Oceanology, Russian Academy of Sciences, Moscow.

POI FED RAS: Pacific Oceanological Institute, Far Eastern Division of the Russian Academy of Sciences, Vladivostok.

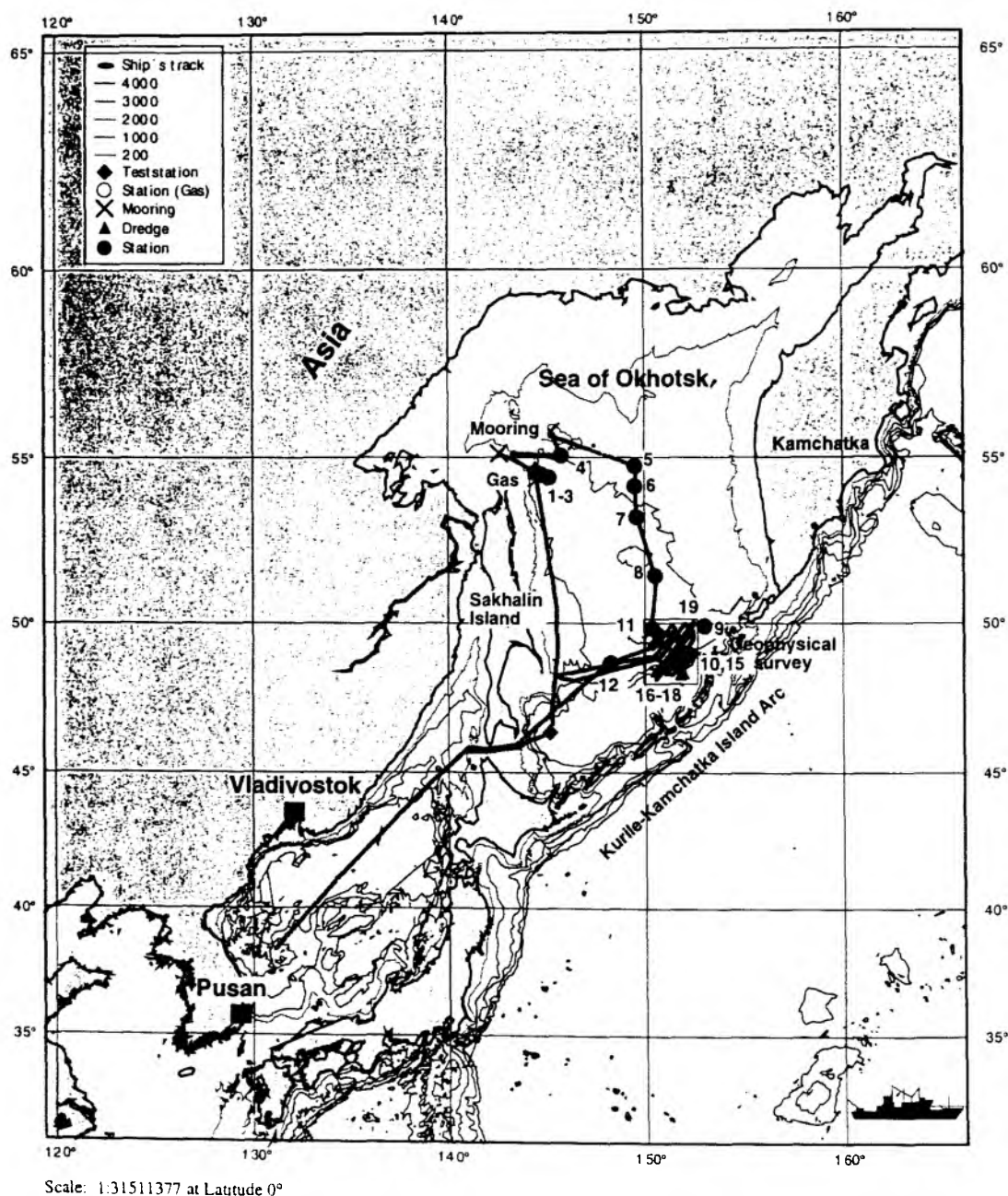


Fig. 1.1: Ship's track of R/V Akademik Lavrentyev during cruise 27 and site locations. The inserted rectangular indicates the detailed geophysical investigation.

Considering that there is a good tradition from the beginning of the joint German-Russian Okhotsk Sea investigations to name expeditions "POSETIVE" (1994) and "GERDA" (1995), we suggest to call this year's expedition "GREGORY" (abbreviation from German-Russian Expedition for Geological/Geophysical Okhotsk Sea Research).

## 2. List of participants

Karp, Boris	Co-chief scientist, seismics (POI FED RAS)
Nürnberg, Dirk	Co-chief scientist, marine Geology (GEOMAR)
Baranov, Boris	Scientific leader, tectonics (IO RAS)
Nikolaev, Sergey	Deputy of chief scientist, gravity (POI FED RAS)
Lelikov, Evgeniy	Deputy of chief scientist, petrology (POI FED RAS)
Karnaikh Victor	Scientific coordinator, Seismics (POI FED RAS)
Astakhov, Anatoliy	Lithology (POI FED RAS)
Botzul, Anatoliy	Seismics (POI FED RAS)
Dergachov, Aleksandr	Lithology (POI FED RAS)
Dozorova, Karina	Tectonics (IO RAS)
Golovan', Anatoliy	Magnetics (POI FED RAS)
Gorbarenko, Sergey	Paleoceanology (POI FED RAS)
Gruetzner, Jens	Marine geophysics (GEOMAR)
Kolpashikova, Tat'ayna	Gravity (POI FED RAS)
Krainikov, Gennadiy	Technician (POI FED RAS)
Matul, Aleksandr	Micropaleontology (IO RAS)
Neufeld, Sergej	Technician (GTG)
Obzhirov, Anatoliy	Gas geochemistry (POI FED RAS)
Prokudin, Vladimir	Seismics (POI FED RAS)
Sibekin, Victor	Seismics (POI FED RAS)
Sudakov, Anatoliy	Seismics (POI FED RAS)
Svarichevskiy, Aleksandr	Geomorphology (POI FED RAS)
Tararin, Igor	Petrology (FEGI FED RAS)
Terekhov, Evgeniy	Petrology (POI FED RAS)
Tzovbun, Nikolay	Magnetics (POI FED RAS)
Valitov, Maksim	Gravity (POI FED RAS)
Vogt, Christoph	Marine geology (GEOMAR)
Wolfsdorf, Jan-Malte	Marine geology (GEOMAR)

FEGI FED RAS: Far Eastern Geological Institute, Far Eastern Division of the Russian Academy of Sciences, Vladivostok.

GEOMAR: Research Center for Marine Geosciences, Christian - Albrechts - University, Kiel.

GTG: GEOMAR Technology GmbH, Kiel.

IO RAS: P.P. Shirshov Institute of Oceanology, Russian Academy of Sciences, Moscow.

POI FED RAS: Pacific Oceanological Institute, Far Eastern Division of the Russian Academy of Sciences, Vladivostok.

### 3. Scientific background and objectives

(B. Baranov, S. Gorbarenko, B. Karp, D. Nürnberg, E. Lelikov, and A. Obzhirov)

#### 3.1 Tectonics

In the Okhotsk Sea, various scientific and industrial organizations of the former USSR carried out geological and geophysical investigations. Most of these studies were performed in areas showing a thick sedimentary cover to search for oil and gas occurrences. These areas are located along Sakhalin Island, the Asian continent, and the Kamchatka Peninsula coasts. The available data allowed to determine the general tectonic and crustal structure, nevertheless, many unsolved problems still remain. The tectonic evolution of the Kurile Basin is one of them.

The Kurile Basin is the greatest and deepest among three basins of the Okhotsk Sea (Fig. 3.1). The so-called back-arc basin is located behind the Kurile Island arc, the existence of which is typical for other north-western Pacific marginal seas, e.g. the Japan and Bering Seas. The maximum depth of the Kurile Basin equals to 3374 m, which is the maximum depth of the entire Okhotsk Sea. The average depth of the Kurile Basin equals to 3300 m.

Previous studies (Galperin and Kosminskaya, 1964; Bikkenina et al., 1987) showed that the Kurile Basin's oceanic crust is covered by a thick sediment pile (velocity of 1.7-2.3 km/s) of up to 5 km. Below, the second layer is characterized by velocities of 4.3-5.2 km/s and a thickness of 2.0-2.8 km. This layer presumably constitutes the top of consolidated volcanogenic-sedimentary rocks. A high velocity layer ( $V_p = 6.8$  km/sec) corresponding to oceanic layer 3 exhibits a thickness of 4-5 km. The Moho discontinuity is recognized at 13 km depth below sea surface.

Based on these results, the Kurile Basin is suggested to have been formed due to back-arc extension, which was followed by seafloor-spreading and the formation of new oceanic crust. Up to now, it is suggested that the spreading axis within the Kurile Basin trends NE-SW being parallel to the Kurile Island Arc. Opening is, thus, suggested to be orthogonal to the spreading axis (Fig. 3.2 a) (Savostin et al., 1983; Kimura and Tamaki, 1986). However, data verifying this geometry, such as linear magnetic anomalies and the structural manifestation of the spreading axis, are still absent. The above mentioned tectonic situation is mainly based on both the general tectonic pattern and the similarity of the northern and southern Kurile Basin slopes.

The impossibility of establishing a correlation between the opening geometry of the Kurile Basin and the Okhotsk rift system furthermore contradicts the tectonic pattern outlined above. The Okhotsk rift system is one of the most remarkable features of the Okhotsk Sea tectonics (Gribidenko, 1990). Its separate parts formed simultaneously with the basin, but exhibit an orthogonal direction of extension in comparison to it.

Recently, Baranov et al. (1995) proposed a new model of the Kurile Basin opening geometry. According to this model, the spreading axis is orientated in a northwesterly direction, orthogonal to both the Kurile Island Arc and the Kurile Basin, suggesting the pull-apart mode of basin opening (Fig. 3.2 b). In such a case, the direction of the Kurile Basin opening parallels the extensional trend of the Okhotsk rift system. Accordingly, both the northern and southern flanks of the Kurile Basin correspond to strike-slip structures along the curves of big circles.

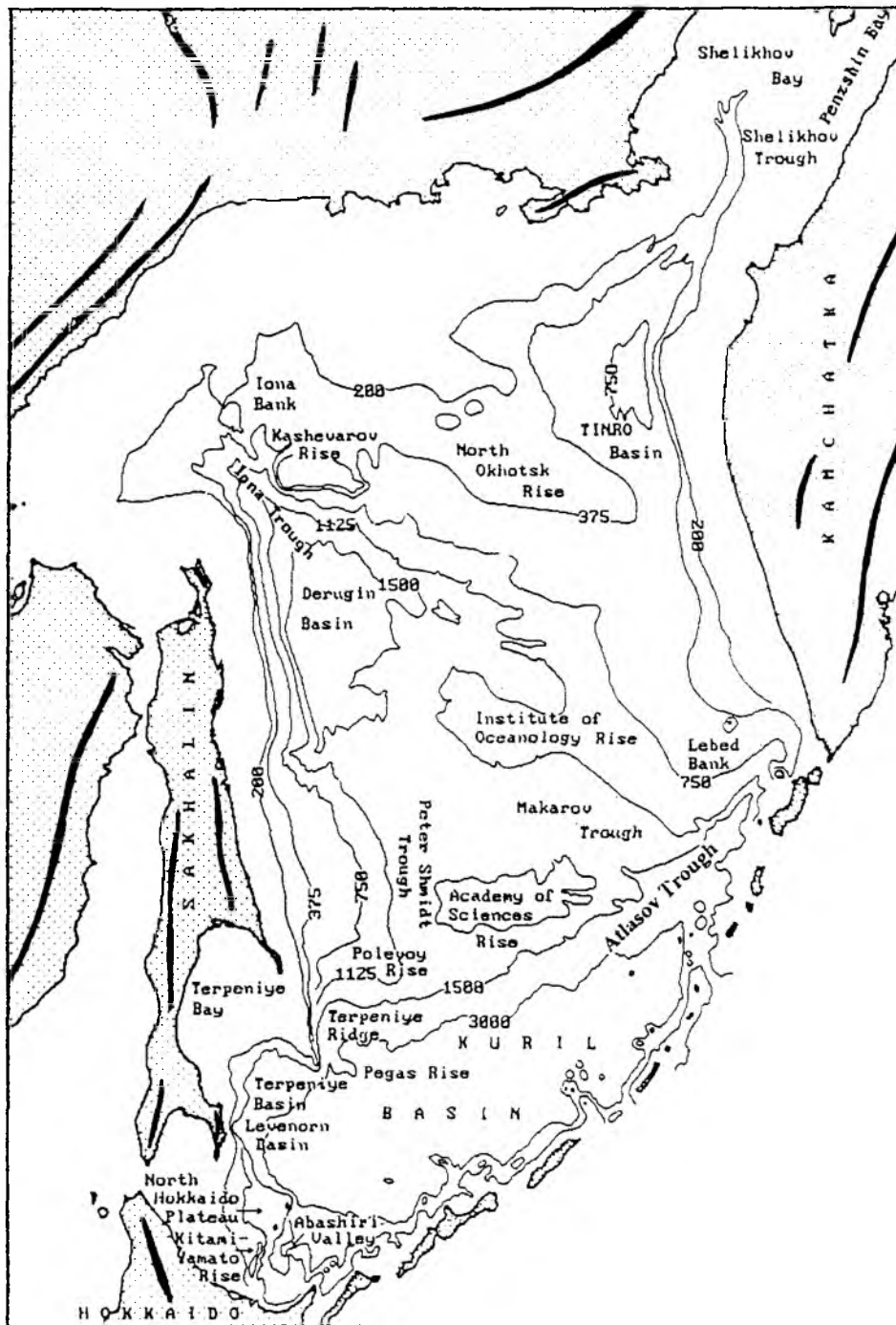


Fig. 3.1: Main morphology elements of the Okhotsk Sea floor. Contours are 200, 375, 700, 1125, 1500, and 3000 m (after S. Svarichevsky). Thick lines indicate mountain ranges on land.

The model can be verified by structural investigations determining the system of conjugate faults and their kinematics. Accordingly, the northern slope of the Kurile Basin is the target of this year's geophysical survey (echosounding, single channel seismic profiling, magnetic and gravity measurements), which will help to understand the tectonic pattern closely related to the initial stage of rifting.

The geophysical studies will focus on:

1. the determination of the fault pattern, and
2. the characterization of displacements along the faults (i.e. normal faults or strike-slip).

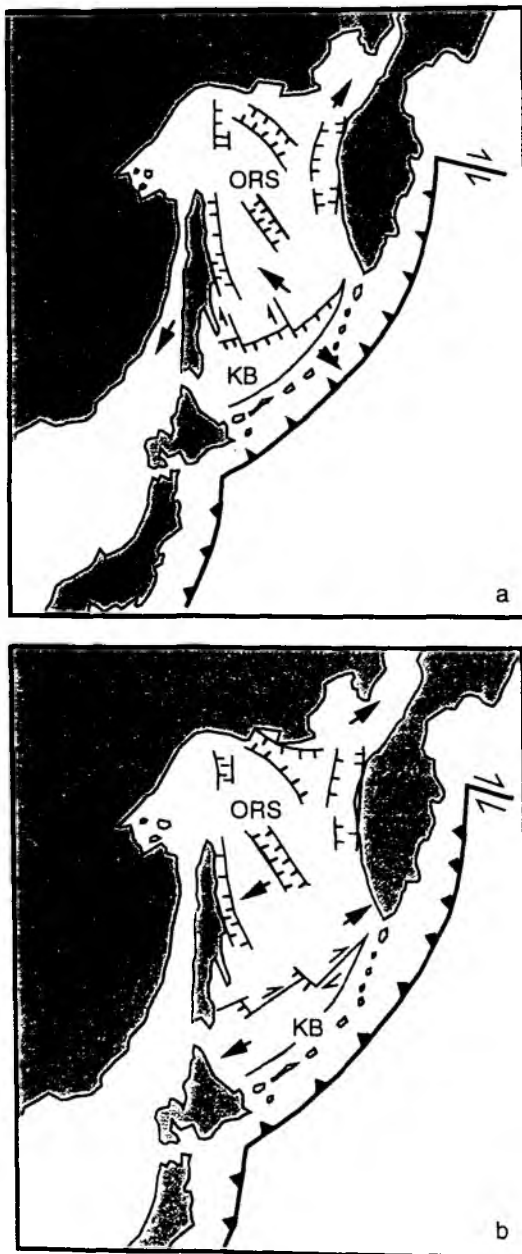


Fig. 3.2: Two geometry models of the Kurile Basin opening. See text for explanation. Thick arrow indicate the opening direction for the Kurile Basin (KB) and the Okhotsk Rift System (ORS). Lines with bars show normal faults, lines with arrow - strike slip. Toothed lines marks trenches.

### 3.2 Petrology

Previous investigations (Geodekyan et al., 1976; Vasiliev et al., 1990; Lelikov, 1992) showed that the Okhotsk Sea has a complex heterogeneous basement structure. In this respect, the central Okhotsk Sea is the best studied area as it exhibits the minimum sediment thickness. In contrast, the periphery of the basin being characterized by deep subsidence and accordingly, maximum sediment thicknesses of up to 8 km (Kharakhinov et al., 1985), remains nearly unknown.

In the central Okhotsk Sea, the basement outcrops are predominantly located on bathymetric uplifts. These uplifts can be traced from Iona Island in the north to the continental rise of the Kuriles in the south. Within this belt, the basement crops out on Iona Bank, Kashevarova Rise, North-Okhotsk Rise, Institute of Oceanology Rise, and Academy of Sciences Rise, as well as on the slopes of the Kurile Basin.

Different institutes of the Russian Academy of Sciences carried out dredgings on these rises during the seventies and eighties. Unfortunately, the dredging stations were not supported by seismic reflection surveys. This, however, is extremely needed in regions characterized by a widely extended sedimentary cover, which may cover basement scarps. On the base of rock material gathered by dredging, the following rock complexes were found:

1. Metamorphic rocks of apparently Paleozoic age;
2. Jurassic and Mesozoic granitoids;
3. Cenozoic volcanic rocks similar in composition to the Kurile-Kamchatka Island Arc volcanites;
4. Mesozoic to Cenozoic sedimentary rocks.

Based on these data, Noklenberg et al. (1994) suggested that the Okhotsk Sea basement consists of terranes, which originated from different geodynamic conditions. Nevertheless, a lot of problems are still unsolved, e.g. how is the boundary between the ancient continental crust occupying the major part of the Okhotsk Sea and the young (Oligocene-Miocene?) oceanic crust manifested in the basement rock composition?

Therefore, a number of dredgings at the northern slope of the Kurile Basin were suggested in order to investigate the boundary between thinned continental crust (Academy of Sciences Rise) and oceanic crust (Kurile Basin). Bedrock sampling accompanied by geophysical surveys and its further petrological analysis is, thus, proposed in order:

1. to examine the rock composition and to determine the type of the earth's crust;
2. to search for volcanic rocks, such as alkaline basalts connected with the rifting process;
3. to determine the basement's physical properties being important for the geophysical (seismic, gravimetric and magnetic) data interpretation;
4. to study the composition and the age of sedimentary rocks outcropping along the Kurile Basin slopes.

### 3.3 Paleooceanography

From the paleoceanographic point of view, the Okhotsk Sea is still one of the poorly investigated basins, although this basin is of extraordinary importance for the understanding of both regional paleoenvironmental changes and global climate changes. The Okhotsk Sea represents a marginal basin characterized by a high terrigenous influx. It, thus, is a unique location at high northern latitudes to obtain

high-resolution records of paleoclimatic and paleoenvironmental changes and to understand the nature of these changes. Changes of water circulation, biological productivity, sea-level, and sea ice conditions connected with global climatic changes during Pleistocene and Holocene times are expressed in this basin better than in the Pacific Ocean.

In the fifties and sixties, Russian scientists started lithological, geochemical and micropaleontological studies within the upper sediment cover of the Okhotsk Sea (Bezrukov, 1955; Zhuze, 1962), but the low content of biogenic carbonate restricted detailed stratigraphical and paleoceanographical investigations in this basin.

During the last years, radiocarbon-dated downcore records of stable isotopes, and diverse geochemical and micropaleontological parameters allowed to set up a reliable stratigraphy, from which preliminary conclusions were drawn concerning the temporally changing paleoenvironment of the Okhotsk Sea (Morley et al., 1991; Gorbarenko et al., 1988; Gorbarenko, 1991, Keigwin, 1995). The majority of the analyzed cores was recovered from the central Okhotsk Sea, mainly from the southern slope of the Academy of Sciences Rise. From these studies it became apparent that environmental changes in the Okhotsk Sea are closely linked to NW-Pacific conditions, but also show distinct individual features (Gorbarenko, *subm.*). For instance, AMS- $^{14}\text{C}$  dated  $\delta^{18}\text{O}$  and  $\delta^{13}\text{C}$  records, carbonate, organic carbon and opal records, and temporal changes in the faunal composition reveal significant paleoenvironmental changes in the Okhotsk Sea during Termination 1A (13-12 ky BP), the Younger Dryas cooling event, and early Holocene times (Gorbarenko et al., *in press*). The Holocene environmental changes were accompanied by the drastic increase of biogenic silica caused by an enhanced biological productivity transforming the basin into a "silica" type basin.

Gorbarenko et al. (1988) pointed out that the increasing productivity during Holocene times did not simultaneously occur in the entire basin, but spread progressively from its open part towards the basin periphery in dependence from the increasing surface water temperatures. During this year's cruise, it will be attempted to assemble detailed records of various paleoenvironmental parameters from different parts of the basin, i.e. in sediment cores located along a NW-SE-trending profile (Sites 4, 5, 6, 7, 8, 9, 12) (Figs. 1.1 and 5.1).

The proposed Sites 1-3 are located in the outflow zone of suspended matter from the Amur river, which flows southward along the eastern Sakhalin slope. The sediment cores will distinctively reflect environmental changes of the northwestern Okhotsk Sea, which is strongly influenced by the Amur river.

In order to study deep water ventilation changes and their influence on the generation of intermediate and deep waters within the Pacific Ocean, sediment cores from different depths will be recovered (Sites 5, 6, 7, 9, and 12). The deep water masses of the Pacific Ocean are the largest reservoir of total dissolved inorganic carbon dioxide (total  $\text{CO}_2$ ). Possible changes in the formation of the Pacific intermediate and deep water masses may allow to further understand variations in the atmospheric  $\text{CO}_2$  content, and further to better understand the global climate.

Recently, Talley (1991) has stressed the importance of the Okhotsk Sea water masses for the North Pacific intermediate water mass formation. Due to the fact that the Okhotsk Sea belongs to the "silica"-type basin,  $\text{CO}_2$  is directly transported from the surface waters to the deep water masses through bioproduction and, thus, serves as a sink for atmospheric  $\text{CO}_2$ . Processes of vertical ventilation and changes of the biological  $\text{CO}_2$ -pump transferring  $\text{CO}_2$  from the atmosphere to the Pacific deep reservoir are therefore of outstanding importance to understand climate change.



### 3.4 Gas geochemistry

During the last twenty years, gas distribution patterns were studied within the water column and in sediments from the Okhotsk Sea. All investigations focussed on the applicability of gas as an indicator for oil-gas prediction, for mapping fault zones, and for searching for gas hydrates, hydrothermal and seeping vents.

As a result, gas anomalies were found in bottom water masses, in distinct horizons of the water column, and within seafloor deposits of the Okhotsk Sea. Here, methane is concentrated in bottom water anomalies located above oil and gas deposits, gas hydrates and fault zones. Methane concentrations in anomalies reach approximately 10000 nl/l. The background methane concentration is about 50-80 nl/l. Gas fluxes within the water column were found in areas where sediments contain gas hydrates (Zonenshain et al., 1987, Obzhairov et al., 1989). They look like plumes on the echosounder records.

The gas distribution within the water column of the Okhotsk Sea resembles the distribution of other marginal seas (e.g. Bering and Japan Seas). The normal pattern, however, disappears in areas with fields of gas anomalies. Since the upward migration of gas is significantly dependent on the saturation state of the water, this process has to be considered when calculating the exact amount of gas reaching the surface.

High concentrations of methane were determined in sediments, mainly in sediments containing gas hydrates (more than 10 ml/l). Sediments showing gas anomalies contain diverse carbonate and sulfide mineral assemblages. Commonly, a distinct horizon keeping gas and preventing gas migration from sediments to sea water is established in sediments at about 0.5 m below sea floor, which interacts with the gas and influences the oxidation-redox processes (Obzhairov, 1993).

With respect to the Okhotsk Sea before 1987, background methane concentrations amount to 30-40 nl/l. Gas anomalies, in contrast, increased to 300-400 nl/l offshore northeast Sakhalin. After 1987, the background methane concentrations increased to 70-80 nl/l, whereas the anomalies showed maximum values of 2000-3000 nl/l. Such drastic increase in methane concentrations may be related to the increased tectonic activity in this area (Neftegorsk earthquake, May 27, 1995;  $M = 7.6$ ). It has to be noted, indeed, that the onshore areas in the vicinity of the East-Sakhalin Fault have not experienced such a change in methane concentrations since 1987. Analog increases of gas concentration were also obtained between the Okinawa Trough and Taiwan (Obzhairov, 1994). Here, the enhanced gas concentrations may also be related to earthquakes in that area, which occurred in 1994 and 1996. It seems possible that the drastically enhanced gas exhalation can be applied for long-term earthquake prediction.

During this year's cruise of "Akademik Lavrentyev" it is planned to study the gas distribution within both the water column and the sediment. Accordingly, the identification of gas occurrences will be used:

1. to estimate the recent tectonic activity and to recognize fault zones;
2. to find gas fluxes and to calculate the gas volume migrating to the water/atmosphere interface;
3. to investigate the interaction between gas fields and mineral assemblages.

4. Methods and instruments

4.1 Geophysical methods

4.1.1 Gravity

(S. Nikolaev and B. Karp)

Four highly damped spring-type sea gravimeters GMNTM (made in Russia) mounted on a gyrostabilized platform GMS-2TM (made in Russia) were installed in a special room aboard the research vessel. The accuracy of the gravimeters is 0.8 mgal. In order to reduce cross-coupling errors, the straight-line model of the two gravimeters was used. The gravity data were written on an analog recorder for visual checking and subsequently stored on a PC486 with a sampling rate of 4 seconds. The gravity observations were started three days before the beginning of the cruise in Vladivostok, where the base gravity point is installed.

4.1.2 Magnetic intensity

(S. Nikolaev and B. Karp)

The magnetic total intensity measurements were performed by the proton magnetometer MBM-1TM (made in Russia). The magnetometer has a measuring range of 20.000 to 100.000 nT and shows an accuracy of 2-4 nT within the total measuring range. The magnetometer receiver was towed by a nonmagnetic cable in a distance of 250 m behind the ship's stern. The magnetic data were written on an analog recorder with a sampling rate of 10 seconds and stored by a PC486 with a sampling rate of 2 seconds.

4.1.3 Seismic

(B. Karp and A. Sudakov)

The energy source used for the single channel seismic reflection (SCS) survey was an airgun (Impuls-1TM, made in Russia) including 3 liter volume firing chambers. It was towed about 20 meters behind the ship in a depth of approximately 4 m. The airgun was fired at a pressure of 10-13 MPa every 10 seconds. Seismic signals were obtained by a one channel hydrophone streamer. Some characteristic features of the streamer are listed in Table 1.

Table 1: Specifications of the one channel hydrophone streamer.

Section name	Length (m)	Number of elements
Lead-in cable:	150	1
Weighted section:	10	1
Stretch section:	50	1
Active section:	100	1
Tail nylon rope:	25	1

The streamer depth was approx. 7 meters and its active part started 200 m behind the ship. Seismic signals were written on an analog line scan recorder and stored by the Digital Seismic Recording System (DSRS) on hard disk of PC486. Within the DSRS it is possible to watch 620 traces on the monitor simultaneously. After storing on hard disk, back ups were additionally made on magnetic-optic disk. The analog recorder has 5 sec sweep and delays from 0.5 to 10 sec in 0.5 seconds steps are possible.

The DSRS and the analog system were developed by the Marine Seismic Laboratory of the Pacific Oceanological Institute. Some characteristics of the DSRS are listed in Table 2.

**Table 2:** Specifications of the Digital Seismic Recording System.

Length of trace:	5 sec.
Start delay:	optional 0 to 4 sec in 1 sec. steps
Sampling rate:	optional 0.5, 1, 2 and 4 ms; here: 2 ms
Data format:	10 bits plus sign (integer 2 bytes)

#### 4.1.4 Bathymetry

(A. Svarichevsky)

Bathymetric mapping was carried out with the echosounding system designed by Elac Corporation (Kiel, Germany), especially designed for the Holming Corporation (Finland). The echosounding system has a fixed impulse power providing a radiated energy of 200W and/or 2kW. The duration of the impulses are 1, 3, and 10 ms, the main frequency is 12 kHz, and the beam width is 100 x 100. The received reflection signal is formed by an antenna of receivers as separate analogous beam of 9.20 x 4.30 width. Depth values were written on an analog echosounder line scan recorder and stored by the echosounder digital system on hard disk (PC486). The analog recorder has a delay of 1 m to 9999 m. Sea water sound velocity was considered to be 1500 m/s. Variations of sea water temperature and ambient pressure were not taken into consideration.

Locations of the geophysical observations were determined applying the GPS navigation system. The receiving set NavTracXL designed by Trimble Navigation was applied to determine the ship's location. All navigation data were stored on PC 486.

## 4.2 Geological and geochemical methods

### 4.2.1 Recovery of deep-sea sediments

(D. Nürnberg)

Seafloor sediments were recovered with the Standard Multicorer (MUC), the GEOMAR gravity corer (GC), and the POI gravity corer. The multicorer usually gains the undisturbed uppermost sediment column and therefore, covers the transition to the gravity corer, which recovers long sediment cores, but often shows disturbed surfaces.

During cruise 27 of RV "Akademik Lavrentyev", 12 multicorer were run. Only two runs failed. 12 GEOMAR gravity cores were taken in total recovering ca. 49 m. Only one corer was damaged. 10 POI corer were recovered successfully (ca. 47 m).

#### 4.2.1.1 Multicorer

(S. Neufeld and J.-M. Wolfsdorf)

The multicorer is a pyramidal metal cage with a fixed frame in its center. The frame consists of an apparatus inhabiting 12 plastic tubes (length 61 cm, diameter 6 cm, open at both sides), and a release mechanism. Additional weights increase the total load of the MUC. Each tube is equipped with two lids, which are fixed in an open position by springs when lowering the device to the seafloor. When reaching the sediment surface, the frame containing the tubes is pushed into the sediment. When again pulling up the device, the springs are deactivated and the lids tightly close the sediment-filled tubes. On average, sediment recovery is ca. 30-40 cm. Further, the bottom water directly overlying the sediment/water interface is trapped within the tubes.

#### 4.2.1.2 Gravity corer

(S. Gorbarenko, S. Neufeld and J.-M. Wolfsdorf)

The GEOMAR gravity corer (GC) applied by the German group consists of a long steel tube (length 5.75 m, diameter 0.18 m), which includes a removeable plastic liner of the same length (diameter 0.125 m). At the lower end, a core catcher prevents the sediment from sliding out of the tube. At the upper end, the tube is fixed to a large weight (1200

kg), which pushes the gravity corer deeply into the sediment. The maximum sediment recovery of 5.75 m can be extended by connecting additional tubes. Dependent of the type of sediment, cores of up to 18 m length can be easily derived. Aboard the ship, the plastic liner is pulled out of the steel tube and sliced into 1-meter segments.

The POI gravity corer run by the Russian geologists has a 8.50 m long steel tube (inner diameter 0.145 m). The 700 kg-weight is directly attached around the upper part of the tube. In contrast to a plastic liner used by the GEOMAR corer, a thin polyethylene sleeve was inserted into the core. After coring, the sleeve taking up the sediment was pulled out and cutted into sections of 1-1.3 m length. Fig. 4.1 compares sediment recoveries obtained by the GEOMAR gravity corer and the POI gravity corer at all locations. Apparently, no correlation either between the locations or the devices can be drawn.

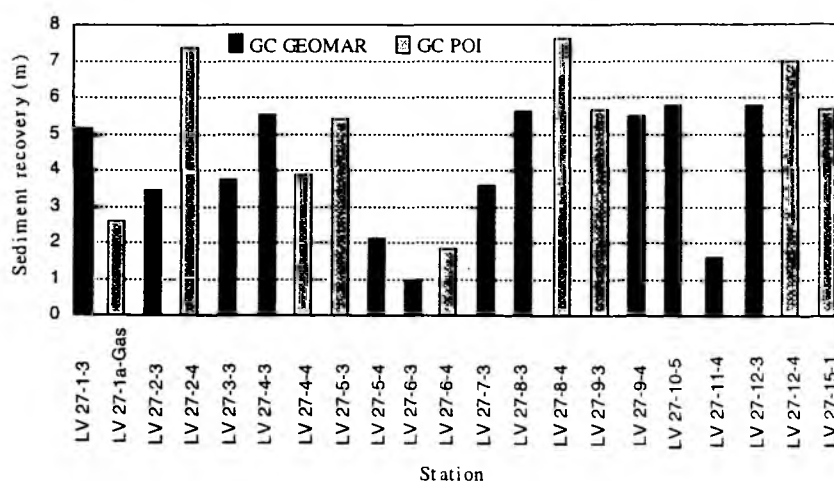


Fig. 4.1: Comparison of the GEOMAR-GC and the POI-GC sediment recovery.

#### 4.2.1.3 Dredging

(E. Lelikov)

Dredging was carried out in order to receive samples from bedrock outcrops. The cylindrical dredge with a diameter of 50 cm and a steel net was operated by a stern winch and an A-frame.

The dredging program followed the detailed bathymetry and seismic reflection profiling in areas, where steep scarps with possible basement outcrops were identified. The dredge was trailed along the seafloor starting at the lower slope towards its upper part. The location of the dredging site was determined by the GPS system aboard the ship at the moment of the first contact of the dredge with the seafloor. The depth of the dredging site was determined by echosounder.

Taking into account that in the Okhotsk Sea ice-rafted material is wide-spread, a detailed analysis of dredge hauls was carried out to determine the lithology of the outcropping bedrocks. The following criteria were used:

1. the shape of the samples (angular, non-rounded);
2. the existence of fresh surfaces formed by tearing away from the bedrock outcrops;
3. similarity of the material in the dredge haul.

### 4.2.2 Sediment sampling and processing aboard the ship

#### 4.2.2.1 GEOMAR approach

(Chr. Vogt and D. Nürnberg)

Up to 7 multicorer tubes were cut into 1 cm slices and stored immediately after coring. The lithology was described prior to sampling. For multicorer tubes, the bottom water and the fluff layer at the water/sediment-interface were sampled. Bottom water was taken for pH and gas analyses (see chapter hydrochemistry). At nearly each station, tubes were also sampled for stable isotope and coarse fraction analyses, organo-geochemical and inorganic-geochemical analyses (GEOMAR), the determination of biogenic silica (GEOMAR), and micropaleontology (AWI). Two tubes were utilized by Russian scientists (hydrochemistry, paleoceanography).

Each 1-meter liner-segment of the GEOMAR gravity corer was cut into work and archive halves and subsequently photographed. The lithology was documented accordingly. For X-ray photography, 25x1x1 cm sediment slices were prepared and stored in plastic lits. Subsamples were routinely taken for smear slide investigations. For selected cores, in addition, 5 ml and 10 ml syringes were taken each 10 centimeter for the determination of the water content, physical properties, stable isotopes, coarse grain fraction, and organic carbon content (Fig. 4.2). An additional 10 ml syringe were taken for siliceous plankton studies. Approximately 100 ml of sediment was sampled each 10 centimeter for inorganic geochemical analyses.

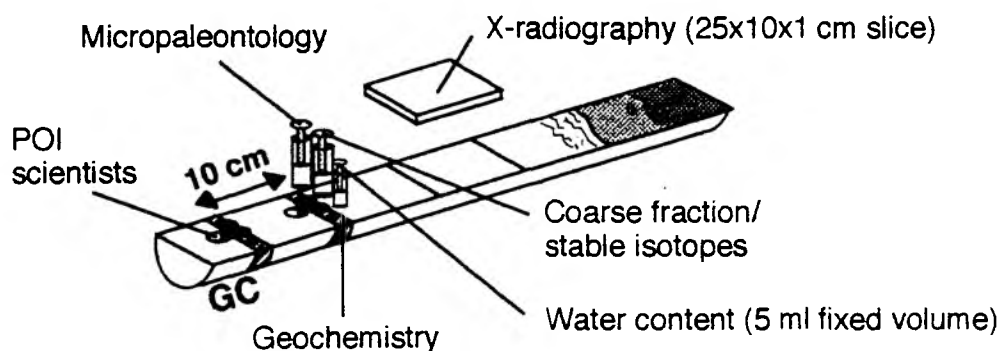


Fig. 4.2: Sampling of GEOMAR gravity core.

Offset by one centimeter, 10 ml syringes were taken for Russian colleagues. In return, the German group received 10 ml syringe samples from the Russian gravity corer each 10 cm. After processing, the cores were stored at +2°C.

Smear slides were prepared for each lithological unit (Table 1A) and subsequently investigated under the microscope. Biogenic and terrigenous sediment components were distinguished. A rough quantification of grain size fractions (sand >63 µm, silt 2 µm - 63 µm, clay <2 µm) and single components was derived by scanning the smear

slide and classifying it into 4 classes of occurrence: rare, common, abundant and rich. This method provides preliminary knowledge of the lithological sediment composition.

##### 4.2.2.2 POI approach

(S. Gorbarenko)

During the cruise following steps of sediment sampling and processing were performed:

1. Sampling for the analysis of gas components and pH-parameter
2. Measurements of humidity and magnetic susceptibility were done every 3 cm by microwave meter (MWM-8) and magnetic susceptibility meter (IMV-2), which is in direct contact to the sediment covered by a polyethylene foil. Data were directly stored on a computer. The devices were designed by the Western Company, Kaliningrad (Russia).
3. Sampling every 20-50 cm for measuring the sediment humidity and density according to the weight method.
4. Visual description, sampling, preparation and the preliminary study of smear slides with the microscope POLAM L-211.
5. Sampling for micropaleontological studies (diatoms, radiolarians, foraminifers, every 2.5-5 cm), oxygen and carbon isotopic analyses (2.5-5 cm), granulometric (10 cm) and geochemical (5-10 cm) measurements.
6. Removal of the clay fraction and classification into the grain size fractions 0.05-0.1 mm, 0.1-0.25 mm, and fractions larger than 0.25 mm for mineralogical analyses of the terrigenous and authigenic sediment components.
7. Selection of heavy minerals (density of more than  $2.89 \text{ g/cm}^3$ ) in the 0.05-0.1 mm fraction (every 20-50 cm) for immersion analysis.
8. For morphometric analyses sampling of quartz granules (every 5-20 cm) in the 0.25-0.315 mm fraction from selected cores.

##### 4.2.3 Gas sampling

(A. Obzhirrov)

For gas measurements samples were taken from both surface and bottom water applying Niskin bottles and multicorer tubes. Sediments recovered by multicorer and gravity corer were also investigated for their gas content. The gas was extracted by a specific vacuum assembly, and subsequently analysed by gas chromatography aboard the ship. Methane and heavy hydrocarbons (ethane, propane, butane and their homologs) were analysed by a flame-ionization detector. Oxygen, nitrogen and carbon dioxide were analysed by a catharometer. The sensibility of the hydrocarbon analyses was 0.00001%, of other gases ca. 0.01%.

##### 4.2.4 Mechanical properties of the sediments

(A. Astakhov and S. Gorbarenko)

The analysis of sedimentary mechanical properties was mainly performed to establish a lithostratigraphy of the Quaternary sediments. In addition, the mechanical properties are necessary to calculate sediment accumulation rates. Since it is difficult to preserve the sediment's natural humidity, humidity measurements were directly carried out aboard the ship, immediately after cutting the core.

Two methods were used: First, the standard weight method and, second, humidity measurements with the MWM-meter. The standard method includes sampling of  $50 \text{ cm}^3$  of non-disturbed sediment, subsequent drying at  $105^\circ\text{C}$  temperature, and weighing before and after drying. On the base of these data, the density of the natural sediment ( $D$ ), the density of the mineral base ( $D_p$ ), the mineralogical density ( $D_t$ ), the volume humidity ( $W_v$ ), and the weight humidity ( $W_w$ ) were calculated applying following equations:

$$D = P_0/V;$$

$$D_p = P/V;$$

$$D_t = P/(V - (P_0 - P)/g);$$

$$W_p = (P_0 - P)/V * g \text{ } 100\%;$$

$$W_w = (P_0 - P)/P_0 \text{ } 100\%,$$

where  $P_0$  and  $P$  are the sediment sample masses before and after drying (g);  $V$  - sample volume ( $\text{cm}^3$ );  $g$  - slime water density ( $\text{g}/\text{cm}^3$ ) (1,00).

#### 4.2.5 Magnetic susceptibility

(J. Grützner)

Records of magnetic susceptibility mainly reflect the content of ferrimagnetic minerals in the sediments. During the cruise, measurements of magnetic susceptibility were obtained with two different methods:

1. Whole core segments (1m length) retrieved with the GEOMAR gravity corer were measured with a Bartington loop sensor (MS2C) in conjunction with a control unit (MS2). The sensor generates a low intensity alternating ( $f=565 \text{ Hz}$ ) magnetic field and any material brought into the sensor changes the oscillator frequency. This frequency information is returned to the control unit where it is converted into a value of magnetic susceptibility. Magnetic susceptibility was measured in SI units ( $\cdot 10^{-5}$ ) in 3 cm intervals along the cores. Artificial minima of magnetic susceptibility usually occurring at both ends of each core section were identified and removed from the data set.
2. Cores collected with the POI-gravity corer were measured with a sensor directly at the sediment surface. Magnetic susceptibility and humidity values were obtained every 2 cm along cores. The magnetic susceptibility was measured in cgs-mode.

For comparison and calibration, some of the cores from the GEOMAR corer were also analysed with method 2 after splitting. Fig. 4.3 shows a comparison of three records of magnetic susceptibility from Site 8. Measurements obtained from Core LV27-8-3 (GEOMAR corer) demonstrate good agreement and comparability between method 1 and 2 (Fig. 4.3 a and b). This comparability is given at all locations except for Sites 1-3, where the sediment has a very weak magnetic susceptibility. In this environment differences in the sensitivity of the two sensors are most likely the cause of inconsistencies between the two methods. Figs. 4.3 b and 4.3 c show a correlation between cores LV27-8-3 (GEOMAR corer) and LV27-8-4 (POI corer). An ash layer, which was found in both cores, is marked by susceptibility maxima at 121 cm in Core LV27-8-3 and at 310 cm in Core LV27-8-4. Below this peak, both records show very similar curvature (shaded area), but, the distances between the maxima are less in Core LV27-8-3. According to these differences, the sediment section in Core LV27-8-3 is compressed by a factor of 1.4 relative to Core LV27-8-4. When comparing the two records it is obvious that the uppermost sediment section (diatomaceous ooze) in Core LV27-8-4, which is characterised by low ( $<25 \cdot 10^{-5} \text{ SI}$ ) magnetic susceptibility, is missing in LV27-8-3.

#### 4.2.6 Micropaleontology

(A. Matul)

For the radiolarian study, the uppermost 1 cm of the surface sediment of the multicorer tubes (MUC) was used. The preparation technique includes the sediment disaggregation and the extraction of organic ingredients by boiling in a weak hydrogen peroxyde solution, washing through a  $50 \mu\text{m}$  sieve, and settling of the residues on slides in Canada balsam. 230-280 specimens per sample were counted, from which the absolute radiolarian content and the relative species concentrations were calculated.

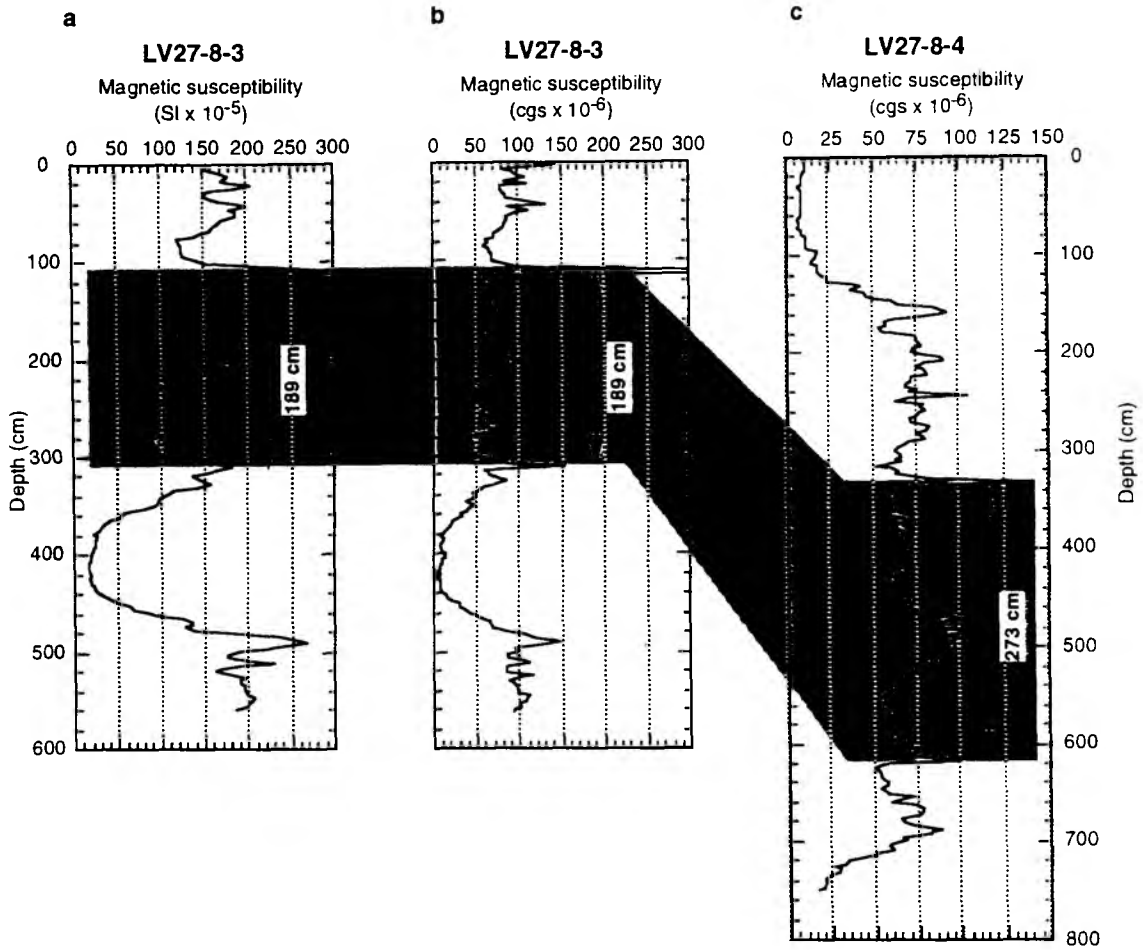


Fig. 4.3: Comparison of magnetic susceptibility records obtained at site 8. Good agreement between measurement methods 1 and 2 is confirmed by the records in 8a and b which were both measured at core LV27-8-3. Correlation of records from LV27-8-3 (GEOMAR-corer) and LV27-8-4 (POI-corer) shows that the sediment section in core LV27-8-3 is compressed by a factor of 1.4 (8b and c).

### 4.3 Hydrographical methods

#### 4.3.1 Plankton net

(D. Nürnberg and Chr. Vogt)

The upper layer of the water column down to 300 m was sampled for plankton. We applied a Nansen Closing Net constructed by Hydro-Bios Apparatebau GmbH, Kiel (Germany), which has a messenger-operated closing mechanism. The conical net part is of synthetic material showing a mesh size of  $55\ \mu\text{m}$  and a total length of 3 m. Below, the net bucket (bronze and nickel-plated) contains the sample net, which also has a mesh size of  $55\ \mu\text{m}$ . Plankton net samples were taken at stations 5, 8, and 10 in intervals from 300-200 m, 200-100 m, 100-50 m, and 50-0 m water depth. At station 8 we failed in sampling the lower intervals due to heavy drift. Here, only the upper 50 m could be sampled. After lifting up the net, it was washed with seawater. The sample was splitted into three subsamples: subsamples for micropaleontological studies (GEOMAR, AWI)



were poisoned with ethanol; the subsample containing living foraminifers was diluted by seawater and stored at +2°C.

#### *4.3.2 Water sampling*

(D. Nürnberg, Chr. Vogt and A. Obzhirov)

At stations 5, 8, and 10 water sampling was performed by 1.75 liter-Niskin bottles (General Oceanic, Inc.), which were lowered by the portside front winch to 300 m, 200 m, 100 m, and 50 m water depth. The Niskin bottle is a cylindrical plastic container, on both ends open, that can be closed by two rubberband-connected lids. Closing of the lids at the proposed water depth is triggered by a small weight falling down along the steel-rope. Surface waters were easily sampled with a bucket at all stations. Sample splits will be investigated for gas content (POI) and oxygen isotopes (GEOMAR).

## 5. Results

### 5.1 Marine geophysics

#### 5.1.1 Bathymetry

(A. Svarichevsky)

The main purpose of the geomorphological survey was to investigate in great detail the Okhotsk Sea bottom relief, especially in the area of the geophysical survey (Fig. 1.1) and in the region of a hydroacoustic anomaly at the northern Sakhalin shelf. In addition, the continuous mapping of the bottom relief during transit was undertaken to find new hydroacoustic anomalies, to further establish their correlation with relief elements, and to explain relief genesis.

The main objectives of the bathymetric study were:

1. Regular square bathymetry survey on the polygon;
2. Echosounder measurements on all the ship tracks;
3. Bathymetry and map support on all geological sites.

In the area of the complex geophysical survey (the Academy of Sciences Rise and the northern slope of the Kurile Basin), the bathymetry mapping was performed along the system of northwesterly and northeasterly directed ship tracks (Fig. 5.1). In average, the main track length is 90 miles. The distance between tracks did not exceed 12 miles. The size of the survey area was approximately 800 square miles. In total, 1310 miles were surveyed within the survey area and about 2000 miles of bathymetric profiles were obtained during transits.

On the basis of these profiles, the bathymetric map was compiled. The map was plotted using the commercial software SURFER. Since the survey tracks were not regularly spaced, and since the track network in its southern part was denser than in the northern part, two maps were prepared, one for the entire study area (Fig. 5.2) and another for the southernmost part (Fig. 5.3).

Specific attention was paid to the eastern flank of the Academy of Sciences Rise. Former investigations allowed to distinguish a large-scale fault and an adjacent submarine Pegas valley. Along with the general submerging of the rise towards the Makarov Trough in the east, its upper part is divided into a series of minor rises. They correspond to basement blocks separated by graben structures. In some places where sediment thickness is reduced basement blocks crop out, the tops of which are cut by abrasion.

Minor rises oriented in a WNW direction are manifested in the bottom morphology. Deep grabens located in this area are filled with sediments and form an accumulative plateau gently inclining towards the Kurile Basin. Here, gouges originated at the contact zone between the outcropping basement blocks and sedimentary layers, which justify a high hydrodynamic activity of the water masses during the forming of this surface.

The eastern part of the Academy of Sciences Rise is restricted by a series of tectonic scarps, faced to the NE towards the Makarov Trough. Their heights reach approximately 200 m.

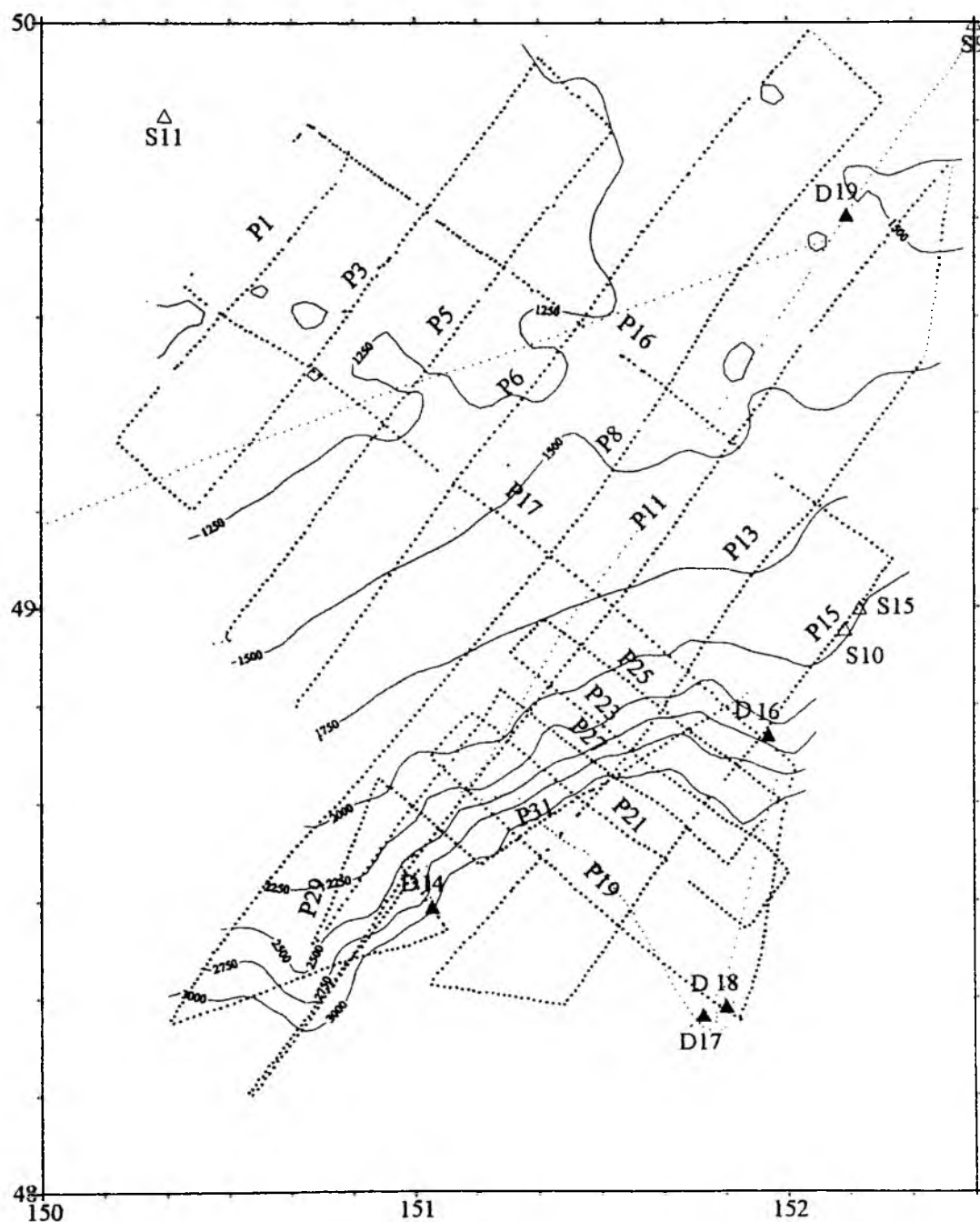
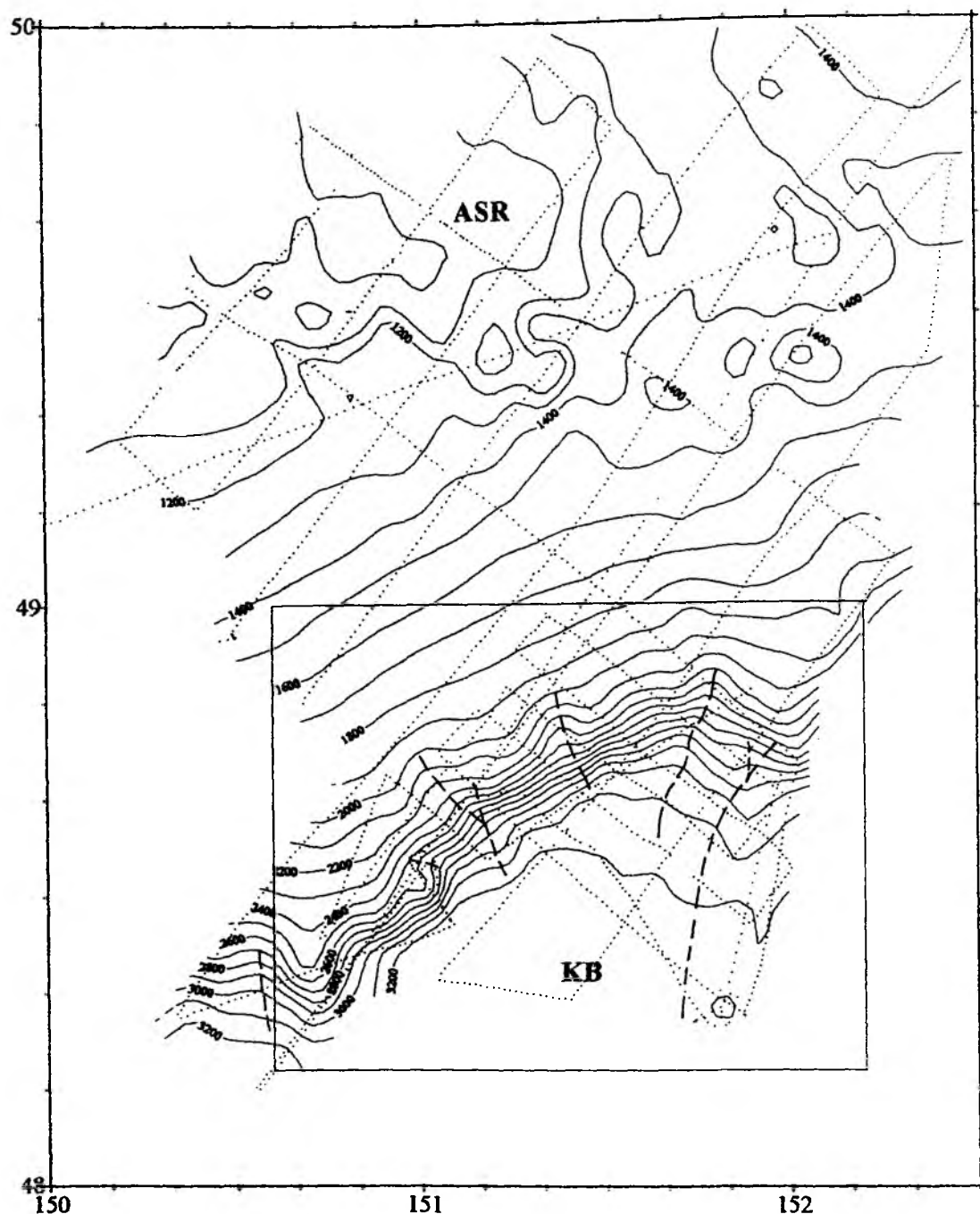


Fig. 5.1: Ship's track lines of the geophysical survey including magnetic - gravity - seismic - bathymetry profiles with their numbers (bold dotted line), bathymetry profiles (dotted line); dredge (black triangles) and gravity core and multicorer (triangle) sites.

The continental slope, separating the central Okhotsk marginal plateau from the Kurile Basin, exhibits a complex morphological structure. The bathymetric position of its top is generally determined by the top level of the corresponding basement block, the sedimentary cover of which is thinned. Further to the Kurile Basin, the slope deep increases. Here, many canyons occur, which are connected to faults and basement block outcrops. At the base of canyons, landslide bodies occur.



**Fig. 5.2:** Bathymetric map of the geophysical survey area. Contour interval is 100 m, broken lines - submarine channel and canyon axis, inserted rectangular is location of detail map in Fig. 5.3. Abbreviation: ASR: Academy of Science Rise; KB: Kurile Basin.

In the regions adjacent to the Kurile Basin at a depth of 3000 m and more, a gently inclined plateau of the continental rise was observed. A submarine channel was also mapped. In addition, the seamount located at the northern boundary of the Kurile Basin was investigated. According to its shape, it is most probably of volcanic origin. The height of the seamount is about 1000 m, the diameter of its base is about 3.5 miles.

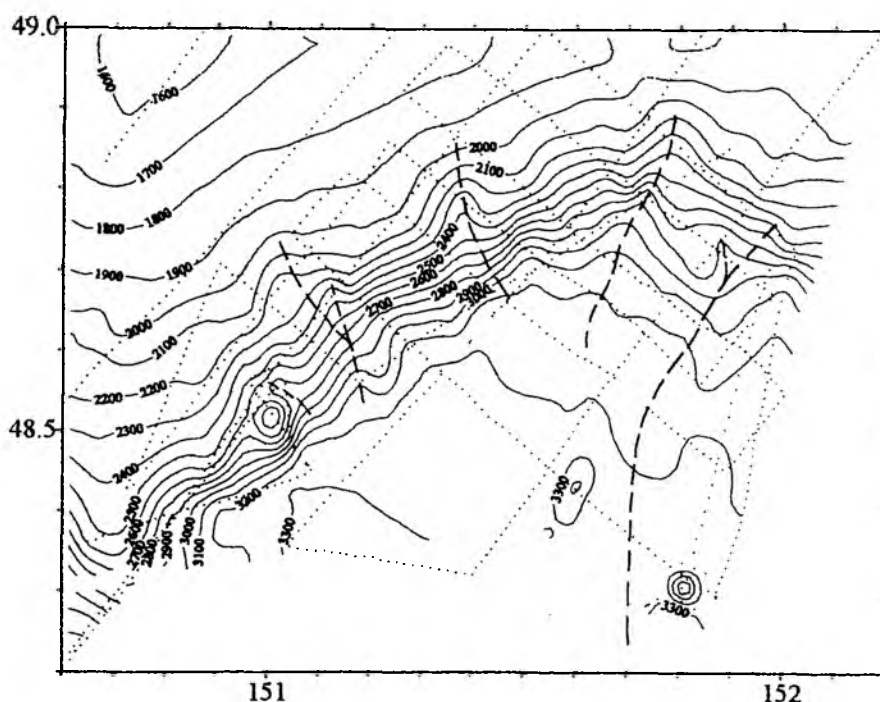


Fig. 5.3: Detail bathymetry map of the Kurile Basin lower slope. Contour interval is 100 m, broken lines - submarine channels and canyon axis.

At the NE Sakhalin shelf, the existence of hydroacoustic anomalies was verified, which were caused by gas seeping (gas plumes). Similar phenomena were discovered for the first time east of the submarine Terpenya Ridge.

#### 5.1.2 Seismic

(B. Karp and V. Karnaukh)

The seismic single channel reflection survey was carried out to obtain a high resolution seismic structure of the study area. The location of the seismic profiles are shown in Fig. 5.1. The total length of the 31 profiles is about 2350 km. The average ship's speed was maintained at 9 knots throughout the survey.

The acoustic basement map constructed from seismic reflection data is given in Fig. 5.4. In general, the seafloor morphology is reflected by the acoustic basement map, except the region between 49°30'N and 49°48'N. Here, the seismic data are inadequate to reflect the complex seafloor morphology in detail. Both, the Academy of Sciences Rise with its steep NE trending slopes and rising from 3.6 s TWT to 2.6 s TWT, and the upper and lower slopes of the Kurile Basin are well recognized on the map. The deep acoustic basement depression with NE strike corresponds to the Kurile Basin. The chain of the small acoustic basement highs lies along the north-western basin slope. The gentle NW trending basement swell intersects the upper basin slope and extends up to the top of the Academy of Sciences Rise. At the top, the asymmetrical basement blocks are recognized in seismic cross-sections (Fig. 5.9). The steep flanks of these blocks face to the north and north-east. The gentle flanks of the blocks form local basement depressions.

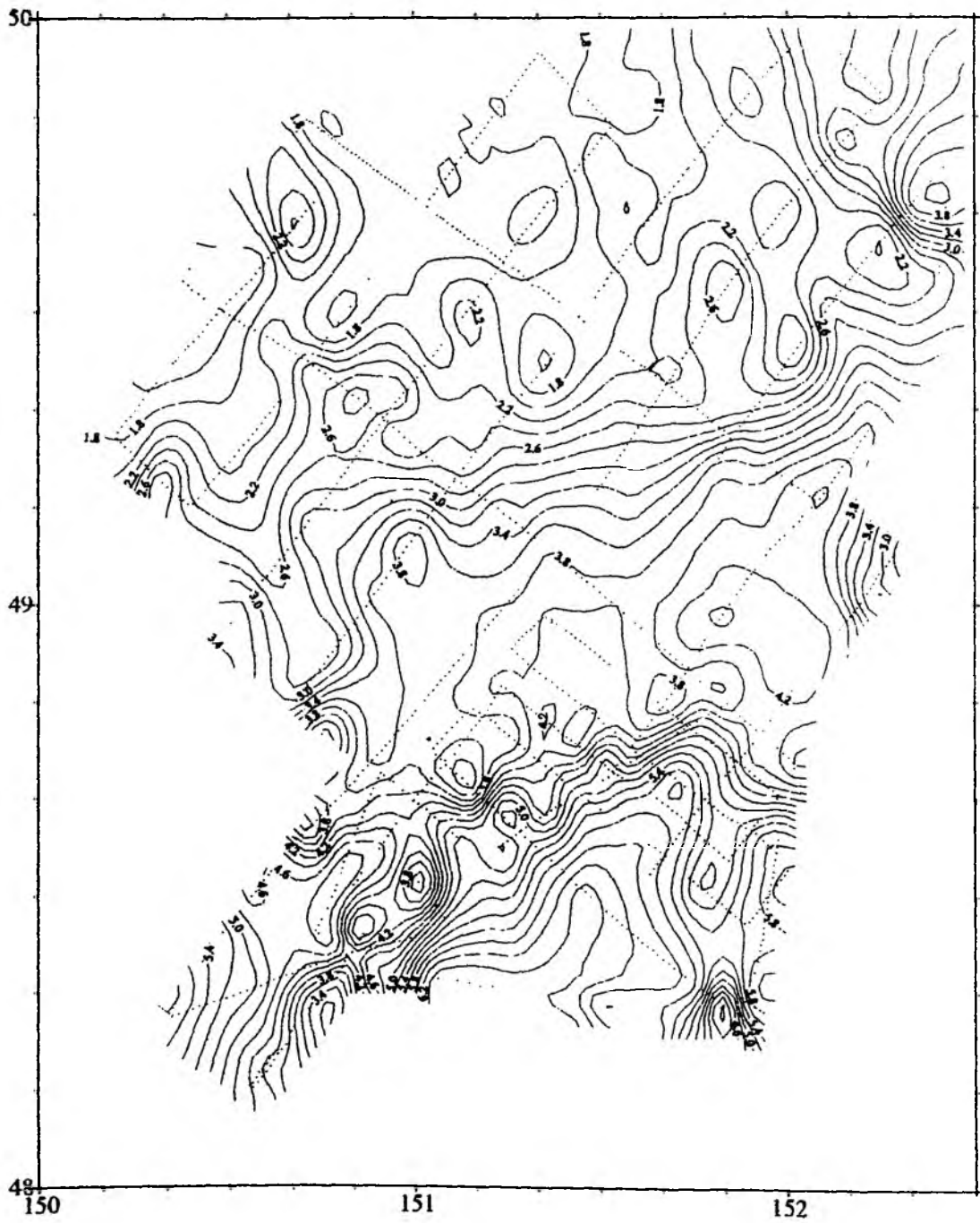


Fig. 5.4: Basement depth contour map of the geophysical survey area in 0.2 sec TWT inter-val.

The major part of the study area is blanketed by sediments (Fig. 5.5). The main depocenters include the Kurile Basin and local basement depressions on the upper basin slope and on the gentle flanks of the asymmetric blocks. The sedimentary thickness exceeds 2.2 s TWT in the Kurile Basin and is up to 1.8 s in the local basement depressions. Acoustic basement is exposed on most parts of the lower basin slope and on the steep flanks of the basement blocks.

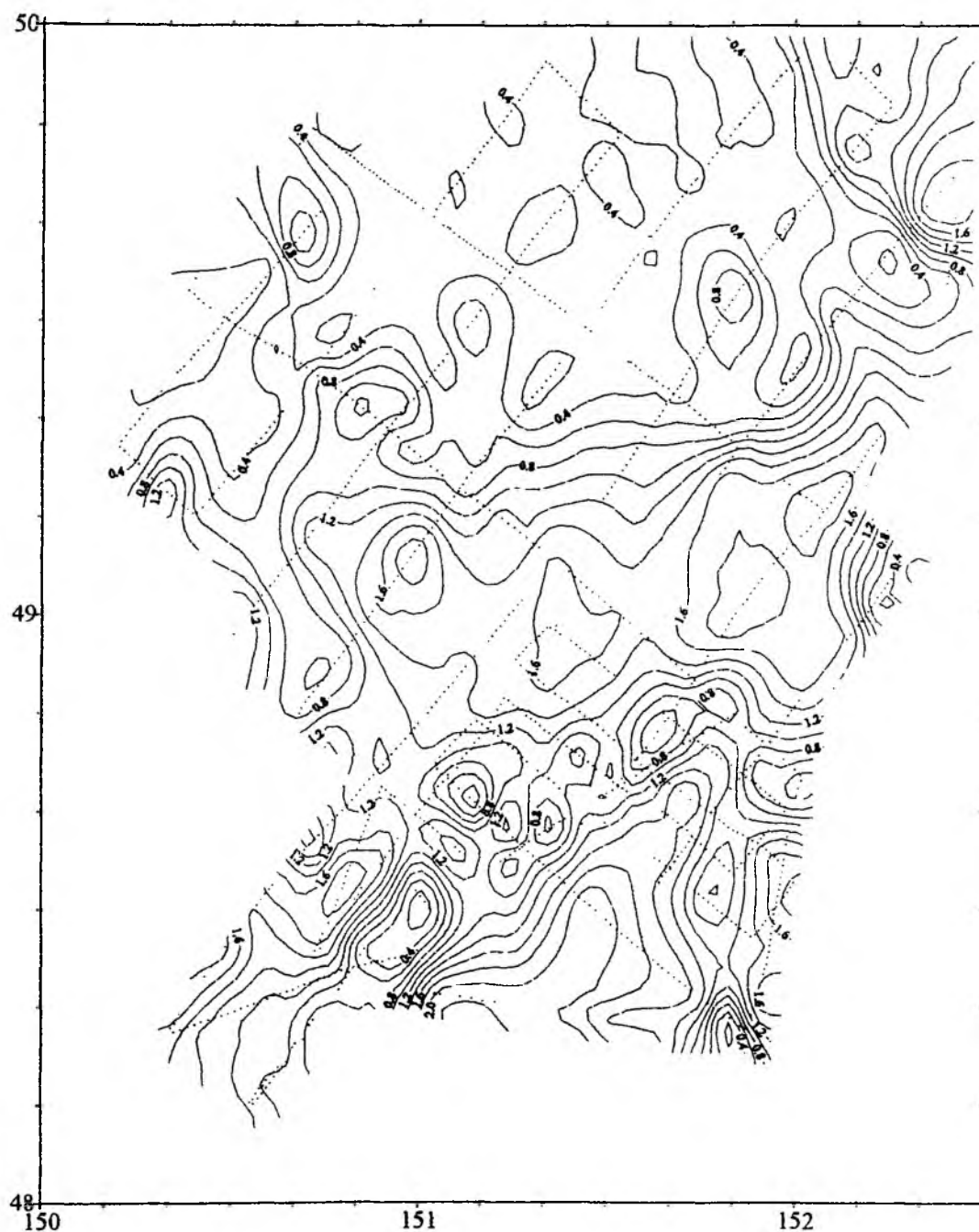


Fig. 5.5: Isopach map of sedimentary layer of the geophysical survey area in 0.2 sec TWT intervals.

#### Stratigraphy of sedimentary layers

The sediment fill of the Kurile Basin is composed of two major acoustic units. The upper acoustic unit is characterized by low frequency stratified reflectors (Fig. 5.6). The high continuity/variable amplitude reflectors from within the unit indicate turbidite deposition alternating with pelagic and/or hemipelagic deposition. The lower acoustic unit is acoustically transparent. The thickness of the upper unit is approximately constant throughout the study area ranging from 0.7 to 0.9 s TWT. The thickness of the

lower unit varies from 0.5 s near the basin slope to 1.2 s at some distance from it. The source of the detrital material deposited as turbidites is the Academy of Sciences Rise. The detritus is transported along submarine channels, which cut the upper and lower basin slope (Fig. 5.2). In most cases, the upper acoustic unit onlaps to the lower basin slope. In places, the upper unit reflection pattern suggests tectonic movements in terms of subsidence. The tectonic movement took place during the lower part of the upper unit accumulation.

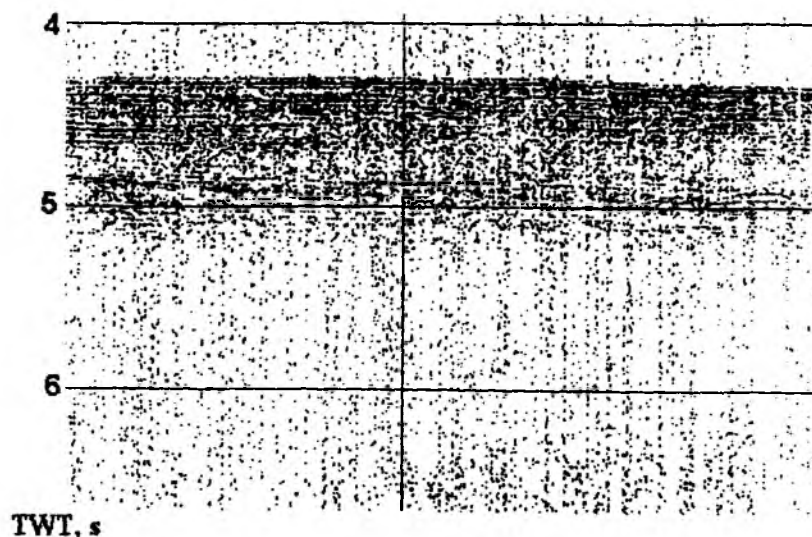


Fig. 5.6: Structure of sedimentary layer in the Kurile Basin. Portion of seismic profile 19.

Sedimentation on the lower basin slope occurs mainly as deposition of detritus transported along canyons and submarine channels. The sedimentary layer includes one acoustically transparent unit. There are numerous slumps. Sea bottom water currents running along canyons and channels form a levee (Fig. 5.7).

The sediment fill of the Kurile Basin upper slope includes two major seismic sequences. The upper sequence is characterized by stratified reflections, whereas the lower sequence is acoustically semitransparent (Fig. 5.8). These seismic sequences are separated by an unconformity. The high-amplitude, laterally continuous reflectors from within the upper sequence indicate deposition of turbidites. Transparent units alternating with high-amplitude reflectors indicate pelagic and/or hemipelagic deposition. We can recognize two major turbidite events in the Kurile Basin slope area. The turbidite events correspond to periods characterized by an enhanced sediment supply to the slope area. Possible mechanisms for the major variations in sediment supply to the slope area include both an eustatic sea-level change and a rapid uplift of the source areas onshore. We have not enough data to differentiate between these possibilities.



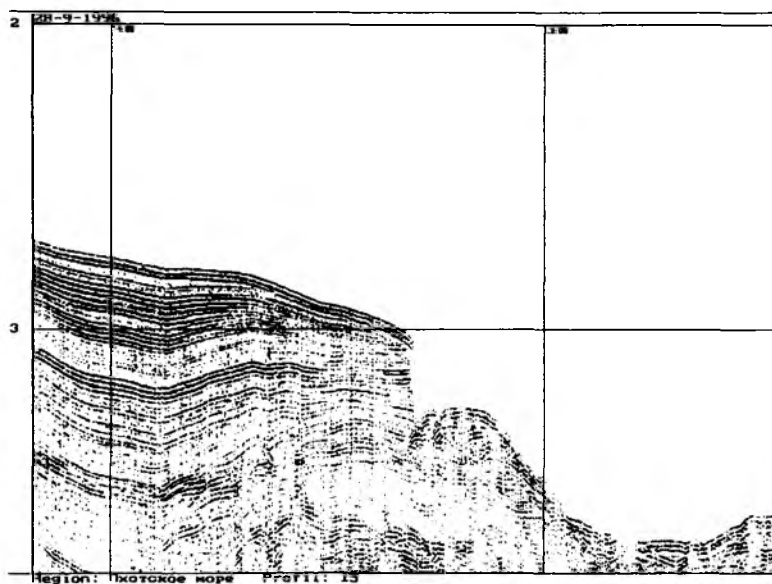


Fig. 5.7: Structure of the Kurile Basin lower slope showing submarine channel and levee. Portion of seismic profile 15.

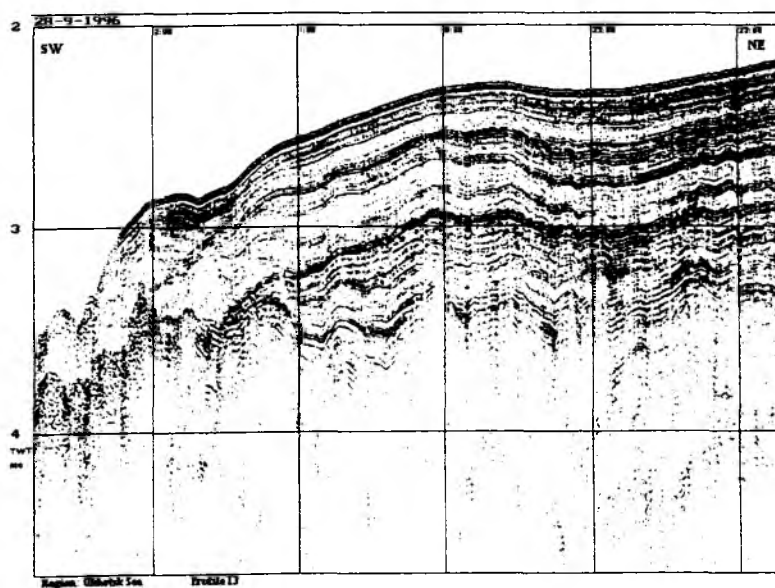


Fig. 5.8: Structure of the Kurile Basin upper slope. Portion of seismic profile 13.

The reflection pattern from both seismic sequences suggests a tectonic movement in terms of subsidence. The rate of the tectonic movement varies with time. It was high during the lower unit deposition and low during the upper unit formation.

The sedimentary sequence lying above the asymmetric blocks, which occur at the top of the Academy of Sciences Rise, consists of stratified units separated by an unconformity (Fig. 5.9). The lower unit lies on the tilted surface of the asymmetric blocks and its reflection boundaries are conform to them. The reflection boundaries of the upper unit are subhorizontal. Almost without exception, submarine channels can be recognized close to the asymmetric block tops, which occur as sea-floor local highs. In places, the seismic reflections below the unconformity are curved downward indicating a subsidence of block surface during sedimentation.

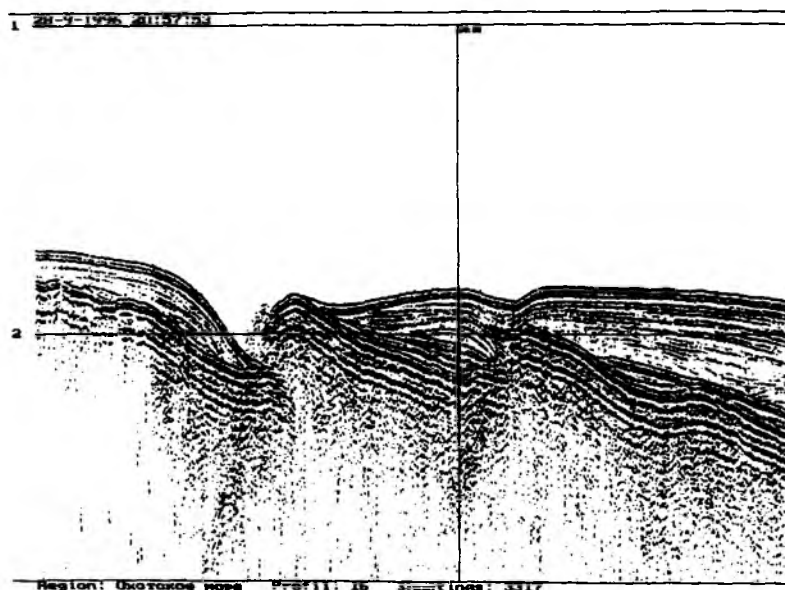


Fig. 5.9: Tilted blocks and structure of sediments on the Academy of Science Rise top. Portion of seismic profile 16.

### 5.1.3 Gravity and magnetics

(S. Nikolaev and T. Kolpashikova)

Gravity and magnetic measurements were carried out simultaneously in the seismic reflection survey. The location of gravity and magnetic profiles is shown in Fig. 5.1. The total lengths of the gravity and magnetic profiles are about 2000 km and about 2300 km, respectively. The magnetic anomaly can be calculated after converting magnetic variations into measured values of the magnetic field. Values of magnetic field variations will finally be obtained at the home lab at Vladivostok. Also, the gravity anomaly field will be calculated after having finished the gravity observations at the basic gravity point in Vladivostok.

For the preliminary presentation of the gravity and the magnetic field, the relative values for gravity and magnetic fields along three profiles were used (Fig. 5.10). The data analysis obtained during the cruise shows that the gravity field gradually decreases from the Academy of Sciences Rise towards

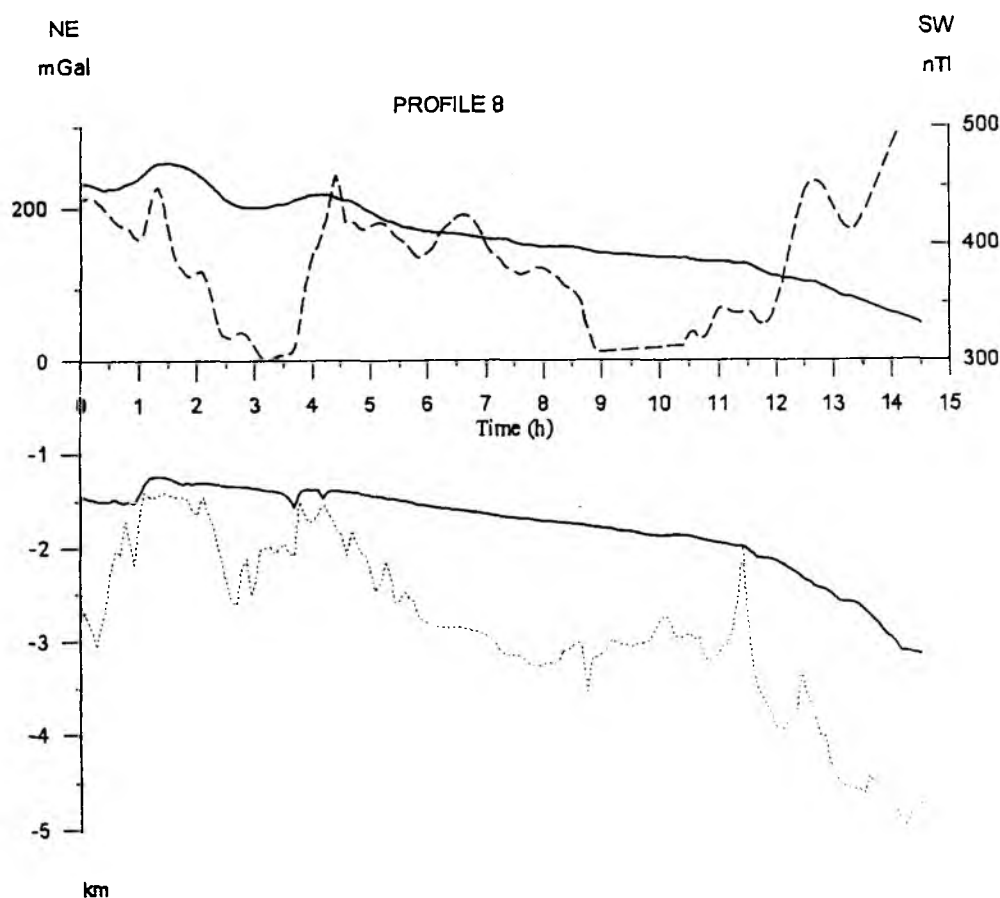


Fig. 10 a: Relative value curves of gravity (solid line) and magnetic (broken line) fields (top). Bathymetry (solid line) and acoustic basement (broken line) profiles (bottom). Location on Fig. 5.1.

the Kurile Basin. The magnetic field is more complicated due to a number of structures within the survey area that can cause the magnetic anomalies. According to the field's morphology, three areas of anomalies can be distinguished. They correspond to the main morphological structures of the survey area.

1. The anomaly area of the Academy of Sciences Rise is well manifested in the acoustic basement relief and characterized by local anomalies of geophysical fields. They are connected with uplifts and troughs of the acoustic basement, probably represented by the volcanogenic-sedimentary rocks.

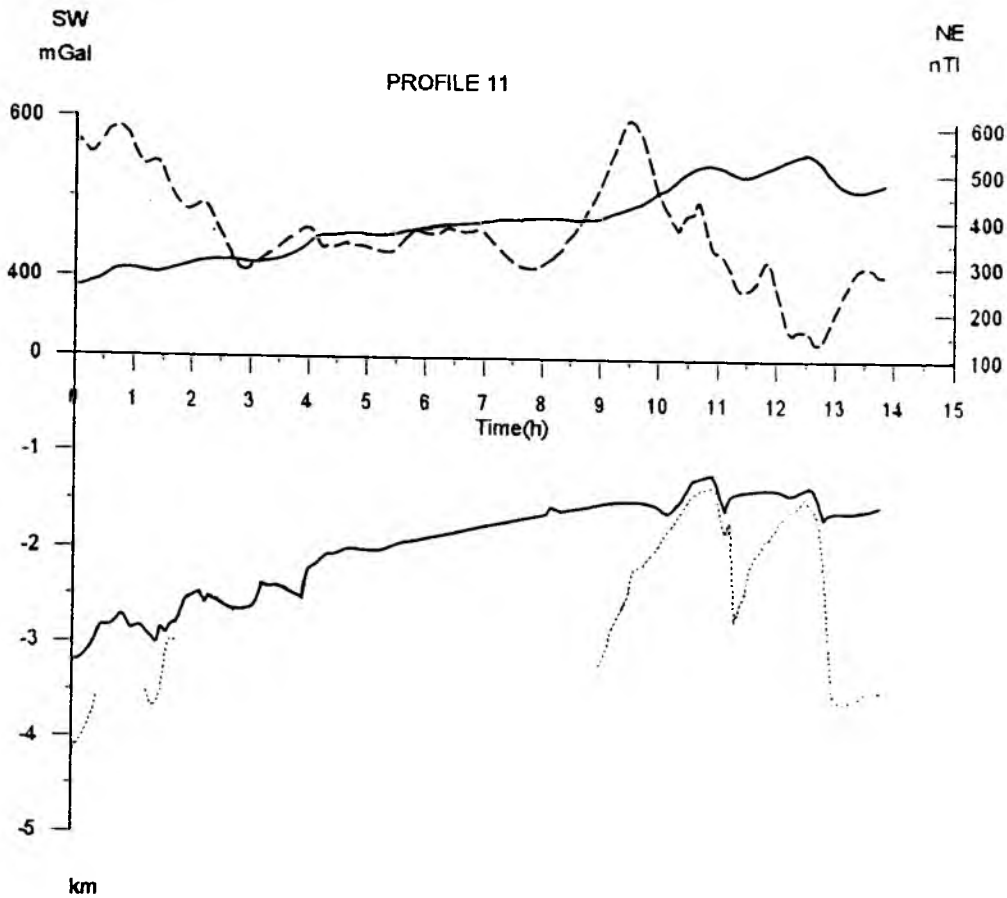


Fig. 5.10 b: Figure captions in Fig. 5.10 a.

2. The anomaly area of the Kurile Basin upper slope adjacent to the area described before is characterized by both the very low gradient of the gravity field and the decreasing values of the magnetic field. It is mainly connected with the enhanced sediment thickness up to 1,5 km. There are no local gravity anomalies in this area. Nevertheless, small local anomalies of the magnetic field were recorded. This fact may be explained by the presence of effusive formations in the lower sedimentary unit.
3. The anomaly area of the Kurile Basin lower slope is characterized by both the increase of the gravity field negative gradient, and the significant increase of the magnetic field. The abrupt changes in the geophysical fields point to the tectonic nature of the boundary between the upper and lower slopes of the Kurile Basin. The large positive gradient of the magnetic field may also be connected to the change in the geological structure of sedimentary layer. Small local anomalies in geophysical fields indicate the variations of the acoustic basement level.

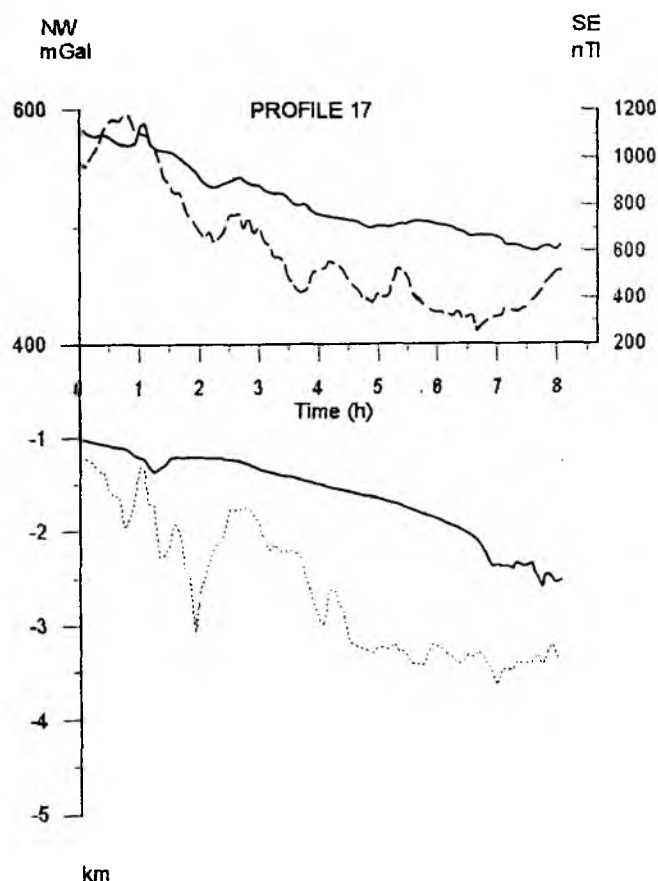


Fig. 5.10 c: Figure captions in Fig. 5.10 a.

## 5.2 Marine geology and geochemistry

### 5.2.1 Bedrocks

(E. Lelikov, I. Tararin, and E. Terekhov)

During the cruise, the bedrock dredging and subsequent petrological investigations were completed on 5 stations, located on the Kurile Basin northern slope, on the Academy of Sciences Rise, and on a volcano within the Kurile Basin (Fig. 5.1, Appendix IV, Table 9A). Dredging sites were chosen at places, where according to seismic reflection data basement outcrops and the upper sedimentary unit occur (Fig. 5.7). Basement rocks were sampled by two dredges (D14 and D19, Fig. 5.1) from 3000 and 1500 m water depths, respectively. At both stations, resembling assemblages of volcanic, sedimentary and plutonic rocks are present. These rocks were dredged in the form of angular blocks and fragments (30\*25\*20 cm to 6\*5\*3 cm), as well as in form of

rubblies, pebbles and rounded boulders. For the characterization of the basement rocks, the non-rounded fragments that apparently represent debris from bed rocks outcrops were considered.

Volcanic rocks demonstrate a broad variety of composition and are represented by the whole series from basalts to dacites. Lavas and tuffs of andesite and dacite dominate with subordinate basalts and tuffs. Some volcanites have metamorphic textures and mineral assemblages indicating some recrystallization at low greenschist facies conditions.

The sedimentary rocks intercalated with volcanic sequences are subordinate and are represented by argillites, alevrolites, greywackes and gravelites. Sometimes, sedimentary rocks are weakly metamorphosed: mica phyllites and even biotite hornfels with thin veins of leucocratic granite occur.

These low temperature alterations of volcanic and sedimentary rocks are apparently of regional nature and are influenced to a lower degree by the intrusions of granitoids. The radiometric K-Ar data for volcanites (basalts, dacites and felsites) from Academy of Sciences Rise (Kornev et al., 1982) justify the sedimentary-volcanic unit to be of Cretaceous age (125, 117, 87 Ma).

Angular fragments of fresh sparse porphyritic clinopyroxene-plagioclase basalts were sampled by dredge LV-27-14. Obviously, this rock type forms dykes connected to a younger (Neogene) magmatism.

A great variety of plutonic rocks was recovered. Biotite and biotite-amphibole granite, granodiorite and quartz diorite could be distinguished. Also few fragments of amphibole gabbro occur. On the Academy of Sciences Rise, granitoids similar in composition to the dredged rocks have a Cretaceous isotopic age (121-75 Ma).

Besides, Fe-Mn crusts were found among the dredged material. The largest crusts were recovered at station LV27-19, where the thickness of Fe-Mn crusts overgrowing silica sponges reaches 5-8 cm.

During this cruise, for the first time the fresh vesicle-poor two-pyroxene-amphibole basalts and basaltic andesites were dredged from the volcanic edifice located in the Kurile Basin. At station D18 (Fig 5.1), several angular fragments of pillow lavas of two-pyroxene-amphibole basalts and basaltic andesites were recovered. Further study of these rocks will allow to estimate the age of the volcanic edifice and its geodynamic position.

The samples of the upper sedimentary unit were obtained at station D16, which is located at an abrupt scarp on the northern slope of the Kurile Basin. Two types of sedimentary rocks were recovered. In the lowest part of the dredge, plate-shaped heaps of light olive gray and dark yellowish brown dense tuff-diatomaceous clays (approximately 45\*35\*20 cm) are present. In the upper part, less dense dusky yellow diatomaceous oozes were found. The first were dredged from the lower part of the scarp, which has a height of 250 m (interval of dredging -2450-2200 m), and characterize the lower part of the young sedimentary unit, whereas the second type of material represents the upper sedimentary unit. The apparent age of these rocks is Miocene to Lower Pliocene.

### Discussion

The preliminary analysis of the dredged rocks shows that the basement of the Academy of Sciences Rise and the northern slope of the Kurile Basin consists of Late Mesozoic sedimentary/volcanogenic rocks, which were intruded by Cretaceous granitoids. This

unit underwent weak regional metamorphism (low greenschist facies), which was followed by contact metamorphic processes connected with the intruding of granitoid massives. There is evidence from the metabasite gravel of the greenschist facies found in the greywackes of the Cretaceous volcanogenic/sedimentary unit recovered on Site D19 that this unit overlies the oldest complex (probably of Paleozoic age) metamorphologically altered in greenschist and epidote-amphibolite facies. These data are compatible with the model that the oldest basement of the Okhotsk Sea is buried by an onlapping Cretaceous unit.

The published data as well as our investigations show that the successive geological development is typical for various morphologic structures in the Okhotsk Sea (Kashevarov Bank, Okhotsk Arch, Institute of Oceanology Rise). All these structures exhibit outcrops of Cretaceous volcanic or sedimentary/volcanogenic rocks intruded by granitoids and old metamorphic basement. Among the dredged fresh basalts, clinopyroxene-plagioclase and two-pyroxene-amphibole basalts and basaltic andesites can be distinguished. The first may represent the rift-related dyke complex in the sedimentary-volcanic Late Mesozoic unit and may be connected with the formation of small extensional basins (pull-apart basins) due to the back-arc spreading in Kurile Basin. The data obtained suggest that two-pyroxene-amphibole basalts and basaltic andesites dredged from the slopes of the seamount in the Kurile Basin apparently have island-arc nature and are connected with Kurile Island Arc magmatism.

#### 5.2.2\* *Sediment stratigraphy*

(S. Gorbarenko)

Various indications derived from diatoms analyses (Zhuze, 1962), oxygen isotope records, AMS- $^{14}\text{C}$  dating, as well as positions of volcanic ash layers, and horizons with enhanced biogenic components (diatoms, foraminifers, total organic carbon) (Gorbarenko et al., 1988; Gorbarenko, 1993) were used to establish a preliminary stratigraphy for the Okhotsk Sea sediments. Wide parts of the Okhotsk Sea surface sediments consist of a typical olive diatomaceous ooze. Diatom analyses performed by Zhuze (1962) revealed that this upper layer of diatomaceous sediment belongs to the Holocene. Previous oxygen isotope investigations and AMS-radiocarbon datings on Core B34-90 from the Academy of Sciences Rise southern slope (Gorbarenko et al., in press) further reveal that the base of the diatomaceous silts age to about 6 ky BP. The underlying terrigenous sediments, which still contain large concentrations of diatoms (weak diatomaceous), were formed approximately 8 ky ago. It has to be mentioned, however, that the upper diatomaceous horizon did not begin to form simultaneously all over the Okhotsk Basin. Especially in the peripheral areas, it formed later due to progressive environmental warming (Gorbarenko, 1991).

The transition between the weak diatomaceous silts and the underlying, dominantly terrigenous sediments is characterized by an increasing carbonate content, which is due to large amounts of planktic foraminifers. This 2-step increase in calcareous plankton dates to approximately 9 and 12 ky, thus corresponding to the glacial terminations T1B and T1A (Gorbarenko et al., in press). The terminations are further characterized by the presence of volcanic ash layers, which were dated to 8.5 and 12 ky BP, respectively (Gorbarenko et al., in press). The lower volcanic ash, which was observed in many cores of the central Okhotsk Sea during this year's cruise, is defined as K-1.

According to micropaleontological and lithological indications, as well as information from the oxygen isotope stratigraphy, the dark gray terrigenous

\* List of the lithology and paleoceanology group and their scientific contribution in Appendix IV.

sediments underlying the upper horizon enriched in biogenic silica, were formed mainly during glacial conditions, i.e. oxygen isotope stage 2 and the upper part of stage 3 (Zhuze, 1962; Gorbarenko, 1991). Accordingly, biogenic components are of minor importance, whereas the significant influence of ice-rafted material must be noted in many cores.

Distinct variations in the coarse fraction (sand, pebbles) and a slightly varying carbonate content in these sediments suggest small but severe environmental changes in the Okhotsk Sea even during the last glacial period. In a number of cores, the terrigenous succession is intercalated by a volcanic ash (K-2), which is dated to approximately 28 ky (AMS- $^{14}\text{C}$  dating of Core 936, Dr. John Southon, personal communication, 1995).

The thick succession of terrigenous glacial sediments is underlain by a diatomaceous ooze characterized by abundant planktic foraminifers and a high total organic carbon content. According to the oxygen isotope records from the central Okhotsk Sea, this biogenic sediment package can presumably be related to the warm isotopic event 3.3 (Gorbarenko, 1991).

Below the diatomaceous horizon, a second sequence of terrigenous sediments follows, which must be related to cool environmental conditions during the lower part of isotope stage 3, stage 4 and the upper part of stage 5. The preceding third diatomaceous horizon accumulated during the interglacial oxygen isotopic event 5e, as inferred from the preliminary isotopic stratigraphy of Core K-105 from the central part of the Okhotsk Sea (Gorbarenko, 1991). The typical succession of relatively warm biogenic and cool terrigenous horizons is also typical for the Bering Sea and the NW-Pacific (Bezrukov and Romankevich, 1960; Gorbarenko, *subm.*).

### 5.2.3 Mineralogy

(A. Derkachev)

#### Mineralogical composition of the sediments

The climate and - in particular - the formation of the sea-ice cover are the most important factors influencing the depositional environment of the Okhotsk Sea. During sea ice formation in the shallow coastal zone, detrital material of all size fractions is entrained into the ice. The coastal ice is later transported by surface currents into the outer parts of the Okhotsk Sea and subsequently, releases its terrigenous freight during ice melting.

Apart from the coarse fraction (pebbles, gravel, boulders) found in Okhotsk Sea seafloor deposits, the silt fraction is of outstanding importance. The analysis of the mineralogical composition of the silt fraction in both coastal zones of the Okhotsk Sea and the deep-sea deposits allows to reconstruct pathways of debris transport from probable source areas to depositional areas. Petelin (1957) already determined the mineralogical associations of the source areas along the coastal zones and was able to relate them to distinct sedimentary Okhotsk Sea provinces (surface layer, 0-10 cm).

In this respect, the mineralogical studies of the terrigenous sediment components play a major role for the reconstruction of the Okhotsk Sea paleoceanography. The estimation of the intensity and the reconstruction of transport paths of debris allow to temporally and spatially reconstruct the pattern of surface currents, and the basin's ice cover during Pleistocene-Holocene times.

Based on the analysis of the mineralogical composition performed on selected sediment samples, source areas of clastic material can be deciphered. According to Table 2A (Appendix IV), Cores LV27-6-4 and LV27-8-4 located in the central Okhotsk Sea are



characterized by the pyroxene group. Clinopyroxene dominates in all samples. The content of minerals typical for granito-metamorphic rocks (aktinolite, granite, chlorite, zircon, turmaline, sphene etc.) on average is lower than 15%. The group of resistant minerals (zircon, turmaline, sphene, anatase) is of minor importance (less than 1%). Downcore mineralogical changes are negligible within the Holocene and Late Pleistocene sediments. Horizons enriched with volcanoclastics, namely volcanic ashes, are the only exceptions.

Within the Holocene sediments, however, a downcore decrease in the silty and sandy fractions can be observed indicating some changes in transport energy and also, revealing information about the constancy of the source area for the clastic material (i.e. West Kamchatka coasts). The similarity between both the studied mineral associations and the associations of the coastal regions of West Kamchatka justifies this supposition (Petelin, 1957). Ongoing studies on the mineral associations and typomorphic features of the minerals will allow to determine transport mechanisms of pyroclastics connected with volcanism on the adjacent coasts.

The mineral composition of the western group of stations (LV27-2-4, LV27-4-4) is quite different from the southeastern sites (Table 2A, Appendix IV). The amount of pyroxenes decreases, but the contents of epidote, aktinolite, chlorite, sphene and hornblende increase. Such mineral associations are due to the weathering of granite-metamorphic rocks. At the same time, the high content of pyroxenes in association with epidote, antipolite, and chlorite justifies the wide development of erosion and transport of the weakly metamorphic volcanogenic rocks. Outcrops of such rocks are known from the western coasts of the Okhotsk Sea. From the morphostructural point of view, they correspond to the Okhotsk-Chukotka Mesozoic volcanogenic belt.

#### Mineralogy of volcanic ashes

In particular, the analysis of the volcanoclastic sediment components allows to identify specific ash layers, which can be used for a lithostratigraphic correlation of the investigated cores. The absolute dating of these volcanic ashes will further allow to correlate them with known volcanic eruptions in the Kurile-Kamchatka region.

The volcanic ashes are the most reliable time markers in the studied cores of the Okhotsk Sea. Two of the most distinctly manifested and well diagnosed ashes can be found. The first is located beneath the Holocene diatomaceous horizon. Its characteristics are: color - grey; structure - silt, prevailing size fraction - 0.05-0.1mm (in comparison, the >0.1 mm fraction is rare). In the interlayer composition, the volcanic uncolored glass of fluidal-fibrous, rarely bubble-clastical sharp prevails. As an admixture, the crystal-clastics present plagioclase, heavy minerals and clastic rocks. Among the heavy minerals, hypersthene (Opx) and augite (Cpx) prevail. Their quantitative relation varies in the different cores (Cpx/Opx=0.54-1.11) (Table 3A). An important diagnostic feature of the ash is the dominance of hypersthene. Dark ore minerals are mainly represented by magnetite. The majority of mineral grains is covered by volcanic glass. For the orthopyroxenes, the isomorphic, long-axis prismatic crystals with weak pleochroism are typical.

The ashes with the above mentioned properties were found in Cores LV27-8-4 (153-155 cm), LV27-15-4 (110-112 cm), LV27-7-3 (51 cm) and presumably, also in Core LV27-5-4 (221 cm). Since the material was not representative (1.5-2 mm lenses), the ash from the last station was conventionally related to this type, although according to the morphology of the glass fractions (the fluidal-fibrous grains prevail) it is similar to them.

The second volcanic ash is located in the gray terrigenous sedimentary unit between stratigraphical horizons III and IV and was investigated in Core LV27-8-4 at 332-334 cm. It has reddish tinge and has a more rough-grained structure in comparison to the first ash (it contains significant amounts of the >0.1 mm fraction). The volcanic ash is represented by the fractions of bubble-cellic transparent (non-colored) glass (fluidal-fibrous fractions are rare). For this ash, clinopyroxene prevails ( $Cpx/Opx=1.74$ ). It is also characterized by a very high content of magnetite (up to 33.5%) quantitatively comparable with clinopyroxene (Table 3A, Appendix IV). The majority of heavy minerals are in the volcanic glass cover. Orthopyroxenes are characterized by short-prismatic idiomorphic crystals. Their combinations with slightly smoothed and melted surfaces are also covered by glass. Volcanic ashes with similar properties were discovered on stations LV27-8-3, LV27-7-3, and LV27-15-3, but their mineral composition has been not studied so far.

#### 5.2.4 Morphometric analysis of terrigenous quartz

(A. Astakhov)

The morphometric analyses of terrigenous sand-sized quartz was carried out to determine the sources and mechanisms of coarse material being transported across the continental slope to the central parts of the Okhotsk Sea. The applied analytical method allows to differentiate between eolian material and material transported by water (Astakhov & Vashchenkova, 1993; Astakhov, 1995).

Among water transported debris, material accumulated in rivers deltas and submarine deltas can be differentiated. Taking into account that the sand-sized material is mainly transported by ice floating into the central Okhotsk Sea, the determination of its sources may provide information about the ice drift direction. Temporal changes within this process may justify changes in paleoceanographic conditions. The reason for applying this method in the Okhotsk Sea is the restricted occurrence of nearshore eolian sediments. They only appear at the North Sakhalin coasts, but are widely spread and have morphometric characteristics typical for eolian sediments (Astakhov & Vashchenkova, 1993).

The investigated 0.25-0.315 mm fraction was separated by sieves and analysed under the microscope equipped with a mirror device (Willets & Rice, 1983). The lengths of three quartz grain axes were measured. Subsequently, the nondimensional morphometrical coefficients were calculated. The data interpretation was made on the base of the modified Cailleux sphericity coefficient (Cailleux, 1952) -  $2c/(a+b)$ , and rollness coefficient -  $c/b$  (Astakhov & Vashchenkova, 1993) ( $a$ ,  $b$ ,  $c$ , - correspondingly long, medium and short grain axes). The roundness estimation was made by comparison with the standard scale (Khabakov, 1946). In each sample, 30 grains were measured.

The most interesting results were obtained in Core LV27-2-4. The drastic change of morphometric characteristics was observed at 160-200 cm core depth. According to the lithostratigraphy, this change took place 4000-7000 years ago. Significant paleogeographical events during this period are unknown. According to the main sediment characteristics, this event occurred after the global climate and sea-level changes 15-8 ky ago. From the morphometrical point of view, the analysed material from the lower horizon samples (see diagram  $c/b - 2c/(a+b)$  on Fig. 5.11) correspond to eolian sediments. The upper horizon, in contrast, is characterized by water transport and even delta sedimentation. Three samples are very similar to the Amur estuarine environment. The samples from the lower horizon resemble eolian sediments from the North Sakhalin coasts (Astakhov & Vashchenkova, 1993).

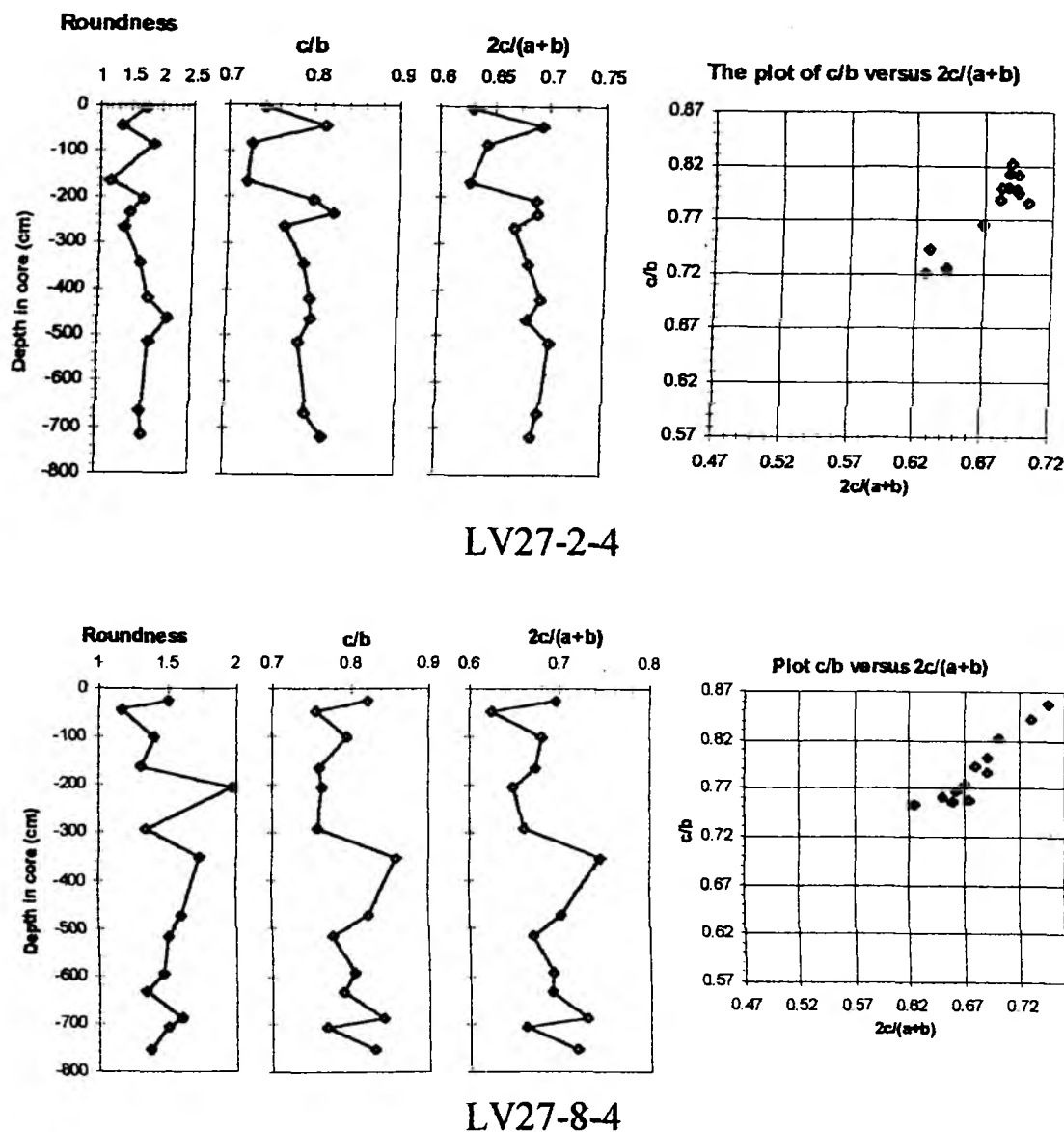


Fig. 5.11: Average roundness and morphological coefficients of quartz grains of 0.25-0.315 mm fraction from sediments of LV27-2-4 and LV27-8-4 cores.

In the sediments from the lower horizon, 10-20% of the quartz grains have a dim small-mesh surface typical for eolian sediments. It is, therefore, supposed that during the formation of the lower horizon (mainly in periods of low sea-level) the floating ice transported the sand material from the adjacent Sakhalin coasts. The possibility of eolian transported dune sands onto the ice surface and the quantification of this process were done by Kononova (1986). During the formation of the upper horizon (that took place when the sea-level was similar to the recent one) significant portions of sand-sized material were transported by the Amur Liman and Sakhalin Bay ice (see Kononov et al., 1975).

We propose that the Holocene change in direction of ice rafting occurred because the aquatories near the East Sakhalin coast were ice-free before the summer monsoon

winds had established. In such case, the NW-directed winter monsoons (November-April) transported the dirty coastal ice from the Sakhalin Bay and Amur Liman towards the south and south-east, and thus, into the region of Core LV27-2 station.

In case of the cleaning from sea ice was delayed and lasted until the summer monsoon period (June-September), as it is supposed for the lower horizon, the coastal ice from the North-East Sakhalin shelf would be transported to the north and north-east.

In Core LV27-8-4, distinct horizons can be differentiated with enhanced values of  $c/b$ ,  $2c/(a+b)$  and roundness, but they are not connected with lithostratigraphic horizons and apparently do not correspond to changes in climatic and paleogeographic conditions. The downcore variations of morphometrical characteristics are rather small. Fig. 5.11 shows that material typical for beach and shelf environments prevail.

A few samples show high values of  $c/b$  and  $2c/(a+b)$ , which is typical for eolian sands, but they exhibit an unusual low roundness. Probably, in this case the high values of morphometric coefficients depend on the existence of pseudorounded grains (e.g. melted crystals of volcanic origin). The interpretation of quartz peculiarities in this core and apparently in other cores from the SW part of the Okhotsk Sea deep-water basin require to conduct additional investigations of the coastal sedimentation of Kamchatka and Kuriles.

5.2.5 Mechanical properties of the sediments  
(A. Astakhov and S. Gorbarenko)

Humidity measurements are shown in Table 5A (Appendix IV), and in Fig. 5.12 and 5.13. The measurements with the MWM-meter correlate well with the weight humidity. Minor differences may be caused due to the following reason: the standard method deals with 50 cm<sup>3</sup> of sediment, whereas MWM-meter measurements are performed applying a sensor square of 10 mm in diameter at the depth of 3-5 mm. Besides, the results of MWM-meter measurements are influenced by air and gas inclusions within the sediment.

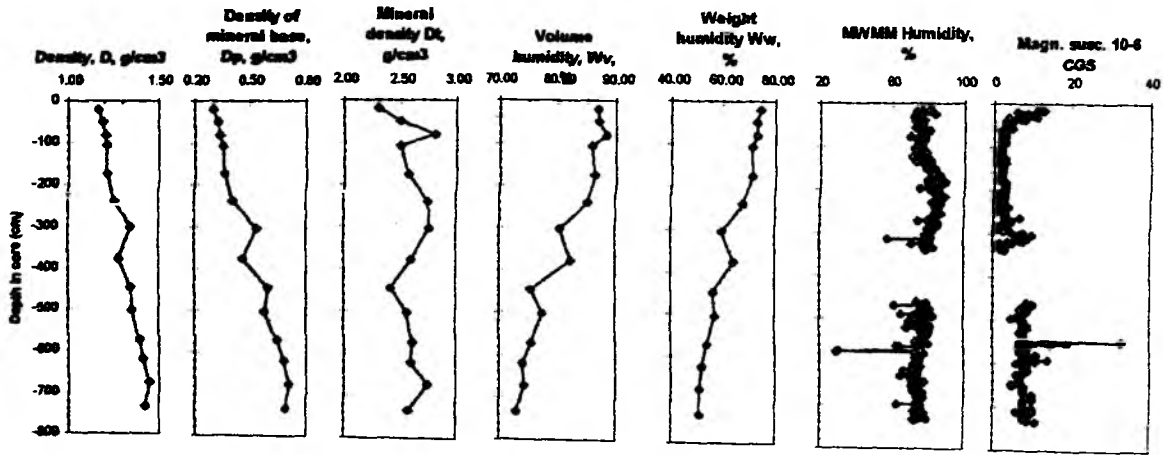


Fig. 5.12: The mechanical properties and magnetic susceptibility of sediment core LV27-2-4.

Obtained density and humidity data for the Holocene layer correlate well with former physical property measurements (Astakhov, 1991). Within all sediment cores recovered,

Holocene diatom oozes exhibit a humidity of more than 80% and a density of the mineral base from 0.2 to 0.5 g/cm<sup>3</sup>. Downcore variations of these parameters in the first line depend on the amount of detrital minerals included within the sediment. In general, the humidity variations are closely connected to the grain size distribution.

In addition, the mechanical properties are also determined by the ratio of siliceous and clayey components versus detrital components. Taking into account that in the central Okhotsk Sea detrital minerals (sand and silt fraction) are transported by floating ice, the variations of their physical properties partly reflect changes of climate conditions.

Apart from the easily identifiable ash layers (Fig. 5.13), layers with sand, pebbles and gravel (low humidity and high density), and clayey horizons (high humidity) can be determined on the basis of their mechanical properties. The increase of density and decrease of humidity through time appears to be rather small. For the Holocene siliceous sediments and for the lithostratigraphic unit IV, density changed from 0.22-0.26 g/cm<sup>3</sup> to 0.33 g/cm<sup>3</sup>, and volume humidity from 89.9 - 92.2 g/cm<sup>3</sup> to 87.9 g/cm<sup>3</sup>.

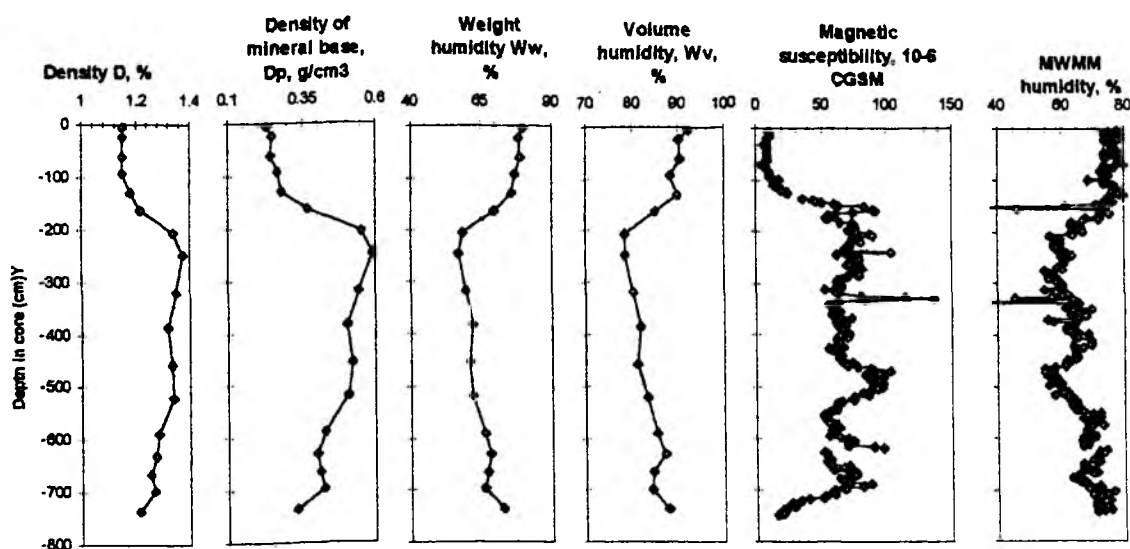


Fig. 5.13: The mechanical properties and magnetic susceptibility of sediment core LV27-8-4.

The most significant increase of density was noted for the siliceous sediments from dredge station LV27-16. The supposedly early-middle Pleistocene (QI-II) diatomite (sample 1) has a density of 1.38 g/cm<sup>3</sup> and a humidity 69.5%. The diatomite of supposedly Pliocene age (sample 2) already has a density of 1.43 g/cm<sup>3</sup> and a humidity of 47.8%. At the same time, only those sediments have physical properties, which come close to the studied Late Pleistocene terrigenous sediment properties. In the vicinity of the dredge station LV27-16, the average density of terrigenous sediments is 1.42 g/cm<sup>3</sup> and its humidity is 52.9%.

The variation of physical properties as a result of postsedimentation and early diagenetic changes seems to be more significant. Sediment carbonate cementation can be definitely determined on the base of MWM-humidity data at 560-580 cm core depth in

Core LV27-2-4 (Fig. 5.12). In the central Okhotsk Sea, the increase of sediment density is frequently caused by sediment cementation due to authigenic clay minerals.

### 5.2.6 Magnetic susceptibility

(J. Grützner)

All magnetic susceptibility (method 1 in SI-units, method 2 in cgs-units) and humidity records (in %) obtained during the cruise are shown in the appendix. Magnetic susceptibility measurements were compared with lithologic information from core descriptions and smear slides. Thus, we were able to correlate strong maxima in magnetic susceptibilities either with large dropstones (e.g. Core 4) or layers of volcanic ash (e.g. Cores 8, 9, 10). These layers are also characterized by low humidity values. Hence, magnetic susceptibility and humidity appear to be anticorrelated.

Calcareous and siliceous biogenic sediments are diamagnetic and, therefore, have commonly low magnetic susceptibilities. Hence, layers of diatomaceous ooze often found in the Okhotsk Sea sediment record and associated with warm climate periods are characterized by susceptibility minima ( $< 40 \times 10^{-5}$  SI) (e.g. Cores 7, 8). Humidity values indicate a higher water content in these layers. A more detailed comparison of lithology and magnetic susceptibility is given in the summary chapters of this report.

Absolute values of magnetic susceptibility show strong regional variations (Fig. 5.14). For comparison of the susceptibility records, we calculated mean values for glacial sediments below the Holocene layer of diatomaceous ooze (maxima associated with ash layers were excluded).

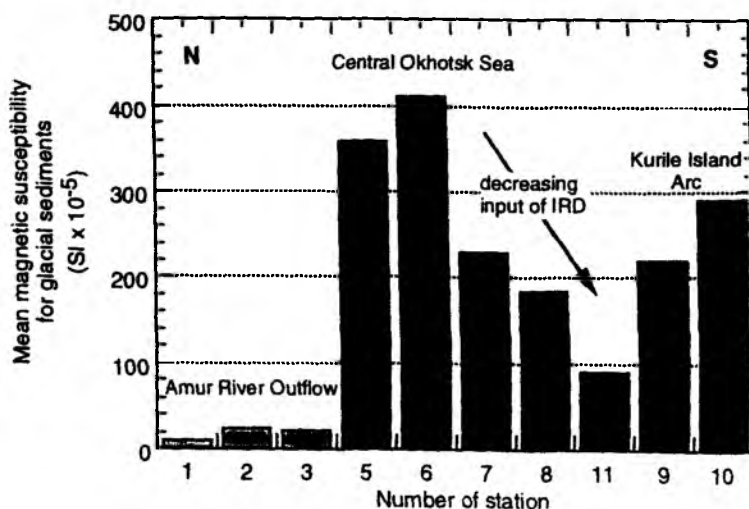


Fig. 5.14: Average values of magnetic susceptibility for glacial sediments from different regions of the Okhotsk Sea.

The sites in the northwestern part of the investigated area (stations 1-3) closest to the Amur river delta are characterized by relatively low magnetic susceptibilities (mean:  $20 \times 10^{-5}$  SI). In the north-south transect of Sites 5 - 11, susceptibilities for glacial sediments show highest average values in the central part of the Okhotsk Sea ( $360-410 \times 10^{-5}$  SI at stations 5 and 6) while susceptibilities decrease towards the south ( $230-90 \times 10^{-5}$  SI at stations 7, 8, 11). For core locations 9 and 10, intermediate magnetic susceptibilities of  $220$  and  $290 \times 10^{-5}$  SI are observed for glacial sediments.

The described pattern is most probably caused by grain size differences in the supply of terrigenous material, which carries magnetic minerals. While terrigenous sedimentation in the Amur river outflow area is dominated by fine grained terrigenous clays, the central and southern Okhotsk Sea is more affected by the input of ice rafted detritus (IRD), which obviously decreased from north to south. We suggest that higher susceptibility values in the vicinity of the Kurile Island Arc are caused by the volcanic ashes rather than by higher amounts of ice-rafted material.

### 5.2.7 Radiolarians in Okhotsk Sea sediments

(A. Matul)

#### Surface sediments

The absolute radiolarian content is relatively low and is approximately similar in all the samples: 1,600-2,800 (in MUC-4 to 8) specimens per 1 g of dry sediment independent of the water depths. The species composition of the radiolarian assemblages does not fluctuate significantly within the analysed samples. Each assemblage contains 24-29 radiolarian forms. 52 radiolarian forms were defined in total (Table 6A, Appendix IV). 19 radiolarian forms occurred in all the samples. The dominant species are *A. micropora*, *A. dubius*, *C. davisiana*, *Ps. gracilipes*, *Pt. hirundo*, *R. boreale*, *S. tabulatus*, *S. glacialis*, *S. pyriformis*, *S. venustum*, *Th. borealis*.

Except for *C. davisiana*, their common percentages vary from 42% to 57%. Therefore, in addition to *C. davisiana*, these species presumably provide the most important portion of the radiolarian assemblages of the Okhotsk Sea.

The relative concentrations of the above listed species do not change considerably across the investigated area. However, a substantial difference between the assemblages of MUC-1 to 3 and the remaining assemblages has to be noted. In the assemblages of MUC-1 to 3, the concentrations of *C. davisiana* increase slightly, whereas the content of *S. tabulatus*, *S. glacialis*, and *S. venustum* drops. The assemblage of MUC-4 to 11 contains rare specimens of *A. aquilonaris*, *E. delicatulum*, *S. pylomaticus borealis*, *S. osculosus*, *S. validispina*, and *Tholospira* sp., which are typical for recent sediments in the North Pacific. In the samples MUC-6, MUC-8, and MUC-11, *L. arachnea* and *S. pyriformis*, typical species for the boreal Pacific, reach their highest concentrations. In the assemblage of MUC-7, *E. acuminatum* was found, which is widely distributed in sediments from the southern parts of the boreal oceanic provinces.

In conclusion, the following radiolarian assemblages could be distinguished in the studied surface sediments :

1. Assemblages MUC-1 to MUC-3 exhibit a relative increase of *C. davisiana* concentrations, whereas typical Pacific species are absent;
2. Assemblages MUC-4 to MUC-11 are characterized by the presence of species typical for the boreal Pacific;
- 2a. Assemblages MUC-7 to MUC-11 show a relative increase of the concentration of Pacific species.

It may, thus, be concluded that the Pacific water masses have a distinct influence on the radiolarian assemblages of the Okhotsk Sea south of 52-53°N.

Two specimens of *A. setosa* were surprisingly found in sample MUC-11. According to Kruglikova (1989 a), this species disappeared in the North Pacific ca. 80,000 years ago. Since the author is familiar with *A. setosa* specimens from many samples from the southern Norwegian Sea, the Labrador Sea, and from Late Pleistocene North Atlantic sediments, the *A. setosa* specimens from sample MUC-11 were accurately identified and fit well to the regular species definition. Since it is questionable that these species are

modern specimens, it is suggested that they are reworked from Pleistocene sediments of the Academy of Sciences Rise.

#### Downcore radiolarian study of Core LV27-8

The radiolarian distribution was analysed in 18 sediment samples from 120 cm core depth to the base (Table 7A, Appendix IV). In all samples, the radiolarian fauna is abundant and highly diverse. The absolute radiolarian content varies between 2,400-3,100 to 5,500-6,900 specimens per 1 g of sediment, and reaches its maximum in the upper and lower diatomaceous ooze units (13,900 and 18,000-32,000, respectively). The number of radiolarian species is not less than 18-25 in each slice showing a significant increase of up to 40 species in the lower diatomaceous ooze unit.

The list of the abundant species (relative concentration more than 1-2%) is almost similar for all the samples (Table 8A, Appendix IV), and does not differ from the modern situation in the central Okhotsk Sea. However, species concentrations vary downcore substantially. Further, radiolarians, which are rare or absent in the present day Okhotsk Sea, occur. *Cr. borealis* is not abundant in modern sediments, but exhibits great concentrations (up to 16.6%) in the 200-690 cm interval. *L. grande*, at present inhabiting the tropical and southern temperate North Pacific areas (Kruglikova, 1989 b), appears only below 480 cm and reaches 38.5%. *A. setosa*, an endemic species of the Arctic and northern North Atlantic (Kruglikova, 1988) and presumably typical for the surface arctic and subarctic waters, was noted at 200-400 cm and 530-743.5 cm depth. The author (Matul, 1994) found high *A. setosa* concentrations (up to 36.6%) in the Younger Dryas sediments of the North Atlantic.

In conclusion, the following radiolarian assemblages were distinguished in Core LV27-8:

1. The assemblage occurring at the 120-182 cm interval is similar to the modern radiolarian assemblages of MUC-1 to MUC 3, with enhanced *C. davisiana* concentrations and only minor influence of the Pacific radiolarian fauna. Probably, this assemblage belongs to the early Holocene (oxygen isotope stage 1).
2. The assemblage occurring at the 200-371 cm interval is defined by an obvious decrease in concentration of *C. davisiana* (21.5-30%), the appearance of *A. setosa* and the significant increase of *Cr. borealis*, which is a typical species for the modern arctic-boreal Pacific. Probably, this assemblage is typical for the Last Glacial (oxygen isotope stage 2). For cores from the south-western Okhotsk Sea, Morley et al. (1991) defined the Last Glacial by a sharp content's decrease and even the absence of radiolarian. At the same time, *C. davisiana* concentrations decrease to a few percents. For core LV27-8, the situation is different: the radiolarian content stays higher than the modern one, and *C. davisiana* is the dominant species. We, therefore, suppose strong lateral differences across the Okhotsk Sea during the Last Glacial.
3. The assemblage occurring at the 400-691 cm interval shows concentrations of the main dominant species (except *C. davisiana*), which are similar to the modern ones. However, the *C. davisiana* content decreases (up to 7.5-16.6%); in slices *C. davisiana* mostly is presented by specimens of oceanic (non marine) style. Below 480 cm, *L. grande* appears, which possibly is a tracer for relatively warm waters. We assume that assemblage 3, in contrast to assemblage 2, is significantly influenced by relatively warm Pacific water.
4. The assemblage occurring at the 710-743.5 cm interval shows increasing *A. setosa* concentrations (up to 46.5%). The *C. davisiana* concentration is relatively high (17.5-42.2%). This assemblage is characterized by many radiolarian forms typical for the modern boreal and southern boreal Pacific (e.g. *A. aquilonaris*, *A. botryocyrtilum*, *A. annulatus*, *A. joergensenii*, *C. laguncula*, *E. acuminatum*, etc., as



well as colonial *Spumellaria* *A. lappacea*?, *Acrosphaera* sp., *Collosphaera* sp.). Probably, a strong contrast existed between the cold surface waters (*A. setosa*, modern Arctic endemic) and warm subsurface and intermediate inflowing Pacific waters.

In conclusion, assemblages 3 and 4 correspond to the last large interstadial (oxygen isotope stage 3), whereas assemblage 4 may indicate its warmest period (stage 3.3).

#### 5.2.8 Sedimentation at the northeastern slope of Sakhalin

(Chr. Vogt, J. Grützner, S. Gorbarenko, A. Astakhov, and D. Nürnberg)

##### Sedimentology

Despite the near continent, the surface and near surface sediments contain high amounts of biogenics, in particular diatoms, mollusc and gastropod shells and carbonaceous shell fragments (Fig. 5.15, for legend see Appendix V). The thickness of the soft dark brown oxidation layer increases with water depth. A 1-2 cm fluff layer was observed at all multicorer stations. The diatomaceous ooze and the predominantly biogeneous horizons are characterized by very low magnetic susceptibility values (Fig 5.15: layer A and B).

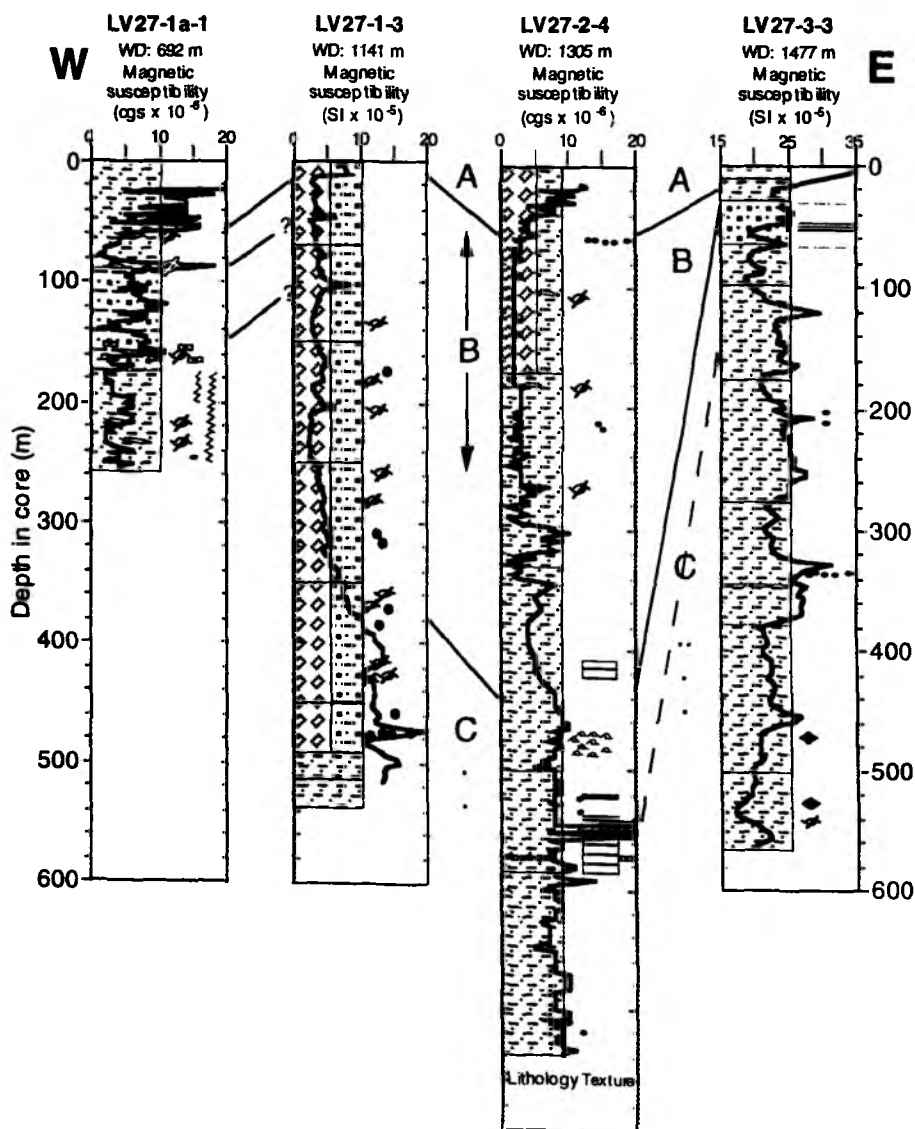
Below the biogenic horizons, transitional sediments with increasing amounts of terrigenous material appear which leads to slightly enhanced magnetic susceptibilities. The deposits contain higher amounts of carbonaceous shell fragments and some randomly distributed pebbles. In several cores, a moderate coarsening of the sediment is obvious (Fig. 5.15: layer B). Down to this core section, olive colors predominate. Further below, gray colors dominate. In core LV27-2-4 significant changes of color and biogenic and mineralogical contents and composition occur at 1.7-1.8 m within layer B (see 5.2.4).

With increasing core depth, hydrogen sulfid odor is typical. Black streaks become abundant, and authigenic pyrite is reported from core LV27-2-4 below 4.2 m. Thus, color, sediment composition and gas formation delineate the prevailing reducing conditions within the sediment. The redox-conditions may have favored early diagenetic alteration of the major magnetic minerals (Fe-oxides) leading to the extremely low magnetic susceptibility values below approx. 50 cm core depth (Fig. 5.15: LV27-1a-1, LV27-2-4). Hence, the drastic increase of the magnetic susceptibility at the core tops may indicate the change between fully reducing and oxygenating sedimentary conditions (Fig. 5.15: layer A).

An increase in the magnetic susceptibility record reflects the change to more terrigenous sediments including increasing amounts of pebbles. Below this increase with its threefold maxima the magnetic susceptibility sticks to the higher level down to ca. 7 m core depth (Fig. 5.15: layer C). The threefold maxima are observed in all slope cores and can be used for correlation (Fig. 5.15, for legend see Appendix V).

Layer B has its base at 4 to 6 m on the upper slope (LV27-1-3, LV27-2-4) and wedges out downslope showing its base at about 0.6 m on the lower slope (LV27-3-3). Hence, decreasing sedimentation rates downslope can be assumed. Below layer B, in layer C at least three maxima of magnetic susceptibility values can be correlated between cores LV27-2-4 and LV27-3-3 (Fig. 5.15, for legend see Appendix V). The most prominent peak is related to a coarsening in lithology in cores LV27-2-4 and LV27-3-3 (gravel layer). In core LV27-2-4 calcareous concretions were observed. The evenly spaced susceptibility peaks in core LV27-3-3 may reflect some kind of cyclicity, though the lithology does not change drastically. It should be noted that at 476-523 cm core depth, large crystals of ikaite (up to 9 cm in length) were found. The calcium carbonate

hexahydrate crystals are assumed to form at cold temperatures in sediments with suboxic to anoxic conditions (Schubert et. al., in press).



**Fig. 5.15:** Tentative correlation of eastern Sakhalin slope cores (54°30' N) based on magnetic susceptibility, physical property and lithology records.

According to sediment density, humidity and water content data the upper part of the "Transitional Zone" is at about 4 m in core LV27-2-4 (Fig. 5.12). In core LV27-1-3 a similar change in the humidity record occurs at 4-4.5 m. Hence, both can be correlated (Fig. 5.15, for legend see Appendix V). The physical property data and the magnetic susceptibility record of the upper part of the "Transitional Zone" correlate well with the records in the cores LV27-4-4 (1-2 m core depth) and LV27-6-3 (0-0.9 m core depth).

### Depositional environment

The diatomaceous oozes of the Okhotsk Sea are of Holocene age. Despite the near continent, the sediments of the northeastern slope of Sakhalin exhibit up to 4 m of diatomaceous ooze or weak diatomaceous sediment (Fig. 5.15). This points to an extraordinarily high bioproductivity during the Holocene. The extreme bioproductivity is presumably driven by the distinctive Okhotsk Sea oceanography. The seasonally changing surface layer is underlain by a cold layer of 100 to 150 m thickness sustained by the production of winter sea-ice, which induces winter convection of the upper water masses (Yang & Honjo, 1996). This "Okhotsk Diocothermal Layer" most effectively prevents vertical exchange of water masses during summer. Thus, nutrient enriched in the surface waters can completely be used up and therefore, contribute to the very high surface water productivity (Tally & Nagata, 1995). The core transect northeast off Sakhalin locates in the eastern part of the Okhotsk Gyre, which counterclockwise moves from the inflow of Pacific waters near Kamchatka across the northern shelf regions to the eastern coast of Sakhalin. It is still not well known how the surface waters of the Okhotsk Sea sustain their high nutrient content (Yang & Honjo, 1996). Admixtures of continental runoff probably provide a lot to the nutrient budget. Near the Amur outflow area, therefore, the surface waters might be strongly enriched in nutrients, causing the extreme accumulation of diatomaceous sediments.

The Holocene age of the diatomaceous ooze would result in sedimentation rates of more than 40 cm/1000 years. The increased content of terrigenous sediment components in layer C, thus, points to a reduction in surface water productivity during the last glacial and the deglacial Termination I. The higher input of terrigenous material may also be due to an increased input of ice-rafted debris. The horizon of ice-rafted material in LV27-3-3 correlates with the thin laminated layer in LV27-2-4 (Fig. 5.15). The laminated area is interpreted as distal turbidity currents.

The stratigraphical framework outlined above states the occurrence of a volcanic ash layer in between the "Transitional Sediments" (Unit II). None of the cores along the transect northeast off Sakhalin exhibits such an ash layer. Most probably, the ash, which presumably originated from the Kurile Islands and was transported northward by wind, did not reach the northern Okhotsk Sea. The decreasing thickness of ash layer K1 from south to north as observed in the central Okhotsk Sea cores, supports this hypothesis.

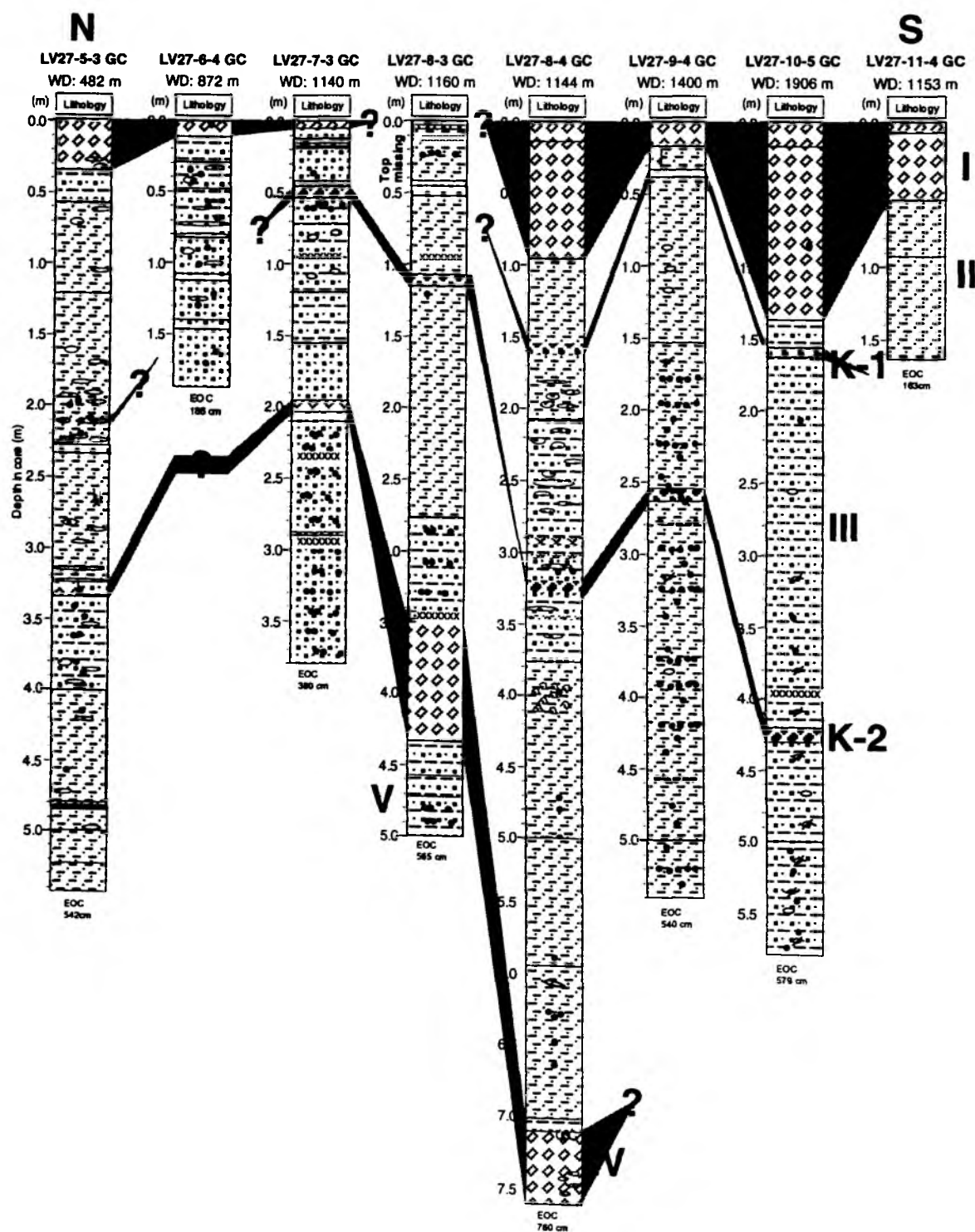
### *5.2.9 Marine geology of the central Okhotsk Sea*

(D. Nürnberg and S. Gorbarenko)

#### Sedimentology

The surface deposits from the central Okhotsk Sea commonly consist of a soft, brown diatomaceous ooze, which is mostly overlain by a ca. 1 cm thick brownish fluff layer. Grain sizes vary accordingly from silty sand to clayey silt depending on the water depth. Approximately 3-4 cm below the surface, the brownish color changes to olive gray typical for the diatomaceous oozes. Calcareous foraminifera and coccoliths are abundant. Due to the dominating biogenic components, the magnetic susceptibility values are extremely low. According to our lithostratigraphical classification, we call the diatomaceous ooze Unit I (Fig. 5.16, for legend see Appendix V).

The diatomaceous ooze is underlain by a "transitional" sediment (Unit II), which is only weakly diatomaceous, but is dominated by terrigenous components. Accordingly, the magnetic susceptibility values increase slightly. Grain sizes vary between sandy silt and clayey sandy silt. The dark olive gray sediment is homogenous and includes reworked lenses of diatomaceous ooze due to strong bioturbation. Occasionally, small pebbles occur. Foraminifers commonly occur and



**Fig. 5.16:** Lithostratigraphic classification of central Okhotsk Sea cores and core correlation (shading) based on lithology and magnetic susceptibility records.

show distinct variations. Within this unit, two ash layers dated to 8.500 a and 12.000 a, were already described (Gorbarenko et al., in press). Within the sediments recovered during this expedition, we only observed one volcanic ash layer (K-1), the age of which is most probably 8.500 a BP. The magnetic susceptibility record exhibits pronounced maxima.

The transitional lithological unit overlays the typical glacial sediment (Unit III), consisting of dark gray sandy to clayey silt and containing abundant dropstones of largely varying size (few mm to ca. 10 cm). The dominating portion of detrital material causes high magnetic susceptibilities. With increasing depth, black streaks and mottles can be observed pointing to the presence of organic matter. Calcareous shell fragments occur, but are rare. Formation of free hydrogen sulfid inferred from an intensive odor, points to the decay of organic matter by the activity of sulphate reducing bacteria under suboxic conditions. Greenish diagenetic horizons must presumably be related to the formation of authigenic clays.

A second layer of volcanic ash (K-2), dated to approximately 28.000 a BP. (Dr. J. Southon, pers. com.), intercalates the glacial unit of terrigenous sediments, thus, relating the glacial deposits to isotopic stage 2 and the upper part of stage 3. It is again characterized by maxima in the magnetic susceptibility records.

Below the glacial succession, the pronounced decrease in the magnetic susceptibility records refer to a second diatomaceous ooze (Unit IV) showing abundant foraminifers, and a high organic carbon content. According to Gorbarenko (1991), this strongly bioturbated sequence belongs to stage 3.3. It is followed by glacial (rest of oxygen isotope stage 3 and stage 4), terrigenous sediments enriched with pebbles (Unit V). Accordingly, the magnetic susceptibility values increase.

#### Depositional environment

Most sediment cores recovered during the 27th cruise of R/V "Akademik Lavrentyev" delineate along a N-S-profile within the central Okhotsk Sea covering a depth range of approximately 1500 m. Nevertheless, lithostratigraphic units described above could be traced over long distances. Fig. 5.16 exhibits the core correlation based on lithology. This correlation is supported by the according correlation of magnetic susceptibility records (Fig. 5.17).

The lower diatomaceous ooze (Unit IV) was only reached by core LV 27-5-3 at the North Okhotsk Rise, and further south by cores LV 27-8-3 and LV 27-8-4 in the Makarov Trough (Fig. 5.16, for legend see Appendix V). In this respect, despite their relatively short lengths, cores LV 27-5-3 and LV 27-8-3 cover the longest time period, since they also intruded lower stage 3 sediments. We suspect that during stage 3.3 the enhanced marine productivity reflected in diatomaceous oozes was mainly initiated by high nutrient supply due to inflowing Pacific surface water masses (Kamchatka Current) favoring a stable water column with relatively warm surface waters comparable to the recent situation. Largely ice-free conditions during the entire year may additionally have contributed favorable environmental conditions for siliceous plankton growth. The fact that the diatomaceous ooze at the northern site is less evolved compared to the southern ones (Fig. 5.16) may be related to different sediment accumulation rates. It may, however, indicate a reduced plankton productivity due to less favorable conditions in the northern part of the Okhotsk Sea during stage 3.3. Perennial sea ice coverage originating in the cold, shallow and low saline coastal waters in the north and subsequently drifting in a direction approximating the Okhotsk-Kurile current system may drastically reduce plankton growth simply by light reduction.

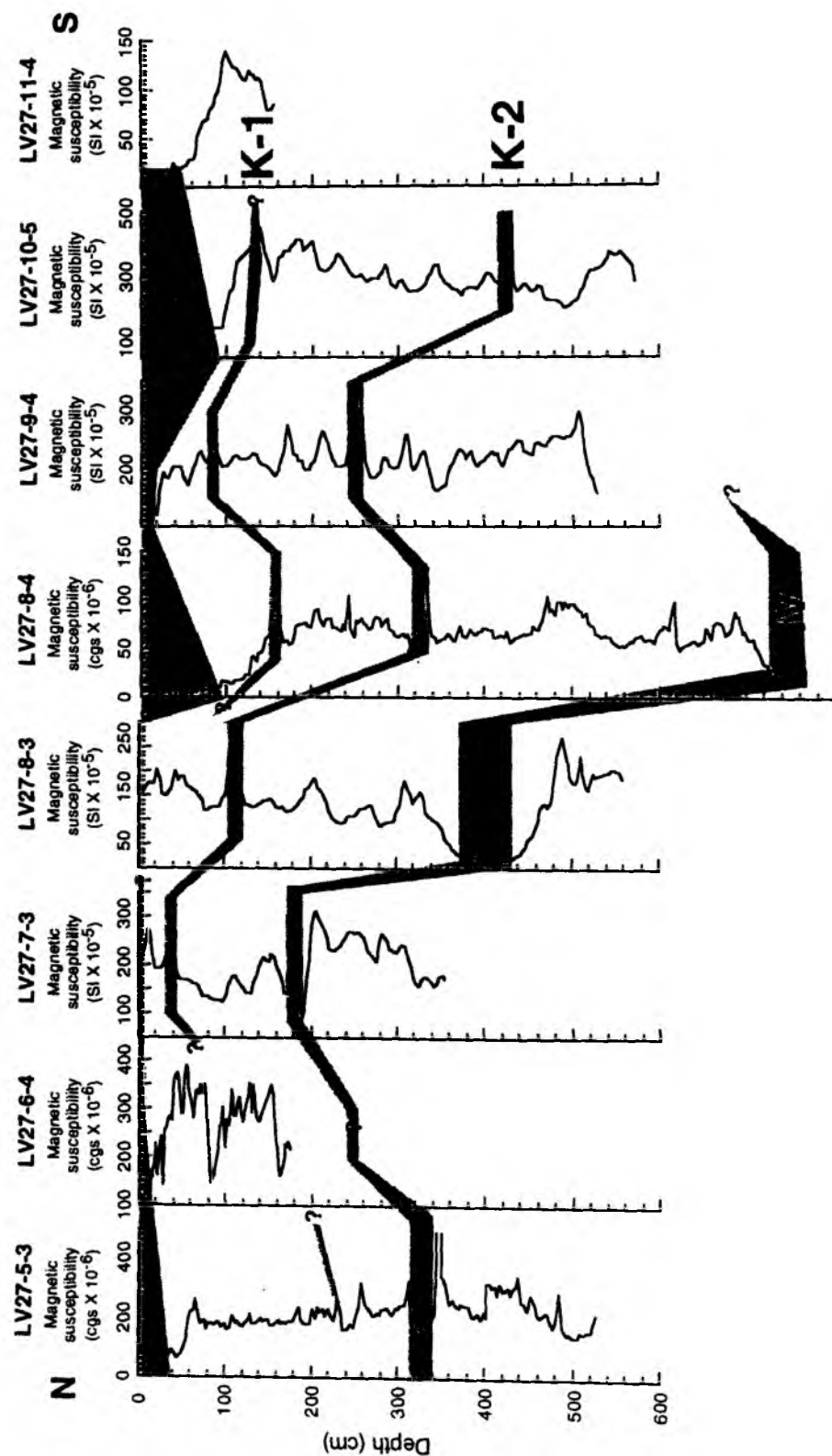


Fig. 5.17: Magnetic susceptibility records of central Okhotsk Sea cores. Core correlation (shading, similar to shading in Fig. 5.16) is based on lithology and magnetic susceptibility records.

Most characteristic for the overlying glacial sediments (Unit III) are the enhanced occurrences of dropstones covering all size fractions (mainly small pebbles of ca. 0.5 cm, but also boulders of up to 10 cm). Since large glacier systems did presumably not exist onshore, sea ice is suggested to be the most important transport agent for the coarse detrital material. Cliff fall and coastal adfreezing, thus, seem to be the most effective entrainment mechanisms. Drifting ice subsequently distributed the pebbles across the entire Okhotsk Sea, releasing its freight during ice-melt in summer. The systematic investigation of ice-rafted detritus within the deep-sea sediments should allow to elucidate both the extension of glacial ice-coverage, and varying transport directions in great detail.

It should be noted in this respect that Arctic Ocean sea ice seldomly includes particles larger than silt-sized. Cliff fall and coastal adfreezing as entrainment mechanisms only play a minor role in comparison to suspension freezing, the dominant entrainment mechanism for fine-grained sea-ice sediments (Nürnberg et al., 1994).

The volcanic ash layer K-2 intercalated within the glacial sequences of most of our cores provides an excellent time-marker and allows to correlate the deep-sea sediments over long distances (Fig. 5.16, for legend see Appendix V). The ash layer is best established in the southern sites (LV 27-10-5, LV 27-9-4, LV 27-8-4, LV 27-8-3), whereas it is not found in the northern site LV 27-6-4. In site LV 27-5-3, only few volcanic particles were found, which may be related to K-2. Such distribution pattern proposes a southern source area for the volcanic ash, e.g. Kurile Islands, and a northerly direction of wind transport becoming less effective in the northernmost parts of our study area.

The transitional, weak diatomaceous sediments (Unit II) overlying the glacial deposits imply a gradual climatic improvement. The influence of sea ice onto deep-sea sedimentation is reduced, since pebbles rarely occur. Diatom concentrations, in contrast, rapidly increase due to improving environmental conditions. The retreating and deteriorating ice cover may reflect the changing surface water current system at that time. In addition, the enhanced light supply and small-scale upwelling at ice edges may have favored plankton growth.

During this climatic improvement, the volcanic ash layer K-1 spread over large areas of the Okhotsk Sea. The volcanic Kurile Islands most probably served as the K-1 source area, since the southernmost sites show a well-evolved ash, whereas the ash is missing in the northernmost sites (LV 27-7-3, LV 27-6-4, and LV 27-5-3).

The transitional, weak diatomaceous sediments gradually change to pure diatomaceous ooze during Holocene times, implying the onset of an extreme siliceous primary productivity. Gorbarenko et al. (1988) mentioned that marine productivity did not simultaneously increase within the entire basin. It is rather suggested that in dependence from increasing surface water temperatures related to the newly establishing surface current system, productivity spread progressively from the southern to the northern parts of the Okhotsk Sea. The preliminary observation that diatomaceous oozes are much thicker at the southern sites compared to the relatively thin oozes at the northernmost sites further suggests that the onset of surface productivity commenced earlier in the southern part contemporaneously with a progressively retreating ice cover from S to N and a stepwise northward intrusion of Pacific surface waters. This assumption, however, needs to be proved by absolute age dating.

### 5.2.10 Gas geochemistry

(A. Obzhirov and B. Baranov)

Gas geochemical analyses were made at 12 stations (see Figs. 1.1 and 5.1). At all of them, the gas component in bottom water samples derived from multicorer tubes was examined. At stations LV27-1, 2, and 4, gas was additionally examined in sediment samples derived from the multicorer. At stations LV27-2, 4, 5, and 8, gas was extracted from sediments obtained by the POI gravity core. At stations LV27-5 and 11, gas was studied in water samples from water depths of 50, 100, 200, and 300 m derived by Niskin bottles. In the sediments and bottom water samples, the pH values were measured. The gas concentrations and pH values measured in water and sediments are listed in Tables 10A and 11A (Appendix IV).

The oxygen and nitrogen concentrations measured in bottom water samples are typical for these depths in the Okhotsk Sea (1.6-2.5 ml/l and 11.9-13.0 ml/l, respectively). In the LV27-7 water sample, the promoted oxygen concentration (3.8 ml/l) and the reduced nitrogen concentration were determined. These conditions may be connected with the mixing up of the bottom and surface waters, which could have occurred during the uplift of the multicorer device. This supposition is verified by a decrease in CO<sub>2</sub> (0.61 ml/l) in this sample. The CO<sub>2</sub> concentrations measured in bottom water (1.40-1.86 ml/l) are rather high, in particular, at site LV27-11 (1.86 ml/l). The same concentrations were obtained in the bottom water from the Paramushir gas seeping (Obzhirov, 1993).

At these stations the most significant difference in bottom water gas composition was observed for the methane distribution. At stations LV27-1 and 2, abnormal methane concentrations were observed (221 and 2000 nl/l, respectively). At other sites, there are background methane concentrations of 20-50 nl/l in the bottom water. At sites LV27-11 and 12, very low methane concentrations were observed (8 nl/l and 12 nl/l, respectively). Such level of concentrations corresponds to the background level of Pacific bottom water and areas where red clays dominate (Obzhirov, 1993).

In water samples taken from the upper horizons (50-300 m) of two stations, the main difference between them exists in their methane distribution. At station LV27-5, it follows the usual distribution law determined earlier (Obzhirov, 1993; see chapter 3), but at station LV27-11 at water depths of 50, 100, and 200 m, the methane concentrations exceed the background level more than 3 times (189 nl/l on 100m).

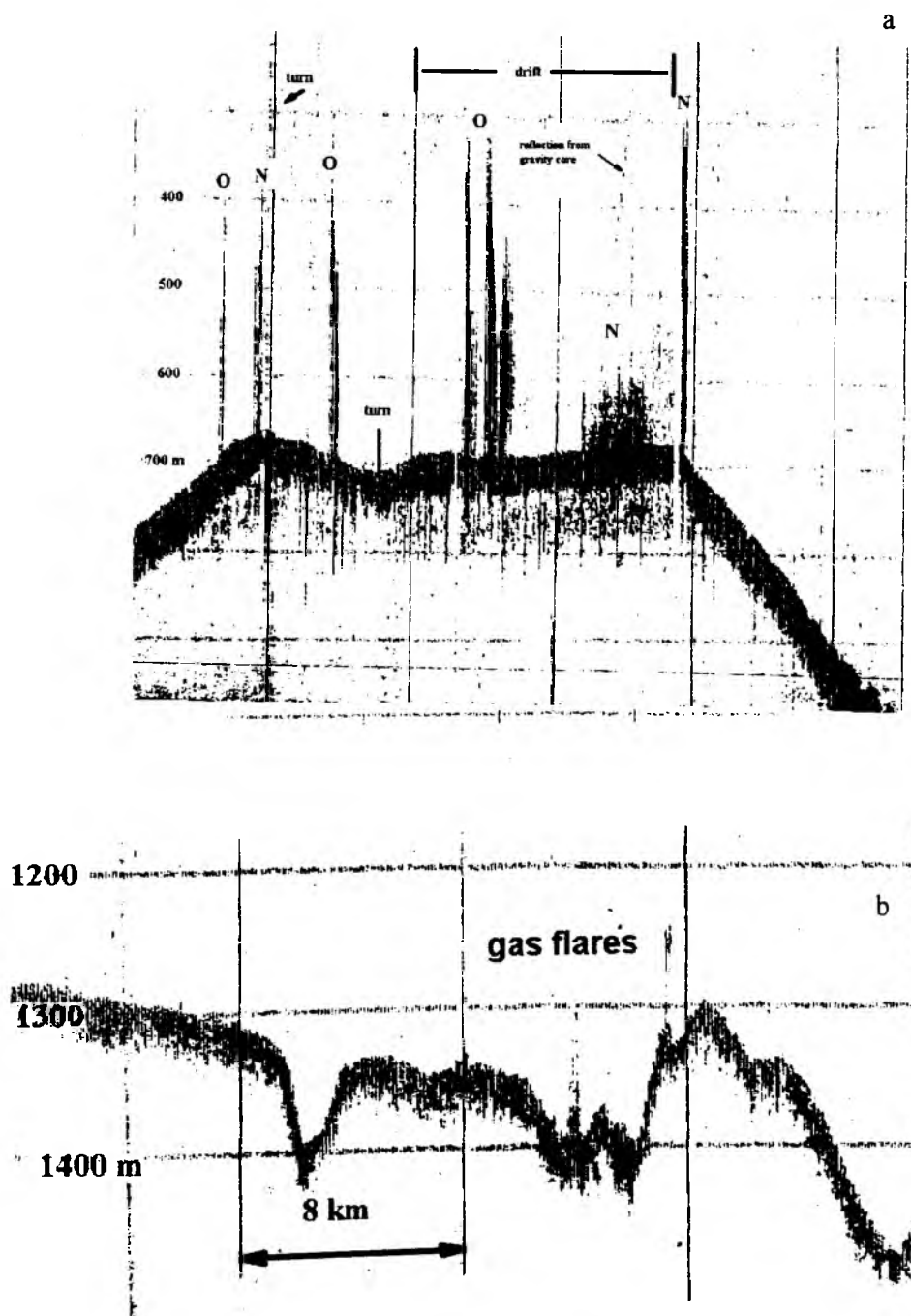
In sediments recovered from stations under investigation, major differences in methane concentrations were observed. The maximum methane volume (10.2 ml/l) was determined at (gas-) station LV27, where on the echosounder record gas plumes were observed. Such plumes were already found in this region earlier (Obzhirov et al., 1989). Here, the sediments contain high concentrations of methane in the entire core, but maximum methane concentrations were determined in its lower part, in the 180-245 cm interval. The low methane concentrations (0.001-0.003 ml/l) were measured in sediments from sites LV27-4, 5, 8, and 10. In sediments from sites LV27-2, 9, and 12, methane concentrations of 0.1-0.3 ml/l were measured. They are 100 times less than the background methane concentrations measured at (gas-) station LV27, but 100 times more than the background methane concentrations typical for the other stations. At site LV27-8 and 10, the methane concentration is increased by two times in comparison to sites LV27-4 and 5.

### Discussion

As it was mentioned above, the most significant amount of methane in bottom sediments was found near the gas plume at station LV27-gas. In this region, methane anomalies of more than 10000 nl/l in the bottom water were already reported (Obzhirov 1993). Also,



gas hydrates were observed in sediments (Ginsburg et al., 1993). At site LV27-gas, gas hydrates were, unfortunately, not observed within the sediments, however, methane concentration anomalies were found exceeding the background level 10.000 times.



**Fig. 5.18:** Echosounder records of the gas plumes offshore northern (a) and southern (b) Sakhalin Island. N shows new gas plumes, O marks old ones. Flare locations are shown on Fig. 5.19 by number 1 and 3, respectively.

The existence of gas plumes and methane anomalies in bottom sediments justify in any case that there must be gas hydrates in the sediments. Such gas plumes usually correspond with the zones of destruction and venting of gas hydrates. This process may begin under the conditions of pressure decrease or temperature increase. Such conditions may be caused by global sea-level changes, volcanic processes, recent tectonic activity, and others.

Site LV27-gas is located in the area of the East-Sakhalin fracture zone, the tectonic activity of which seems to have increased recently. The following facts verify this phenomena:

1. the increase of methane concentrations in abnormal and background fields of the bottom water is at least 10 times higher during the period after 1987 compared to the period before 1987;
2. the continuous gas seeping (plumes) recorded by echosounding techniques during the period between 1988 and 1996;
3. the discovery of new sites of gas seeping (plumes) not far from site LV27-gas (Fig. 5.18a).

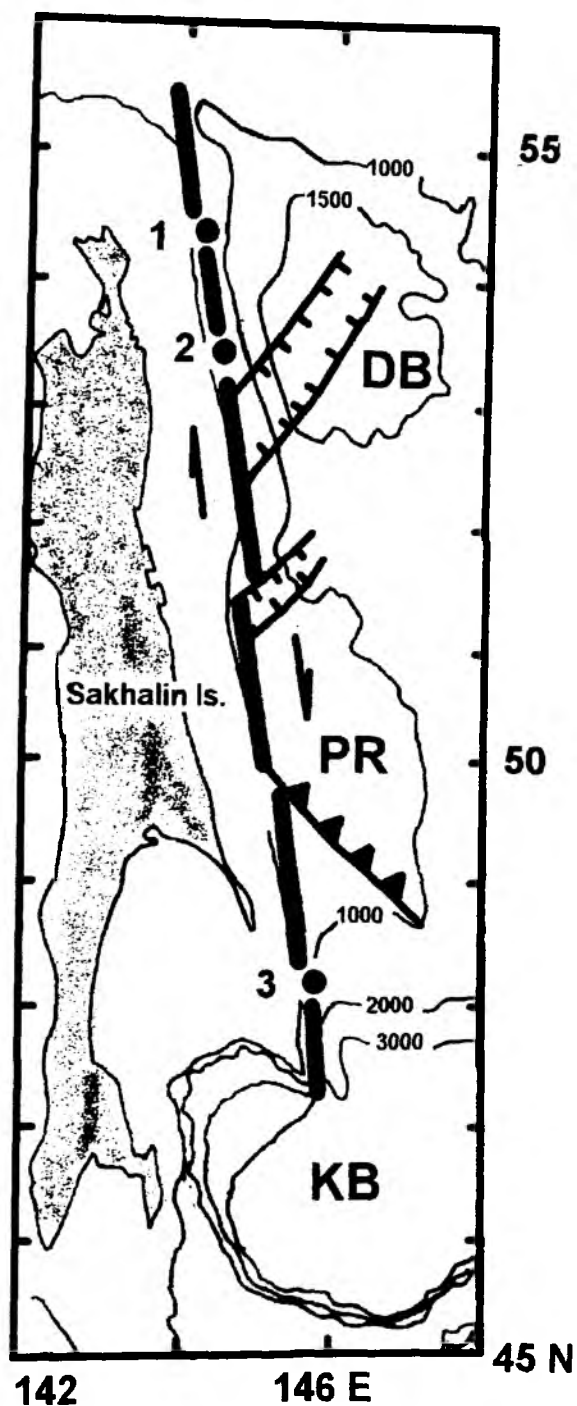
New gas seepings were discovered inside the field, which was earlier defined and studied (Obzhairov, 1993; Ginsburg et al., 1993). According to the location of known gas seepings, it is oriented orthogonal to the Sakhalin continental slope at water depths of 672-865 m. Moreover, during this expedition two gas plumes were found 150 miles southward in water depths of 1320-1400 m (Figs. 5.18 b and 5.19). These plumes are located on small mounds showing heights of about 15-20 m, which may represent mud volcanos.

All known gas fields on the Sakhalin continental slope are obviously connected with the East Sakhalin fault zone (Fig. 5.19). This zone represents the eastern restriction of the Sakhalin shear zone, which can be traced over a distance of more than 2000 km and separates the Amur and Okhotsk plates (Baranov et al., 1996). The East-Sakhalin Fault is a dextral strike-slip structure, as deduced from the existence of extensional feather structures. These structures are located in the Derugin Basin, where they were carefully investigated during the joint German-Russian expedition on RV "Professor Gagarinsky" in 1995 (Baranov et al., *subm.*). The Polevoy Ridge located in the south may correspond to a reverse fault zone.

The area mentioned should be mapped in detail for the determination of the recent tectonic pattern. Such mapping may serve as the base for finding new gas seeping fields and to understand their nature. Nevertheless, it is possible to use the data sampled during this year's expedition to:

1. testimate the volume of methane seeping from the sediments into the water and from the water into the atmosphere;
2. estimate, in a broader sense, the global cycles of natural methane and its influence on global climate change; and/or
3. predict future earthquakes, such as the Neftegorsk earthquake.

The suggestion that methane can penetrate from the water into the atmosphere is supported by the discovery of abnormal methane concentrations in the upper horizons of sea water at site LV27-11. The methane concentrations here exceed the balance with the atmosphere 2-3 times. In the bottom water of this station, however, the lowest methane concentration was 8 nl/l. This discrepancy indicates that the methane does not originate from the bottom sediments. The methane anomaly is rather connected to both the seasonal cycle of microbiotic productivity and the transportation of methane by water masses. If the second assumption is true, the seep providing methane from the bottom sediments must be located at some distance to site LV27-11



**Fig. 5.19:** Location of the gas seeping fields offshore Sakhalin (solid points) and East Sakhalin strike-slip zone (thick line with arrows). Fields 1 and 2 were known before (Obzhairov, 1993; Ginzburg et al., 1993). Field 3 was finding in this cruise. Toothed line indicates reverse fault, line with bars shows normal fault. DB - Derugin Basin, PR - Polevoy Rise, KB - Kurile Basin.

It must be noted that at site LV27-11 high CO<sub>2</sub> concentrations (1.86 ml/l) were found in the bottom water along with very low methane concentrations. This may be due to both the low tectonic activity of the geological structures, and the existence of ancient intrusive complexes, dislocated by faults, along which the gas migrates from the earth's interior to the sea water.

### Conclusions

1. Large amounts of methane were observed in the bottom sediments in areas where gas vents are active.
2. It is suggested that at site LV27-11 the surface water masses have higher methane concentrations than the balance concentrations with air.
3. It is supposed that the region of site LV27-11 is characterized by passive tectonics.
4. The newly discovered gas seeps are located in the vicinity of the East-Sakhalin Fault Zone and may be due to the recent tectonic activity in this area. In this case both gas hydrates and gas and oil deposits may be the sources of methane.

The future detailed investigation of this region would allow to estimate the volume of methane penetrating from the earth's crust into the atmosphere, and its contribution to the global climate change.

### **5.3 Plankton investigations**

(D. Nürnberg and Chr. Vogt)

#### a) Foraminifers

Plankton sampling focussed on studying of calcareous foraminifers, siliceous diatoms, and radiolarians. One basic assumption of paleoceanographic studies using planktic assemblages is that the planktic organisms accurately reflect surface water conditions both now and in the past.

In this respect, stable oxygen isotope analyses within planktic foraminifers are widely accepted to be a powerful paleoceanographic tool for the reconstruction of water mass circulation and surface water temperatures. Nevertheless, there are major uncertainties in understanding the formation of the stable oxygen isotope signal. Recent studies point out that the stable oxygen isotope signal within the water the foraminifers live in is slightly different from the signal preserved in living foraminifers. Further, the isotope signal differs between living and dead foraminifers. The plankton net studies in combination with water sampling represent one further step to understand these vital effects.

In the Okhotsk Sea, the water column is clearly stratified. Below 50 m, temperatures are commonly below 0°C, whereas above, surface temperatures increase to 14°C during summer. Based on temperature and salinity data, Alderman (1996) calculated calcification depths of 40-20 m for the dominating planktic foraminifers *N. pachyderma* sin. and *G. bulloides*. Accordingly, we took plankton nets in different intervals down to 300 m water depth. For comparison of living foraminifers (if possible), dead assemblages down to 300 m water depth, and core-top foraminifers oxygen isotope analyses will be performed at the home laboratories, and will hopefully contribute important insights into vital effects perturbing the stable oxygen isotope signal of surface waters.

#### b) Siliceous plankton

Due to their diversity, excellent fossilization and their known ecology, radiolarians and diatoms are widely used for paleoceanographic reconstructions. Plankton net studies and future deployments of sediment traps will document seasonal changes in the distribution and flux of siliceous plankton assemblages in surface waters of the high

latitude, the seasonally ice-covered NW Pacific. Parallel to the plankton net work, sampling of the water column will provide necessary information on the hydrography and nutrient content. Both plankton net studies and water sampling will further help to interpret the siliceous plankton signal preserved in the sea floor deposits.

During this year's cruise, we started performing vertical net sampling of the uppermost 300 m water column, which gives insight into the depth and diversity distribution of siliceous plankton in dependence from hydrography and nutrient supply. Knowledge about the life habitat of different species is of great value for paleoceanographic interpretations.

In particular, the investigation of the radiolarian species *Cycladophora davisiana*, which is common in Okhotsk Sea surface waters, is of large interest. Except for the Okhotsk Sea, this species occurs in high concentrations only in glacial deposits. These glacial *C. davisiana* peaks can be well correlated over long distances and provide excellent stratigraphic time-markers in high latitudes. However, in paleoceanographic reconstructions, they lead to "non-analog" situations, since conditions for production and sedimentation are not known well enough. Since *C. davisiana* is well known from Okhotsk Sea surface sediments and Holocene sequences, the *in situ* documentation of occurrence and living conditions will provide necessary information for paleoceanographic interpretations.

#### 5.4 Conclusions

During expedition LV27 of RV "Akademik Lavrentyev", in total ca. 100 m of sediment cores were recovered from different morphological structures of the Okhotsk Sea (N - S, E - W profiles). Cores were retrieved from approximately 500 m to 2000 m water depth. Lithological descriptions of sediments, measurements of magnetic susceptibility, humidity, and preliminary mineralogical and micropaleontological analyses were performed aboard the ship, which allowed to determine temporally and spatially changing climatic and environmental conditions.

The investigations reveal drastically changing conditions from the Last Glacial to deglaciation and Holocene times, which are closely related to the paleoceanographical and climatic development in the Okhotsk Sea. During glacial times, a strong influence of ice-rafted debris on the deep-sea sedimentation was observed in the northern and central parts of the sea. Sea ice as the major transport agent for the dropstones apparently covered large areas of the Okhotsk Sea, though the ice cover is not assumed to have behaved as a rigid ice cover during the entire year. During deglaciation times and the beginning Holocene, the influence of sea ice on the depositional environment successively decreases, whereas plankton productivity drastically increases, changing the environment to a "silica-type" basin. Such change was closely related to the establishing surface current system, which was connected to NW-Pacific oceanography. Retrieved cores from the Sakhalin slope show high sedimentation rates. The high resolution records will help to decipher the paleoceanographic and climatic changes in the Okhotsk Sea in great detail.

## 6. Tectonic structure of the northern Kurile Basin slope: Implication to the Okhotsk Sea geodynamics

(B. Baranov, B. Karp, and K. Dozorova)

### Introduction

It is well known that the margins of oceanic basins formed as a result of continental crust breakup conserve the structural pattern, which existed during the initial stage of this process. This is also typical for back-arc basins such as the Kurile Basin. The Kurile Basin is underlain by oceanic crust. However, on its northern and southern flanks, according to the dredging data, Jurassic and Cretaceous granites crop out. It is, therefore, concluded that it initially formed on continental crust.

We, thus, suppose that the structural pattern on the flanks of this structure remained the same as the pattern formed during both the breakup and the initial rift stage. Its tectonic analysis will provide the opportunity to determine the trend and the kinematics of the fault zones and further, to reconstruct the direction of the basin opening. As it has been mentioned previously, these objectives were the main purpose of the geophysical survey during this year's cruise. The results of the bathymetric and seismic surveys were used for the tectonic purposes accordingly. Gravimetry and magnetic survey data will be used after processing in the home labs.

The survey area is located on the northern slope of the Kurile Basin and embraces the eastern part of the Academy of Sciences Rise. Its northern flank faces to the Makarov Trough, its southern slope deepens towards the Kurile Basin (Figs. 3.1 and 6.1). Before the cruise results are described and interpreted, we will briefly inform about the general location and description of these structures.

### General description

The Okhotsk Sea Basin can be divided into three major provinces: the Kurile Basin, the Central Okhotsk Province and the Northern Okhotsk Province, being characterized by different morphologies and hypsometric levels (Figs. 3.1 and 6.1). The first province is represented by the deep-water Kurile Basin, showing water depths of more than 3000 m in the southernmost part. Water depths in the central Okhotsk Sea, which is characterized by the most complex morphology, are limited by the 1000 m contour line. Several bathymetric features are located here: the Institute of Oceanology and Academy of Sciences Rises, the Peter Shmidt and Makarov Troughs, and the Derugin Basin. The third province occupies the northernmost and shallowest part of the Okhotsk Sea.

The Central Okhotsk Province encompasses the central part of the Okhotsk Sea. It has a triangular shape, and the wide part of this triangle looks to the south towards the Kurile Basin. The sea floor of the Central Okhotsk Province is rough. The relief amplitude is approximately 800 m. The Institute of Oceanology and the Academy of Sciences Rises and the Derugin Basin can be defined within this area. The Institute of Oceanology Rise and the Academy of Sciences Rise are located in its central and southern parts, respectively, separated by the Makarov Trough (Figs. 3.1 and 6.1).

The shape of the Academy of Sciences Rise closely resembles a triangle, the northern side of which is oriented in north-westerly direction. The southern side is oriented in north-easterly direction, and the western side shows a N - S strike. Its size reaches almost 200 miles in E - W direction, and is about 100 miles in its central part from the north to the south. The top is represented by a plateau extending in W - E direction. The width of the top is about 50 miles, whereas the E - W - extension is about 150 miles. The minimum water depth is 894 m. The top looms 400-500 m above the Makarov Trough

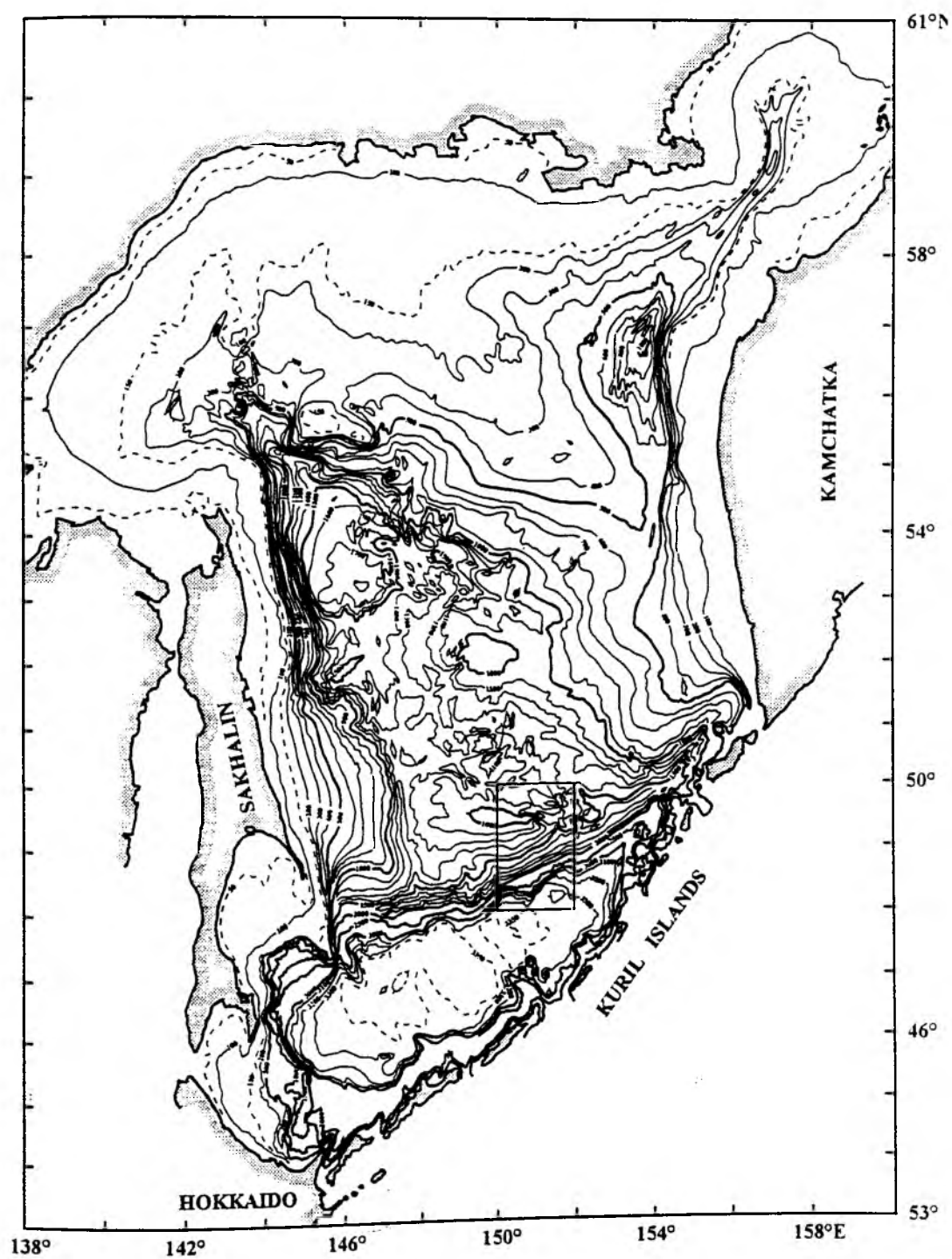


Fig. 6.1: Bathymetry map of the Okhotsk Sea (compiled by A. Svarichevsky). Inserted rectangular shows the area under investigation. Contour interval is 100 m, additional contour is 150 m.

situated to the north, and ca. 2400 m above the Kurile Basin floor. The most remarkable feature of its northern slope and eastern closing is the existence of several scarps. The tectonically induced scarps can distinctly be seen on the contours in Fig. 6.1.

The Kurile Basin contours also have a triangle-like shape. The width of the basin bed is up to 120 miles in the west, but eastwards it wedges out and passes into the narrow Atlasov Trough, which rises to the Kamchatka continental slope. The basin floor represents a smooth abyssal plain, which is weakly inclined to the south-east and slightly raised near the borders.

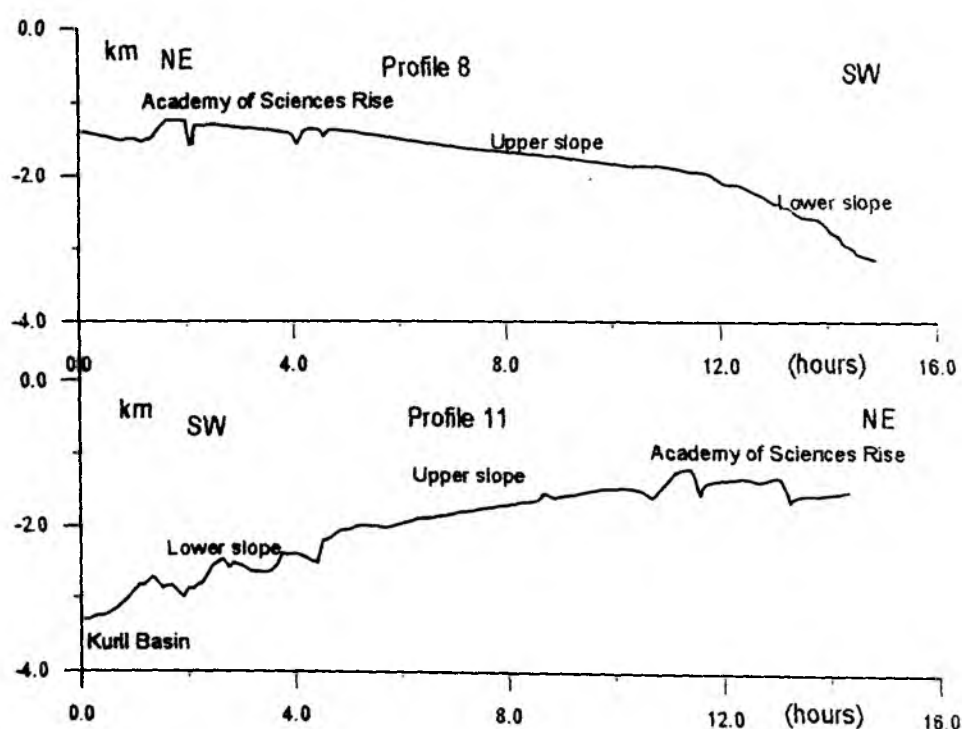


Fig. 6.2: Bathymetry profiles showing main morphology elements of the studied area on northern Kurile Basin slope. Locations of profiles are shown in Fig. 5.2.

The Kurile Basin slopes and their continental rises exhibit a complex morphology and, therefore, the contours of the basin abyssal plain are relatively complicated. Attention is drawn to the fact that the northern slope has a zigzag-shaped character (Fig. 6.1). It consists of a series of rectilinear segments with north-eastern and north-western strikes. It is remarkable that the north-eastern segments are longer, and each of them is shifted in a right-lateral sense, when moving from SW to NE. It was proposed that the NE sides oriented in the same direction as the Kurile Basin in general correspond to normal faults. In this case, the shorter NW segments should correspond to strike-slip faults. According to this suggestion, all previous reconstructions of the Kurile Basin (Savostin et al., 1983; Kimura and Tamaki, 1986; Jolivet et al., 1990) assume a basin



opening in NW direction (see Fig 3.2 a). There is a second type of opening mode in discussion (see Fig. 3.2 b), and we will check both modes using the obtained data.

#### Preliminary interpretation

According to both the structural features apparent on the sea floor and the basement morphology (see Figs. 5.2, 5.4 and 6.2), the studied area can be subdivided into four parts:

1. The top and the northern slope of the Academy of Sciences Rise;
2. The upper southern slope of the Academy of Sciences Rise;
3. The lower southern slope of the Academy of Sciences Rise;
4. The Kurile Basin floor.

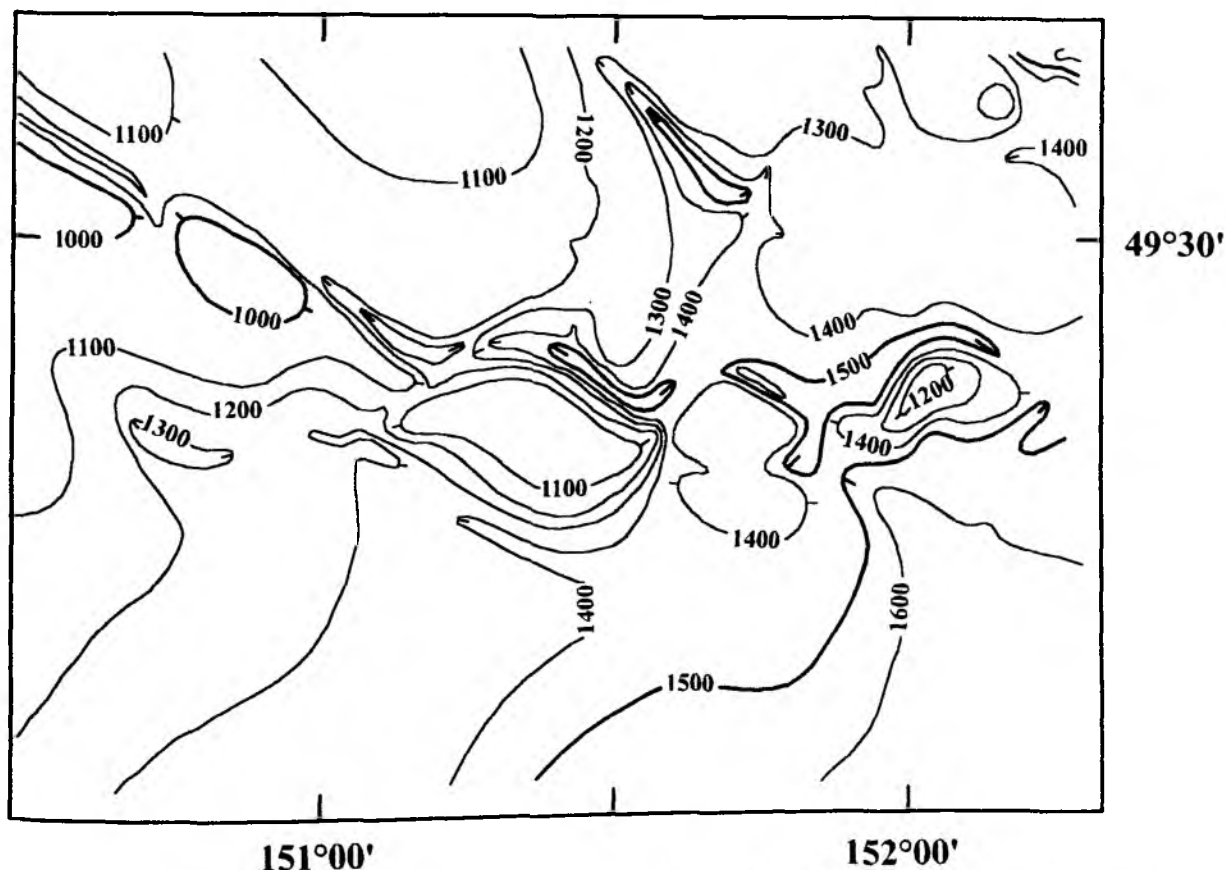
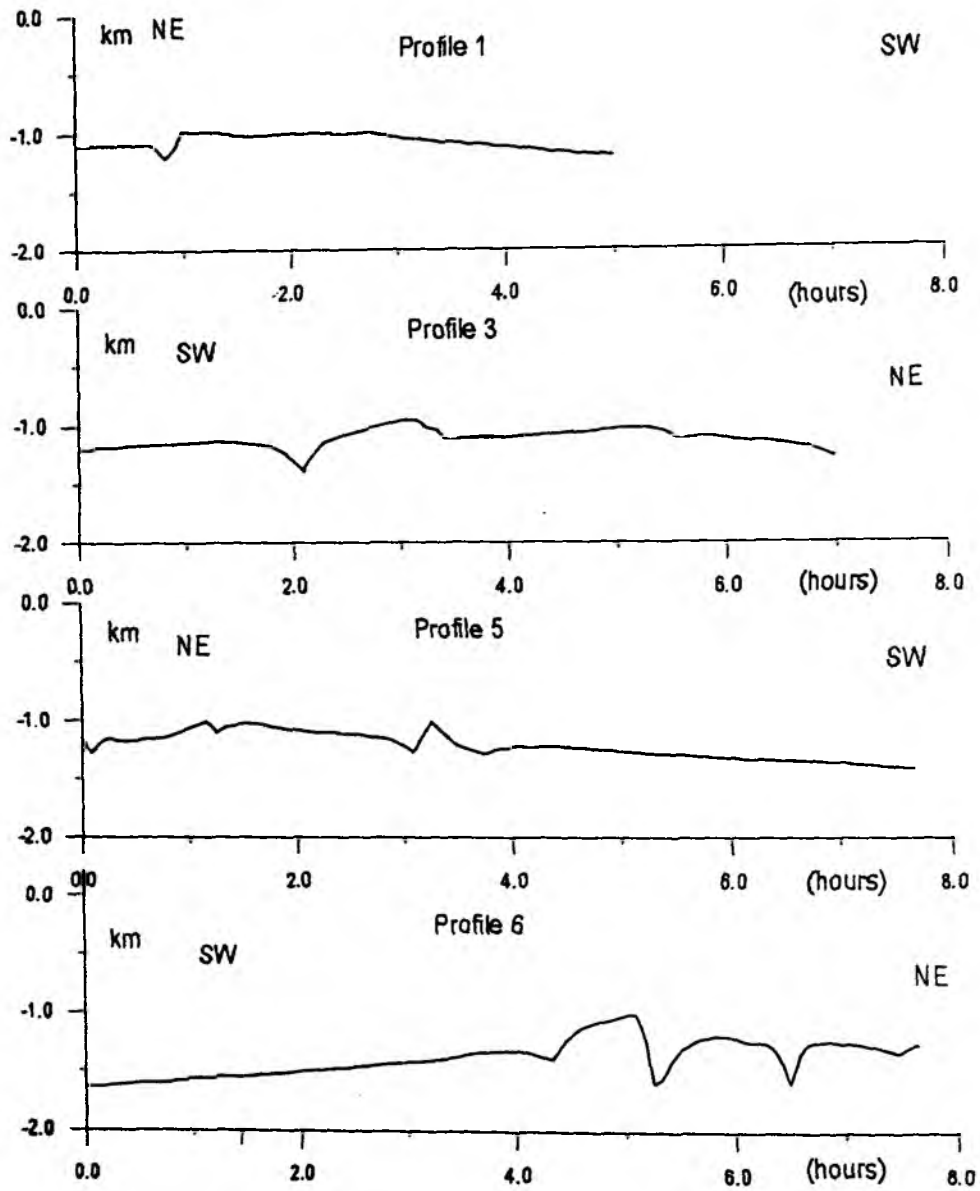


Fig. 6.3: Bathymetry map of the Academy of Sciences Rise top. Top of the rise consists of several blocks shifted each other. S-like depression on the block feet indicates that the sense of movement was a dextral one. This map was drawn with additional data which were obtained before.

#### Relief and basement morphology

a) Top and northern slope of the Academy of Sciences Rise:

Within the area of investigation, the top surface of the rise deepens from the west to the east from 1000 m to 1200 m and more. The rise does not represent a single structure, but consists of several blocks trending in WNW direction (Fig. 6.3). The blocks are asymmetrical, their steep slopes mainly face to the NE and the gentle slopes to the SW (Fig. 6.4). The height of the steep slopes reaches 600 m. The blocks are distinctly recognized in the bottom relief, but much more clearly they can be seen in the basement structure (Fig. 6.5.). According to their morphology,



**Fig. 6.4:** Bathymetry profiles across the Academy of Sciences Rise top, showing tilted blocks. Locations of profiles are shown in Fig. 5.1.

these blocks are tilted and originated during extensional conditions. Obviously, the tops of some of them were located above sea level, since they were cut by erosion (see prof. 8 on Fig. 6.2).

The blocks are arranged in several linear uplifts. The most remarkable is the one which corresponds to the top of the Rise. It is important to note that the blocks are shifted relative to each other in a left-lateral sense when looking from W to E. The existence of S-like depressions near the block bases (see Fig. 6.3) indicating dextral shear zones, allows to suppose that the displacement was a right-lateral one.

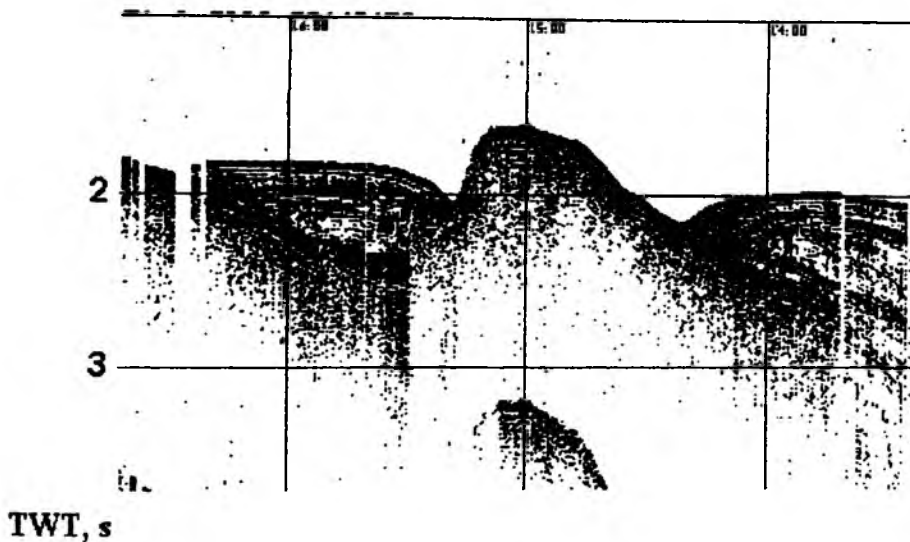


Fig. 6.5: Tilted block on the Academy of Sciences Rise top. Portion of seismic profile 11.

The gentle slopes of the blocks face to the SW. At the 1200-1400 m depth contour they immediately transfer into the prominent rise slope. The upper part of this gentle bend can be observed in water depths of 1900-2100 m. The lower slope dips more steeply to the bottom of the Kurile Basin and its foot is located at depths of 3000-3300 m.

b) Upper slope of the Academy of Sciences Rise:

The upper part of the slope has a simple and smooth bottom relief, because the basement structures are covered by sediments with thicknesses of more than 2 km. Within the survey area, the upper part of the slope generally trends in northeasterly direction. In some places, the slopes change to the WNW direction and then resembles the strike of the Academy of Sciences top. The relief of upper slope is quite differentially manifested in the acoustic basement surface (compare Figs. 5.2 and 5.4).

A graben-like structure is observed in the basement relief, trending in northwesterly direction oblique to the general trend of the slope, and opening towards the Kurile Basin (Fig. 6.7). The western boundary of this area is represented by the acoustic basement high, stretching in northwesterly direction (i.e. under an angle to the general slope trend) from the top of the Academy of Sciences Rise to the Kurile Basin. The eastern boundary of the basement structure corresponds to the rise slope, according to the deepening from its top surface. It must be emphasized that the slope contour, according to the basement relief, has a zigzag shape, and its trend is determined by two directions (NE and NW). The area is totally compensated by sediments and is accordingly not manifested in the bottom relief.

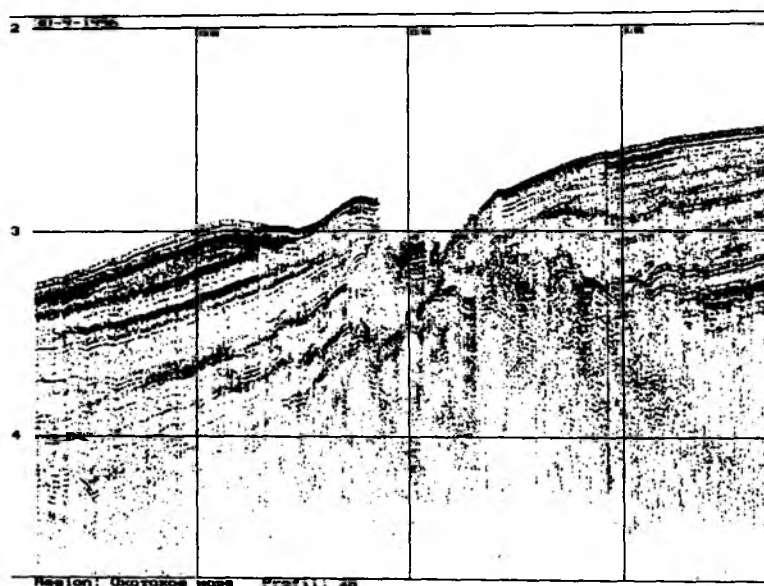


Fig. 6.6: Seismic cross-section showing tilted blocks on the lower slope. A canyon cuts the upper sedimentary unit near the block. Portion of seismic profile 28.

c) Lower slope of the Academy of Sciences Rise:

As it was noted above, the basin slope base has zigzag contours and an *en-echelon* structure determined by NW and NE directions. The area of investigation, thus, contains the NE segment of the structure, which connects two northwesterly striking segments.

The tilted blocks typical for the Rise top again appear in the lower slope zone. They were seen in both the bottom relief (see Fig. 6.2, profile 11) and the basement relief (Fig. 6.6). Thus have northwesterly strikes and are displaced against each other in the right-lateral sense. The blocks are almost covered by sediments. They are manifested in the bottom relief only in the southwestern part of the slope. In the northeastern part of the slope, their strike is determined by canyons striking in northwesterly direction (Figs. 5.3 and 6.7).

Dredging on the slope of one of the blocks revealed that it is composed of ancient volcanogenic and intrusive rocks (see chapter 5). At the same time, basic rocks of younger age were dredged. It must be noted in this case that an isometric seamount of about 500 m height is located on one shoulder of this block (see Fig. 5.3). Apparently it is a volcanic edifice, which originated during the initial stage of rifting. Further analyses of these rocks will presumably clarify the tectonic situation.

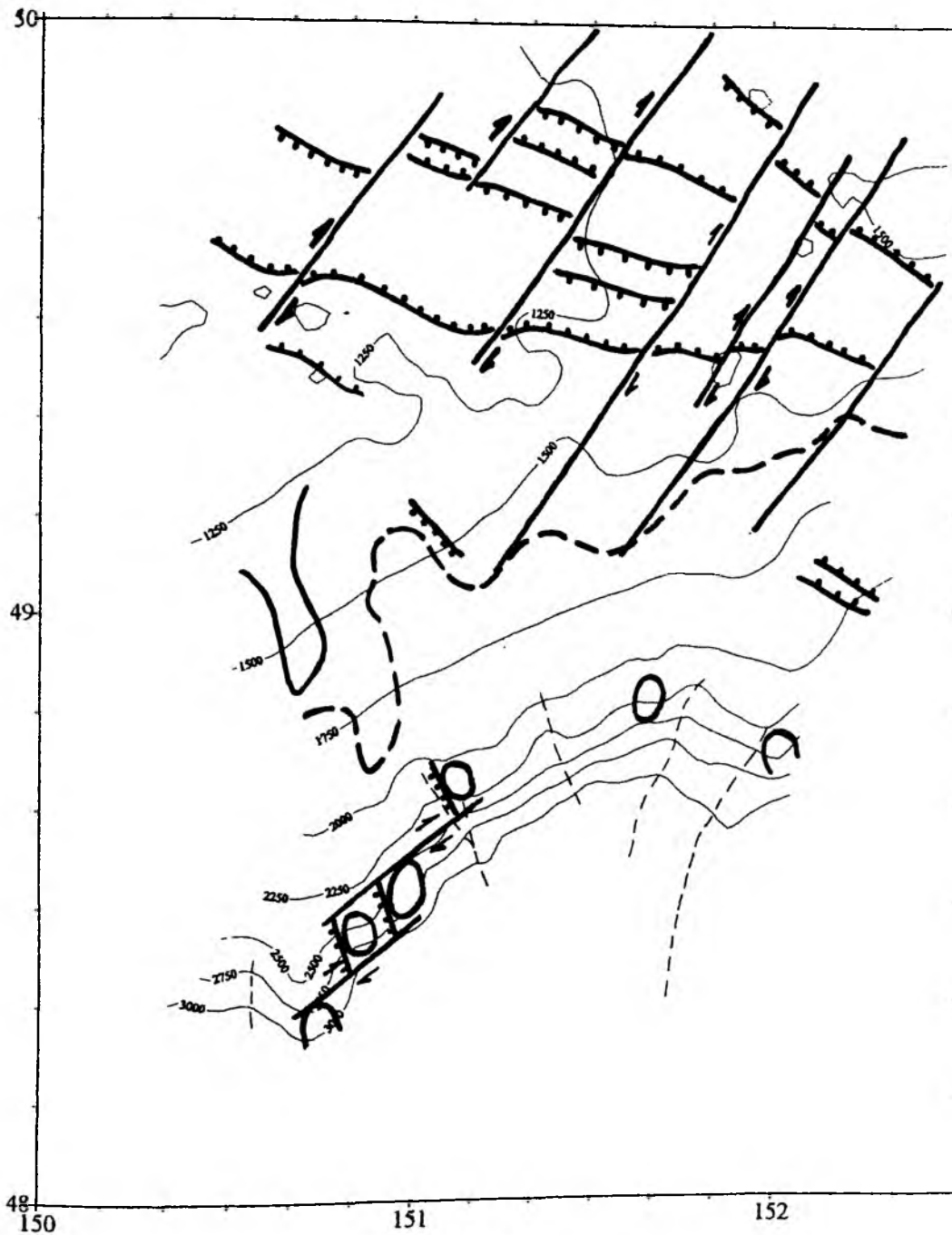


Fig. 6.7: Structural map of the studied area on the northern Kurile Basin slope. Thick lines show basement highs on upper and lower slope. Thick broken lines outline graben-like structure on the upper slope. Broken line with arrows - shear zones. Broken line marks axes of the canyons on the lower slope and submarine channel inside the basin. Contour interval is 250 m.

d) Bottom of the Kurile Basin:

The basin floor of the study area is at approximately 3200-3300 m water depths. The maximum depth is 3330 m. The sea floor is smooth and gently deeps from the slopes towards its central part in concordance with the basement relief. There are two features in the bottom relief, which were determined by the basement morphology. The

first structure at water depths of about 1000 m is the seamount in the SE corner of the area (Figs. 5.3 and 5.4). Dredging showed that this seamount is a submarine volcano (see Chapter 5). We hope that additional investigations will help to solve the following problems: Does this volcano belong to the recent Kurile subduction zone, or does it represent the oceanic basement of the basin. The second structure is related to the basement high that deepens from the northwestern segment of the slope in southwesterly direction.

Apart from these structures connected to the basement relief, the basin bottom is further divided by two submarine channels. One of them can be traced into the basin for at least 15 miles (see Fig. 5.3). The channels are the continuations of two large canyons, cutting through the northwestern part of the slope. The channels are bound by levees, the heights of which are more than 100 m in the upper parts of the canyons. The canyons trend to the NE and cut through the slope near the basement highs, which are covered by sediments. The depths of the canyons are 200-300 m and on their western flanks the upper sedimentary unit crops out. Dredging showed that this unit consists of tuff-diatomaceous clays and diatomaceous oozes (see chapter 5). According to the preliminary stratigraphy worked out by A. Matul, their age is Upper Miocene to Lower Pliocene.

### Tectonics

The relief forms of the sea floor and the basement described above justify that the study area is characterized by two main structural trends, namely WNW-NW and NE striking features. These directions are determined by two types of faults - normal faults and strike-slips (Fig. 6.7). Normal faults are distinctly manifested in the bottom relief as scarps with heights of up to 600 m. According to the basement relief, the visible displacement reaches 2 km.

Normal faults bound the tilted blocks, structures typical for extensional conditions. Their planes face to both the NE and the SW, forming graben and semi-graben structures. The tilted blocks are most distinctly manifested at the top and the northern slope of the Academy of Sciences Rise, and to a lesser degree on the lower slope. They are absent within the basin. At the Academy of Sciences Rise, normal faults strike in WNW direction. On the lower slope, their strike changes to NW, i.e. structures apparently rotate clockwise towards the basin.

The strike-slip zones are most distinctly seen at the Academy of Sciences Rise, and are determined by the displacements of basement blocks. They have NE strike and are generally longer than normal faults. According to the NE curving of the basement contours of graben-like structure, they may continue into the upper slope zone. On the lower slope, a small clockwise rotation of strike-slip faults takes apparently place. The existence of S-like structures, as it is clearly seen in Fig. 6.3, allows to suppose that there are dextral displacements along the faults and that the entire region belongs to a dextral shear zone.

### Discussion and conclusions

It is proposed that from Paleocene times up to present time, the structural features of North-East Asia were shaped by the interaction of two major plates - the North-American and the Eurasian plates (Savostin and Drachev, 1988). During the entire time period, the Okhotsk Sea was situated in between these plates so that its geodynamic situation was entirely determined by the location of the North-American/Eurasian pole of rotation. Before Early Oligocene times, the rotation pole was located near Japan. Therefore the area to the north of it was in the extensional mode. From Oligocene times on up to present day, the pole was situated to the south of the Okhotsk Sea for the entire period, although a number of small pole displacements occurred. Accordingly, the

Okhotsk Sea was always under compressional mode. Nevertheless, extensional structures, namely the Okhotsk rift systems and the Kurile Basin, could form during this time.

Gnibidenko (1995) suggested that the Kurile Basin originated during Oligocene-Miocene times due to the movement of the Okhotsk plate away from the Kurile-Kamchatka subduction zone (Zonenshain and Savostin, 1979). The second extensional area belongs to the Okhotsk rift system. The majority of the related structures are oriented orthogonal to the Kurile Basin trend. Some of them began to originate simultaneously with the basin in Oligocene times, severely preventing consistent plate tectonic reconstructions for this region. It has, thus, to be noted that it is still not clear how the existence of the Okhotsk Sea extensional structures are connected with subduction processes within the Kurile-Kamchatka trench during Cenozoic times (Gnibidenko, 1990).

The data obtained during this cruise reveal that on the Kurile Basin northern slope, extensional structures are widely developed. They are manifested in both the sea floor and the basement reliefs by tilted blocks, grabens, and semi-grabens. The structural pattern of the study area is further characterized by two fault systems: NW striking normal faults and NE striking dextral shear zones, thus, showing the orientation as the Okhotsk rift system structural pattern.

The above mentioned tectonic pattern of the northern Kurile Basin slope gives rise to suppose that it did not extend across, but along the basin trend, i.e. it opened as a pull-apart basin. We conclude that the Kurile Basin and Okhotsk rift system formed due to a single mechanism. The opening can be most perfectly described by the Okhotsk Sea clockwise rotation around the pole, which is located off the Okhotsk Sea northwestern coast. Such movement may be caused by the convergent motion between the North-American and Eurasian plates.

In this line it is further proposed that the different parts of the rift system originated during different time periods: Paleogene-Lower Miocene times, Neogene-Quaternary times and Middle Miocene-Quaternary times (Kharakhinov et al. 1985). The successive rift formation can apparently explain the complex structural pattern of the rift system. This mode does not agree in every aspect with the pattern obtained in supposition with the Okhotsk plate rotation around the non-moving pole, since it is the pole, which describes the general opening of the rift system and the basin since Oligocene times.

Since Oligocene times up to present day, the rotation pole between the North-American and Eurasian plates repeatedly changed its position (Savostin and Drachev, 1988). It could have consequently influenced the Okhotsk plate motion parameters, which caused the non-simultaneous opening of both the Okhotsk Sea rift system and the Kurile Basin. For example, the structural pattern of the Derugin Basin rift system, as obtained on the 16-th cruise of RV "Professor Gagarinsky" (Baranov et al., *subm.*), does not correspond to the pattern of the northern Kurile Basin slope and can not be obtained from the same pole. This area is situated near the Amur/Okhotsk Sea plate boundary. Here, the extensional process began only in Miocene-Pliocene times, and was caused by the right-lateral displacements along the Sakhalin shear zone. According to the basement structure, extensional processes are widespread in the entire Okhotsk Sea. This fact justifies that the deformations did not only took place along the Okhotsk Sea boundaries, but also in its inner parts, i.e. the Okhotsk plate moved not as a rigid body during Cenozoic times (or there were many jumpings of a plate boundary). Within the rift system, the extensional processes stopped at the stage of rifting, whereas in the Kurile Basin they continued up to the spreading stage and the formation of new oceanic crust.

## 7. Conclusions and perspectives

The results obtained during the GREGORY expedition allow to specify the regions, which are interesting from the tectonic and environmental point of view for further investigations within the KOMEX framework. The offshore eastern Sakhalin region is among the most important ones. The discovery of new gas plumes justifies the existence of vast areas of gas venting, stretching along the eastern Sakhalin coast. This area corresponds to the active shear zone separating the Okhotsk and Amur plates.

It is well known that gas seeps are widely spread on the inner slopes of deep-sea trenches - the regions of recent subduction representing convergent plate boundaries. The offshore eastern Sakhalin region, however, is related to the second plate boundary type - transform fault zones. The evaluation of how important such zones are in the global gas balance compared to the gas contribution from subduction zones seems to be of extreme importance.

Up to now, the future KOMEX project only plans to include the gas monitoring of the near Sakhalin region. The complex investigations performed during the GREGORY expedition including the first mapping of active fault zones, the finding of new gas fields, and the *in situ* gas geochemical survey and flux estimations underline that this region is undoubtedly interesting from the paleoceanological point of view, because it is located within the Amur river outflow area.

The investigations devoted to the origin and formation of marginal seas were a major task during this expedition. The appearance of tensional structures under the overall compressional conditions (back-arc basins in subduction zones, such as the Kurile Basin) were discussed from the very beginning of the plate tectonic theory. Several models were suggested to explain the origin of such back-arc basins.

The clockwise rotation model of the Okhotsk plate explaining the mode of formation of the Kurile Basin and other extensional structures in the Okhotsk Sea (e.g. Derugin and TINRO Basins) were initially proposed for examination. The first step in this direction was already done during the GERDA expedition (16th cruise of RV "Professor Gagarinsky", 1995, Derugin Basin). During the GREGORY expedition, this work was successfully continued within the Kurile Basin.

The TINRO Basin is the third one among the biggest basins of the Okhotsk Sea. Its structure is not clear so far, hence it certainly represents one of the key regions in understanding the Okhotsk Sea history and modern kinematics. Juxtaposition of its structural pattern with those of the Kurile and Derugin basins may allow to verify the model of the Okhotsk Sea Basin formation. The TINRO Basin can therefore be proposed as the second major research object for future investigations. Besides, this area is extremely important with regard to gas fluxes.

It is known that the TINRO Basin is filled with sediments containing gases. Since it is located on the boundary between the Okhotsk and North-America plates, it represents a highly active geodynamic regime. Active faults, in fact, must occur in this area contributing the conduits for gases being released from the sea floor deposits and transferred through the water column to the atmosphere. The investigations on gas release in the TINRO Basin may be the same as in the offshore eastern Sakhalin area.

Another tectonically important area is located between the Institute of Oceanology and Academy of Sciences rises and corresponds to the Kashevarov linear zone. It is situated adjacent to the Derugin Basin, and apparently possesses another structural pattern. In paleoreconstructions, this zone is regarded as a linear shear zone, which is connected



with the Kurile Basin opening in NW direction. The data obtained during this cruise allow to conclude that the basin opened in northeasterly direction. Hence, the geodynamics of the Kashevarov linear zone again appear to be amazing, i.e. it is still unclear whether it is a big shear zone or an extensional structure consisting of elements oriented in the same direction as those in the Kurile Basin.

During the 27th cruise of RV "Akademik Lavrentyev", the research program was entirely fulfilled. Significant and original results in both geological and geophysical respect were obtained. Some of them have even a unique character. Moreover, the GREGORY expedition allowed to specify most important regions for future studies and to determine the perspectives of the joint German-Russian geological and geophysical investigations in the Okhotsk Sea. This expedition can, therefore, be estimated as a successful beginning of the KOMEX project.

## 8. References

- Alderman, S.E. (1996): Planktonic foraminifera in the Sea of Okhotsk: Population and stable isotope analysis from a sediment trap.- MS-thesis, Massachusetts Institute of Technology: 99 pp.
- Astakhov, A.S. (1991): Physics-mechanical features and absolute masses of Holocene sediments of the Okhotsk Sea.- *Pacific Geology*, 2: 50-55 (in Russian).
- Astakhov, A.S. (1995): Genesis and sources of the east China sea shelf sediments based on quartz-granes morphometric analysis.- *Terrestrial, Atmospheric and Ocean Sciences*.- 6(N1): 65-74.
- Astakhov, A.S., Vagina, N.K., Gorbarenko, S.A., et al. (1988): Velocities of Holocene sedimentation in the Sea of Okhotsk.- *Pacific Geology*, 4: 1-14 (in Russian).
- Astakhov, A.S. and Vashchenkova, N.G. (1993): Morphometric analysis of terrigenous quartz for lithodynamical and paleogeographical reconstructions.- *Lithologia i poleznie iskopaemie*, 5: 106-117 (in Russian).
- Baranov, B.V., Dozorova, K.A., and Svarichevsky, A.S. (1995): Cenozoic kinematics of the Okhotsk plate: opening of the back-arc basin and Okhotsk rift system.- Abstracts of the International Lithosphere Program Workshop, Miyagi, Japan.
- Baranov, B.V., Drachev, S.S., and Pristavakina, E.I. (1996): The geodynamics of active plate boundaries in the Arctic region.- *CASP Report*, 638: 126 pp.
- Baranov, B.V., Karp, B.Ya., Dickmann, Th., Dozorova, K.A., and Karnauch, V.N. (subm.): Tectonics of the central Ionian Rift, Eastern Derugin Basin (Okhotsk Sea).- *Tectonics*.
- Bezrukov, P.L. (1955): On the migration and velocity of siliceous sediments accumulation in the Okhotsk Sea.- *Doklady Akademii Nauk*, 103(N3): 473-476 (in Russian).
- Bezrukov, P.L. and Romankevich, E.A. (1960): To stratigraphy and lithology of the sediments of the Northwestern Pacific.- *Doklady of Academy of Science USSR*, 130(N2): 417-420 (in Russian).
- Bikkenina, S.K., Anosov, G.I., Argentov, V.V., and Sergeev, K.Ph. (1987): Crustal structure of the southern Okhotsk Sea according to seismic data.- *Science Publ.*, Moscow: 86 pp. (in Russian).
- Cailleux, A. (1952): Morphoskopische Analyse der Geschiebe und Sandkörner und ihre Bedeutung für die Paläoklimatologie.- *Geol. Rdsch.*, 40: 11-19.
- Galperin, E.I. and Kosminskaya, I.P. (1964): Structure of the Earth's crust in the transitional zone from the Asian continent to the Pacific Ocean.- *Moscow, Science Publ.*: 307 pp. (in Russian).
- Geodekyan, A.A., Udintsev, G.B., Baranov, B.V., et al. (1976): Bedrocks of the Central Okhotsk Sea.- *Soviet Geology*, 6: 12-31 (in Russian).
- Ginsburg, G.D., Soloviev, V.A., Cranston, R.E., Lorenson, T.D., and Kvenvolden, K.A. (1993): Gas hydrates from continental slope, offshore Sakhalin Island, Okhotsk Sea.- *Geo-Marine Letters*, 13: 41-48.

- Gnibidenko, G.S. (1990): The Rift System of the Okhotsk Sea.- Proceeding of the First International Conference on Asian Marine Geology, China Ocean Press, Beijing: 73-81.
- Gnibidenko, G.S., Hilde, T.W.C., Gretskeya, E.V., and Andreev, A.A. (1995): Kurile (South Okhotsk) Backarc Basins.- In: Backarc Basins: Tectonics and Magmatism, B. Taylor (ed.), Plenum Press, New York: 421-449.
- Gorbarenko, S.A. (1991): Stratigraphy of the upper Quaternary sediments of the Central Okhotsk Sea and their paleoceanography using  $\delta^{18}O$  and other methods.- *Okeanologiya*, 31(6): 1036-1042 (in Russian).
- Gorbarenko, S.A. (subm.): Stable isotope and lithologic evidence of late-glacial and Holocene oceanography of the Northwestern Pacific and its marginal seas.- *Quaternary Research*.
- Gorbarenko, S.A., Kovalukh, N.N., Odinkova, L.Y., et al. (1988): Upper Quaternary sediments of the Okhotsk Sea and reconstruction of paleoceanological condition.- *Tikhookeanskaya geologiya*, N2: 25-34 (in Russian).
- Gorbarenko, S.A., Chekhovskaya, M.P., and Southern, J.R. (in press): Detailed changes of the Central Okhotsk Sea paleoceanography during last glaciation-Holocene.- *Okeanologiya*.
- Jolivet, L., Davy, P., and Cobbold, P. (1990): Right-lateral shear along the northwest Pacific margin and the India-Eurasia collision.- *Tectonics*, 9: 1409-1419.
- Keigwin, L.D. (1995): Northwest Pacific paleoceanography.- In: Global fluxes of carbon and its related substances in the coastal sea-ocean-atmosphere system, Proceeding of the 1994 Sapporo IGBP Symposium, S.Tsunogai et al., (eds.), M. and J. International, Yokohama, Japan: 473-478.
- Khabakov, A.B. (1946): On indexes of roundness of pebbles.- *Soviet Geology*, N10: 98-99. (in Russian)
- Kharakhinov, V.V., Tereshchenkov, A.A., Baboshina, V.A., and Pudikov, E.G. (1985): Sedimentary basin tectonics of the Okhotsk Sea region.- Review of the Mingasprom, Ser.: Geology and prospecting of the marine oil and gas deposits, 2, 32 pp. (in Russian).
- Kimura, G. and Tamaki, K. (1986): Collision, rotation and back arc spreading: The case of the Okhotsk and Japan Seas.- *Tectonics*, 5, 389-401 pp.
- Kononov, Yu.I., Morik, V.A., and Petrik, N.S. (1975): Ice cover and its significance in sediment formation of Nevelskoy Strait.- In: Problems of Pacific ocean geography, Vladivostok: 64-67 (in Russian).
- Kononova, N.N. (1986): Eolian landscapes of the sea coast.- Far East State University Press, Vladivostok: 104 pp.
- Kornev, O.S., Neverov, Yu.A., Ostapenko, V.F., et al. (1982): The results of geological dredging in the Okhotsk Sea from RV "Pegasus" (21 Cruise).- In: Geological structure of the Okhotsk Sea Region, Vladivostok: 36-51 (in Russian).
- Kruglikova, S.B. (1988): Radiolarians (Polycystina) from the bottom Arctic sediments.- Academy of Sciences of USSR Transac. Geol. series, 1: 92-101 (in Russian).

- Kruglikova, S.B. (1989a): Radiolarian zonal stratigraphy.- In: Neogene-Quaternary paleoceanology (on micropaleontological data), M.S. Barash (ed.), Moscow, NAUKA Press: 67-70 (in Russian).
- Kruglikova, S.B. (1989b): Quaternary radiolarian zonal stratigraphy, datum levels. In: Neogene-Quaternary paleoceanology (on micropaleontological data), M.S. Barash (ed.), Moscow, NAUKA Press: 85-89 (in Russian).
- Lelikov, E.P. (1992): Metamorphic complexes of the marginal seas of Pacific.- Vladivostok, Dal'nauka: 168 pp. (in Russian).
- Leonov, A.K. (1960): Regional oceanography. Part I. Leningrad.- Gidrometeoizdat Press: 765 pp. (in Russian).
- Matul, A. (1994): On the problem of paleoceanological evolution of the Reykjanes Ridge region (North Atlantic) during the last deglaciation based on radiolarian study.- *Oceanology*, 34(6): 881-889 (in Russian).
- Morley, J.J., Heusser, L.E., and Shackleton, N.J. (1991): Late Pleistocene/Holocene radiolarian and pollen records from sediments in the Sea of Okhotsk.- *Paleoceanography*, 6(1): 121-131.
- Noklenberg, W.J., Parfenov, L.M., Monger, J.W.H., Baranov, B.V., et al. (1994): Circum-North Pacific tectono-stratigraphic terrane map.- U.S. Department of the Interior, U.S. Geological Survey, Open-file report, 94: 216pp.
- Nürnberg, D., Wollenburg, I.W., Dethleff, D., Eicken H., Kassens, H., Letzig, T., Reimnitz, E., and Thiede, J. (1994): Sediments in Arctic sea ice - Implications for entrainment, transport and release.- *Marine Geology*, 119: 185-214.
- Obzhirov, A.I. (1993): Gas geochemical fields in bottom water of seas and oceans.- Science Publ., Moscow: 139 pp. (in Russian).
- Obzhirov, A.I. (1994): Dissolution gas distribution in sea water columns North-Eastern Taiwan.- The Fifth Seep and Voce Conference, NTU, Taiwan: 141-150.
- Obzhirov, A.I., Kazansky, B.A., and Melnichenko, Yu.I. (1989): Effect of the sound scattering in the Okhotsk Sea water.- *Pacific Geology*, N2: 119-121 (in Russian).
- Petelin, V.P. (1957): Mineralogy of silt-sand fraction of the sediments of the Okhotsk Sea.- *Proceeding of Institute of Oceanology USSR*, 22: 77-138 (in Russian).
- Savostin, L.A., Zonenshain, L.P., and Baranov, B.V. (1983): Geology and plate tectonics of the Sea of Okhotsk.- In: *Geodynamics of the Western Pacific*. T.W.H. Hilde and S. Uyeda (eds.): 189-221.
- Savostin, L.A. and Drachev, S.S. (1988): Cenozoic compression in the New Siberian Islands and its relationship with the opening of the Eurasian Basin.- *Oceanology*, 28(5): 775-781 (in Russian).
- Schubert, C.J., Nürnberg, D., Scheele, N., Pauer, F., and Kriews, M. (in press): Carbon isotope depletion in ikaite crystals: Evidence for methane release from the Siberian shelves?.- *Geomarine Letters*.

- Talley, L. (1991). An Okhotsk Sea anomaly: implication for ventilation in the North Pacific.- *Deep-Sea Research*, **38**: 171-190.
- Talley, L.D. and Nagata, Y. (1995): The Okhotsk Sea and Oyashio Region.- *Inst. of Ocean Sci., Sidney, B.C., Canada*: 227 pp.
- Vasiliev, B.I., Putintsev, V.K., Makarovskii, B.A., Svyatogorova, N.N., and Selivanov, V.A. (1990): Bedrocks complexes of the Okhotsk Sea submarine rises.- In: *New data on geomorphology and geology of West Pacific*, V.P. Bobykina, B.I. Vasiliev, and G.M. Tomolov (eds.), Vladivostok: 5-16 (in Russian).
- Willetts, B.B. and Rice, M.A. (1983): Practical representation of the characteristic grain shape of sands: a comparison of methods.- *Sedimentology*, **30**: 557-565.
- Yang, J. and Honjo, S. (1996): Modelling the near-freezing dichothermal layer in the Sea of Okhotsk and its interannual variations.- *Journal of Geophysical Research*, **101**(C7): 16421-16433.
- Zhuze, A.P. (1962): Stratigraphy and paleontological investigations in the North-West Pacific.- *Academy of Sciences Publishing House*: 258 pp (in Russian).
- Zonenshain, L.P., Murdmaa, I.O., Baranov, B.V., Kuznetsov, B.V., Kuzin, V.S., Kuzmin, M.I., Avdeyko, G.P., Stunzhas, P.A., Lukashin, V.N., Barash, M.S., Valyasko, G.M., and Diomina, L.L. (1987): An underwater gas source in the Okhotsk Sea to the west from Paramushir Island.- *Oceanology*, **27**(5):795-800 (in Russian).
- Zonenshain, L.P. and Savostin, L.A. (1979): *Introduction to Geodynamics*.- Moscow, Nedra: 311pp (in Russian).

**Appendix I**  
**Research Vessel "Akademik M.A. Lavrentyev"**

## Research Vessel "Akademik M. A. Lavrentyev"

The research vessel "Akademic M.A. Lavrentyev" was built by Hollming LTD. in Rauma, Finland in 1984. The ship is named in honor of Academician M.A. Lavrentyev - a famous Russian mathematician, the first Head of the Siberian Branch of the Academy of Sciences of the USSR. Parameters of the ship are listed in Table 1.

Table 1: Research Vessel "Akademic M.A. Lavrentyev"		
	Length over all	75.5 m
	Depth	4.5 m
	Width	14.7 m
	Displacement	2712 t
	Gross weight	2318 GRT
	Net weight	695 t
	DWT	886 t
	Main engine capacity	1x 2576 KW
	Speed	13 knots
	Crew	43
	Scientific party	28

Seven winches are installed on the ship decks including seismic one. The winch locations are shown in Fig. 1A. Parameter of winches are listed in Table 2.

**Table 2: Description of winches**

Number	Name	Description
1	Seismic	One drum, 4.5 km long seismic streamer
2	Cable	One drum, 8.5 km long 18.0 mm of diameter wire rope or cable, pull force is 10 t
3	Wire rope	One drum, 5.0 km long 6.0 mm of diameter wire rope, pull force is 2.5 t
4	Cable	One drum, 10.0 km long 6.45 mm of diameter cable, pull force is 2.4 t
5	Cable	One drum, 7.5 km long 15 mm of diameter cable, pull force is 2.4 t
6	Cable	Three drums, each drum for 2.0 km long 10 mm of diameter cable, pull force is 0.8 t
7	Wire rope	One drum, 3.0 km long 13mm of diameter cable, pull force is 2.0 t

There are 11 laboratories including geological, seismic, gravity and bathymetry labs. High air pressure for the airgun is provided by 2 electric air compressors (EK - 7TM, made in Russia). The capacity of each of them is 13 liters per minute (air pressure - 19 Mpa). Air compressors can be used one at a time.

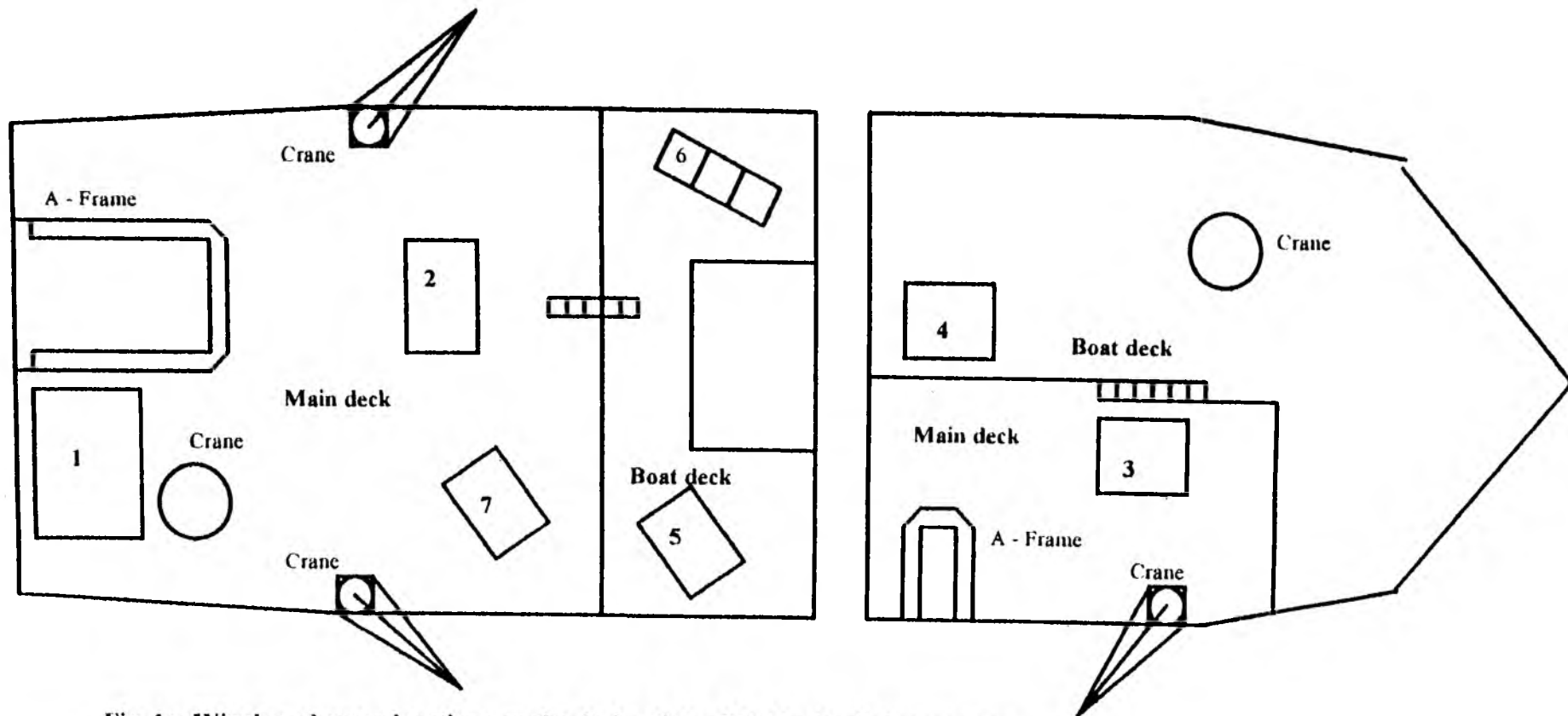


Fig. 1a. Winch and crane locations on the decks of the RV Akademik Lavrentiev



## **Appendix II**

### **Station coordinates**

## Station list

Station		Tool	Date/Time	Latitude	Longitude	Water depth (m)	Penetration (m)	Remarks
LV27-test			15.09.1996 12:29	46°23.21	145°09.91	3301		
	-1	Water sampler	15.09.1996 12:32	46°23.21	145°09.91	3301	100	empty
	-2	Water sampler	15.09.1996 12:39	46°23.21	145°09.91	3301	100	closed
	-3	Pinger	15.09.1996 12:53	46°23.21	145°09.91	3301		test o.k.
	-4	Plankton net	15.09.1996 13:33	46°23.21	145°09.91	3301	0-50	closed
LV27-1			17.09.1996 8:10	54°35.02	144°27.02	1130		
	-1	Water sampler	17.09.1996 8:10	54°35.02	144°27.02	1130	surface water	
	-2	Multicorer	17.09.1996 8:54	54°34.56	144°28.36	1148	0.36	
	-3	Gravity Corer (GEOMAR)	17.09.1996 11:05	54°33.81	144°28.11	1141	5.16	
LV27-Gas			17.09.1996 14:15	54°26.71	144°04.85	700		
	-1	Gravity Corer (POI)	17.09.1996 14:37	54°26.59	144°04.58	692	2.58	
LV27-2			17.09.1996 17:10	54°30.42	144°44.98	1303		
	-1	Water sampler	17.09.1996 17:39	54°30.19	144°45.32	1301	surface water	
	-2	Multicorer	17.09.1996 17:52	54°30.11	144°45.33	1273	0.35	
	-3	Gravity Corer (GEOMAR)	17.09.1996 19:25	54°29.84	144°45.27	1301	3.51	
	-4	Gravity Corer (POI)	17.09.1996 21:49	54°30.15	144°45.14	1305	7.38	
LV27-3			18.09.1996 0:02	54°25.01	145°08.18	1480		
	-1	Water sampler	18.09.1996 0:05	54°24.83	145°08.41	1476	surface water	
	-2	Multicorer	18.09.1996 0:34	54°24.83	145°08.41	1476	0.45	
	-3	Gravity Corer (GEOMAR)	18.09.1996 2:07	54°24.60	145°07.60	1477	3.76	
Mooring			18.09.1996 12:00	55°06.79	142°37.27			
	-1	Water sampler	18.09.1996 12:00	55°06.79	142°37.27		surface water	
LV27-4			19.09.1996 4:20	55°03.66	145°44.26	855		
	-1	Water sampler	19.09.1996 4:20	55°03.66	145°44.26	855	surface water	
	-2	Multicorer	19.09.1996 4:57	55°03.43	145°44.08	860	0.27	
	-3	Gravity Corer (GEOMAR)	19.09.1996 6:05	55°03.22	145°44.19	865	5.52	
	-4	Gravity Corer (POI)	19.09.1996 3:18	55°03.54	145°44.16	857	3.88	
LV27-5			20.09.1996 12:30	54°45.03	149°30.02	487		
	-1	Plankton Net	20.09.1996 13:28	54°47.05	149°29.85	478	see sampling sheet	
	-2	Water sampler	20.09.1996 15:01	54°48.82	149°30.43	467	300,200,100,50	
	-3	Gravity Corer (POI)	20.09.1996 13:07	54°46.09	149°29.91	482	5.42	
	-4	Gravity Corer (GEOMAR)	20.09.1996 13:55	54°47.41	149°29.92	476	2.11	upper 33cm not in liner
	-5	Multicorer	20.09.1996 16:05	54°49.56	149°32.22	462	0.22	
LV27-6			20.09.1996 20:00	54°10.04	149°30.07	909		
	-1	Water sampler	20.09.1996 20:15	54°10.04	149°30.07	880	surface water	
	-2	Multicorer	20.09.1996 20:42	54°09.81	149°30.09	878	0.3	
	-3	Gravity Corer (GEOMAR)	20.09.1996 21:48	54°09.87	149°30.33	868	1	
	-4	Gravity Corer (POI)	20.09.1996 22:52	54°09.73	149°30.09	872	1.85	
LV27-7			21.09.1996 4:45	53°15.49	149°34.71	1142		
	-1	Water sampler	21.09.1996 4:45	53°15.49	149°34.71	1142	surface water	
	-2	a. Multicorer	21.09.1996 5:28	53°14.85	149°34.50	1172		empty
	-2	b. Multicorer	21.09.1996 6:39	53°14.28	149°34.37	1150	0.39	
	-3	Gravity Corer (GEOMAR)	21.09.1996 8:28	53°15.27	149°35.73	1140	3.58	
LV27-8			21.09.1996 21:40	51°29.90	150°30.41	1145		
	-1	Water sampler	21.09.1996 21:40	51°29.90	150°30.41	1145	surface water	
	-2	Multicorer	21.09.1996 22:03	51°29.82	150°30.73	1147	0.31	
	-3	Gravity Corer (GEOMAR)	21.09.1996 23:05	51°29.88	150°32.46	1160	5.63	
	-4	Gravity Corer (POI)	22.09.1996 0:05	51°30.32	150°34.29	1144	7.6	
LV27-11			22.09.1996 10:48	49°50.17	150°20.16	1136		
	-1	Plankton Net	22.09.1996 11:05	49°50.41	150°20.04	1143	0-50m	cancelled- rough sea
	-2	Water sampler	22.09.1996 11:24	49°50.63	150°19.64	1143	300,200,100,50	
	-3	Multicorer	22.09.1996 12:45	49°51.06	150°19.07	1151	0.38	
	-4	Gravity Corer (GEOMAR)	22.09.1996 13:47	49°51.10	150°19.59	1153	1.62	
LV27-10			01.10.1996 9:33	48°57.57	152°08.32	1909		
	-1	Multicorer	01.10.1996 10:15	48°57.74	152°09.34	1911	0.25	
	-2	Plankton Net	01.10.1996 11:10	48°57.76	152°10.24	1924	300	net not closed. broken
	-3	Water sampler	01.10.1996 12:15	48°57.76	152°10.07	1918	300,200,100,50	
	-4	Plankton Net	01.10.1996 13:30	48°57.70	152°09.67	1913	== sampling sheet ==	
	-5	Gravity Corer (GEOMAR)	01.10.1996 15:07	48°57.36	152°08.29	1906	5.78	upper 18cm not in liner
LV27-15			01.10.1996 16:30	48°59.85	152°11.72	2007		
	-1	Gravity Corer (POI)	01.10.1996 17:12	49°00.01	152°11.63	1991	5.67	
LV27-16			01.10.1996 20:10	48°46.76	151°56.17	2455		
	-1	Dredge	01.10.1996 21:12	48°46.86	151°57.01	2455		

Station		Tool	Date/Time	Latitude	Longitude	Water depth (m)	Penetration (m)	Remarks
LV27-17			02.10.1996 6:15	48°18.21	151°46.60	3280		
	-1	Dredge	02.10.1996 7:19	48°18.11	151°46.44	3281		
LV27-18			02.10.1996 12:25	48°19.48	151°50.13	3190		
	-1	Dredge	02.10.1996 13:30	48°19.06	151°50.24	2945		
LV27-9			03.10.1996 8:06	49°59.88	152°30.35	ca. 1370		echolot not accurate
	-1	Water sampler	03.10.1996 8:06	49°59.88	152°30.35	ca. 1370	surface water	
	-2	Multicorer	03.10.1996 9:01	50°00.47	152°28.62	ca. 1370	-	empty
	-3	Gravity Corer (POI)	03.10.1996 10:34	50°01.00	152°25.07	ca. 1430	5,64	
	-4	Gravity Corer (GEOMAR)	03.10.1996 12:40	50°00.76	152°28.43	ca. 1390	5,5	
LV27-19			03.10.1996 16:30	49°40.36	152°09.58	1572		
	-1	Dredge	03.10.1996 16:57	49°39.82	152°09.60	1503		
LV27-12			04.10.1996 8:45	48°42.00	148°13.01	1293		
	-1	Water sampler	04.10.1996 8:45	48°42.00	148°13.01	1293	surface water	
	-2	a. Multicorer	04.10.1996 9:19	48°41.76	148°13.55	1291	-	empty
	-2	b. Multicorer	04.10.1996 10:15	48°42.50	148°14.38	1296	0,35	
	-3	Gravity Corer (GEOMAR)	04.10.1996 11:23	48°43.49	148°14.77	1301	5,8	
	-4	Gravity Corer (POI)	04.10.1996 12:22	48°44.51	148°14.41	1291	6,96	

## **Appendix III**

### **Track coordinates**

**Table                      Track coordinates**

Profile number	Latitude	Longitude	Profile number	Latitude	Longitude
LV27-1	49° 46.79N	150° 46.48E	LV27-17	49° 33.68N	150° 23.27E
	49° 17.13	150° 12.11		48° 43.76	152° 01.08
LV27-2	49° 17.13	150° 12.11	LV27-18	48° 43.76	152° 01.08
	49° 10.15	150° 23.87		48° 17.74	151° 52.20
LV27-3	49° 10.15	150° 23.87	LV27-19	48° 17.74	151° 52.20
	49° 56.41	151° 20.07		48° 44.91	151° 02.93
LV27-4	49° 56.41	151° 20.07	LV27-20	48° 44.91	151° 02.93
	49° 49.29	151° 31.79		48° 49.09	151° 09.39
LV27-5	49° 49.29	151° 31.79	LV27-21	48° 49.09	151° 09.39
	48° 57.73	150° 29.84		48° 27.16	151° 53.09
LV27-6	48° 50.04	150° 40.93	LV27-22	48° 27.16	151° 53.09
	49° 58.98	152° 04.11		48° 32.55	152° 00.02
LV27-7	49° 58.98	152° 04.11	LV27-23	48° 32.55	152° 00.02
	49° 51.79	152° 15.04		48° 55.03	151° 16.13
LV27-8	49° 51.79	152° 15.04	LV27-24	48° 55.03	151° 16.13
	48° 17.80	150° 20.50		48° 58.76	151° 21.00
LV27-9	48° 17.80	150° 20.50	LV27-25	48° 58.76	151° 21.00
	48° 32.53	150° 58.94		48° 40.40	151° 58.63
LV27-10	48° 33.04	151° 00.52	LV27-26	48° 40.40	151° 58.63
	48° 10.26	150° 33.12		48° 33.64	151° 50.35
LV27-11	48° 10.26	150° 33.12	LV27-27	48° 33.64	151° 50.35
	49° 45.36	152° 26.36		48° 51.48	151° 14.10
LV27-12	49° 45.36	152° 26.36	LV27-28	48° 51.48	151° 14.10
	49° 26.10	152° 22.53		48° 25.79	150° 44.11
LV27-13	49° 26.10	152° 22.53	LV27-29	48° 25.79	150° 44.11
	48° 21.87	151° 03.00		48° 42.45	150° 54.12
LV27-14	48° 21.87	151° 03.00	LV27-30	48° 42.45	150° 54.12
	48° 19.20	151° 24.06		48° 33.75	151° 10.62
LV27-15	48° 19.20	151° 24.06	LV27-31	48° 33.75	151° 10.62
	49° 04.75	152° 16.88		48° 49.79	151° 50.41
LV27-16	49° 04.75	152° 16.88			
	49° 33.68	150° 23.27			

## **Appendix IV**

### **Tables**

## **List of lithology and paleoceanology group and their scientific contribution**

<b>D. Nürnberg, S. Gorbarenko:</b>	<b>Scientific supervising</b>
<b>A. Astakhov:</b>	<b>Lithological description, magnetic susceptibility, humidity and density measurements, morphometric analysis, smear slide analysis</b>
<b>A. Derkachev:</b>	<b>Lithological description, mineralogical analysis, smear slide analysis</b>
<b>J. Grützner:</b>	<b>Magnetic susceptibility measurement</b>
<b>S. Gorbarenko:</b>	<b>Magnetic susceptibility and humidity measurement</b>
<b>A. Matul:</b>	<b>Micropaleontological analysis (radiolarians)</b>
<b>S. Neufeld:</b>	<b>Technical handling of equipment</b>
<b>D. Nürnberg:</b>	<b>Lithological description, smear slide analysis</b>
<b>Chr. Vogt:</b>	<b>Lithological description</b>
<b>J.-M. Wolfsdorf:</b>	<b>Lithological description</b>
<b>All the participants: coring and sampling.</b>	

Table 1 A: Smear slides taken and prepared during the expedition from the GEOMAR group.

KOMEX '96																		
Akademik M.A. Lavrentyev																		
Station	LV 27-1-3 MUC	LV 27-1-3 SL	LV 27-2-3 MUC	LV 27-2-3 SL	LV 27-3-2 MUC	LV 27-3-3 SL	LV 27-4-3 SL	LV 27-5-4 SL	LV 27-6-3 SL	LV 27-7-2 MUC	LV 27-7-3 SL	LV 27-8-2 MUC	LV 27-8-3 SL	LV 27-9-4 SL	LV 27-10-1 MUC	LV 27-10-5 SL	LV 27-11-4 SL	LV 27-12-3 SL
Latitude	54°34.56	54°33.81	54°30.11	54°29.84	54°24.83	54°24.60	55°03.22	54°47.41	54°09.87	53°14.28	53°15.27	51°29.82	51°29.88	49°51.10	48°57.74	48°57.36	49°51.10	48°43.49
Longitude	144°28.36	144°28.11	144°45.31	144°45.27	145°08.41	145°07.60	145°44.19	149°29.92	149°30.33	149°34.37	149°35.73	150°30.73	150°32.46	150°19.59	152°09.34	152°08.29	150°19.59	148°14.77
Water depth (m)	2148	2141	1273	1301	1476	1477	865	476	868	1150	1140	1147	1160	1153	1911	1906	1153	1301
Depth in core (cm)	1,62																	
	2 x surface	20	2 x surface	2	2 x surface	1	2	40	0	1 x surface	1	1 x surface	1	0	2 X Surface	20	5	25
	60			16		15	80	50	20		3		4	15		60	21	60
	100			27		25	30	80	49		18		10	30		90	60	90
	140			40		35	19	120	88		35		20	38		100	80	103
	180			48		50	50	130			48		40	45		140	110	120
	220			57		60	90	160			59		43	55		159	150	133
	250			70		70	120	190			80		49	65		170		150
	270			93		110	138	210			90		55	80		190		170
	300			120		140	150				92		70	120		210		190
	340			150		170	170				120		80	150		250		210
	360			180		200	200				140		89	360		257		232
	400			210		230	230				160		110	400		290		255
	440			230		270	250				180		115	440		310		290
	470			250		300	260				190		120	460		350		310
	500			263		350	300				199		140	490		390		340
	520			287		380	330				210		170	520		410		380
	539			320		420	350				230		190	539		428		410
				340		460	370				250		220			460		450
				352		490	400				280		240			464		490
						520	440				288		270			490		510
						550	470				295		290			500		540
							500				320		320			530		580
							540				320		350			560		
											350		370			579		
											370		380					
													400					
													420					
													430					
													435					
													450					
													460					
													470					
													480					
													520					
													560					



**Table 2A: Heavy mineral composition in sediments of Okhotsk Sea (size Fraction 0.05-0.1 mm, specific weight >2.89 g/cm<sup>3</sup> ) (%)**

Mineral	LV27-2-4 (0-10)	LV27-2-4 (120-130)	LV27-2-4 (260-270)	LV27-2-4 (710-720)	LV27-4-4 (0-10)	LV27-4-4 (206-207)	LV27-4-4 (330-335)	LV27-6-4 (0-5)	LV27-6-4 (170-178)	LV27-8-4 (10-20)	LV27-8-4 (510-520)	LV27-8-4 (732-740)
Cpx	12.13	11.46	16.03	18.39	24.73	19.96	21.72	27.2	27.3	28.82	21.04	30.18
Opx	9.43	6.77	4.83	7.18	7.44	9.76	5.88	11.53	4.72	8.13	6.19	7.16
Ol	0.54	--	--	--	--	--	--	--	1.05	0.25	--	0.25
bgHb	25.34	29.17	29.26	29.89	13.13	24.22	21.94	17.19	14.96	16.47	16.09	19.69
bHb	3.23	1.04	1.02	0.57	0.22	1.12	0.9	0.90	1.31	0.74	--	1.02
OHb	0.54	--	0.51	0.29	0.44	1.12	0.45	0.90	1.05	0.74	0.99	0.77
Ep	20.75	19.53	21.88	20.1	20.79	16.19	21.72	11.09	13.65	13.05	10.15	10.49
Act	8.09	5.21	4.83	5.46	1.97	3.55	1.81	2.04	2.36	1.48	2.23	2.30
Gar	1.62	0.52	1.02	1.72	0.44	1.33	0.33	0.90	0.52	0.25	0.99	0.51
Chl	2.96	4.17	3.84	4.02	3.06	1.58	1.13	0.68	1.84	2.46	2.48	0.51
Me	0.27	--	0.25	--	0.66	--	0.68	0.23	--	--	--	0.26
Tou	0.27	--	--	--	--	0.22	--	--	--	--	0.25	--
Ap	0.54	1.04	1.53	0.86	0.44	0.44	0.9	--	0.79	0.25	--	0.25
Sph	1.08	0.52	1.02	0.29	0.22	0.44	0.23	--	--	0.25	0.5	0.26
Zi	--	0.26	0.25	--	0.44	--	0.23	--	--	--	--	--
cMi	1.35	2.34	1.27	1.15	0.88	0.89	0.9	0.68	0.79	--	2.48	0.77
gMi	4.04	3.65	3.05	3.16	0.66	2.00	0.9	0.23	1.57	2.22	9.90	1.79
bMi	1.08	1.82	1.27	1.65	0.44	0.67	0.68	0.45	0.26	1.97	7.92	1.02
Ca	0.27	0.26	--	--	0.22	0.22	--	0.23	--	0.49	--	--
Rf	3.23	10.94	6.36	4.12	6.56	4.98	6.35	17.87	17.59	13.05	7.67	12.28
Op	3.24	1.3	1.78	1.15	14.01	11.31	13.35	7.92	8.67	7.39	11.14	9.97

*Notes for tables*

Minerals: Cpx-clinopyroxene, Opx-orthopyroxene, Ol-olivine, bgHb-brown-green hornblende, bHb-brown hornblende, OHb-basaltic hornblende, Ep-epidote, Act-actinolite, Gar-garnet, Chl-chlorite, Me-anatase, silimanite, Tou-tourmaline, Ap-apatite, Sph-sphene, Zi-zircon, cMi-colourness mica, bMi-green mica, bMi-brown mica, Ca-calcite, Rf- rock fragments, Op-opaque mineral (ilmenite, magnetite).

**Table 3A. Heavy mineral composition in ash layers**  
(size fraction 0.05-0.1 mm)

<b>Mineral</b>	<b>LV27-8-4 (153-155)</b>	<b>LV27-15-4 (110-112)</b>	<b>LV27-7-3 (51)*</b>	<b>LV27-8-4 (332-334)</b>
<i>Cpx</i>	23.96	20.45	34.28	34.91
<i>Opx</i>	25.0	37.37	30.85	20.05
<i>Ol</i>	1.3	0.25	-	-
<i>bgHb</i>	15.1	1.52	4.86	0.71
<i>bHb</i>	-	-	0.29	-
<i>Ep</i>	5.21	1.26	2.29	0.71
<i>Act</i>	-	-	0.29	-
<i>Gar</i>	-	-	-	-
<i>Chl</i>	-	0.25	0.29	0.24
<i>Ap</i>	0.52	0.76	0.57	0.24
<i>Zr</i>	-	-	-	0.24
<i>cMi</i>	-	0.25	-	-
<i>gMi</i>	-	0.51	-	-
<i>bMi</i>	-	-	0.57	-
<i>Rf</i>	16.67	10.01	6.57	9.43
<i>Op</i>	12.24	27.27	19.15	33.49

*Notes of tables*

\* - size fraction 0.05-0.01 mm, Op- prevaile magnetite.

Station/ Gear	Plankton Net	Surface Water	Water Column	Bottom Water	Fluff Layer	Surface Sediment	Near Surface Sediment	Sediment Column	German GC	Russian GC
LV27-Test-1		A.G								
LV27-Test-2			A.G.R							
LV27-Test-4	A.G.R									
LV27-1a-1									R	
LV27-1-1		G								
LV27-1-2				A.G.R	A.G	A.G.R	A.G.R			
LV27-1-3								A.G.R		
LV27-2-1		A.G								
LV27-2-2				A.G.R	A.G	A.G.R	A.G.R			
LV27-2-3										G.R
LV27-2-4										
LV27-3-1		A.G								
LV27-3-2				A.G.R	A.G	A.G.R	A.G.R			
LV27-3-3								A.G.R		
Meerburg		A.G								
LV27-4-1		A.G								
LV27-4-2				A.G.R	A.G	A.G.R	A.G.R			
LV27-4-3								A.G.R		G.R
LV27-4-4										
LV27-5-1	A.G.R									
LV27-5-2		A.G	A.G.R							
LV27-5-3				A.G.R	A.G	A.G.R	A.G.R			
LV27-5-4								A.G.R		G.R
LV27-5-5										
LV27-6-1		A.G								
LV27-6-2				A.G.R	A.G	A.G.R	G.R			
LV27-6-3								Radiography		
LV27-6-4										R
LV27-7-1		A.G								
LV27-7-2				A.G.R	A.G	A.G.R	A.G.R			
LV27-7-3								A.G.R		
LV27-8-1		A.G								
LV27-8-2										
LV27-8-3				A.G.R	A.G	A.G.R	A.G.R			
LV27-8-4								A.G.R		G.R
LV27-9-1		A.G								
LV27-9-3										
LV27-9-4									R	
LV27-10-1								Radiography		
LV27-10-2			A.G.R	A.G.R						
LV27-10-3										G.R
LV27-10-4	A.G.R									
LV27-10-5										
LV27-11-1	A.G.R							A.G.R		
LV27-11-2		A.G.R	A.G.R							
LV27-11-3				A.G.R	A.G	A.G.R	A.G.R			
LV27-11-4										
LV27-12-1		A.G.R						Radiography		
LV27-12-2			A.G.R							
LV27-12-3				A.G.R	A.G	A.G.R	A.G.R			
LV27-12-4								Radiography		
LV27-15-1									G.R	G.R

A-> Alfred Wegener Institute, Bremerhaven, Germany

G-> GEOMAR, Kiel, Germany

R-> Russian paleoceanographic scientific party incl. hydrochemistry

Radiography-> Core opened, but only radiography taken

Table 5 A: Mechanical properties of sediments

Core number	Depth in core (cm)	Sediment density D, g/cm <sup>3</sup>	Density of mineral base Dp, g/cm <sup>3</sup>	Mineral density Dt, g/cm <sup>3</sup>	Volume humidity (porosity) Wv, %	Weight humidity Ww, %
LV27-2-4	-20	1.17	0.30	2.31	87.00	74.37
LV27-2-4	-48	1.19	0.32	2.51	87.14	72.98
LV27-2-4	-81	1.21	0.33	2.81	88.38	73.05
LV27-2-4	-106	1.21	0.35	2.51	86.02	71.07
LV27-2-4	-175	1.22	0.35	2.57	86.24	70.93
LV27-2-4	-238	1.26	0.40	2.76	85.32	67.83
LV27-2-4	-303	1.34	0.54	2.77	80.58	59.94
LV27-2-4	-377	1.28	0.46	2.60	82.40	64.27
LV27-2-4	-447	1.35	0.59	2.42	75.56	56.12
LV27-2-4	-504	1.35	0.58	2.57	77.58	57.42
LV27-2-4	-572	1.40	0.64	2.61	75.42	54.06
LV27-2-4	-621	1.42	0.68	2.60	74.00	52.27
LV27-2-4	-674	1.45	0.70	2.74	74.34	51.36
LV27-2-4	-733	1.43	0.69	2.58	73.16	51.34
LV27-4-4	-4	1.52	0.84	2.63	68.12	44.83
LV27-4-4	-20	1.53	0.82	2.86	71.30	46.53
LV27-4-4	-87	1.53	0.86	2.61	67.16	43.94
LV27-4-4	-147	1.61	1.00	2.55	60.58	37.63
LV27-4-4	-177	1.62	0.98	2.72	63.86	39.38
LV27-4-4	-214	1.65	1.05	2.68	60.94	36.83
LV27-4-4	-244	1.55	0.88	2.63	66.42	42.88
LV27-4-4	-302	1.59	0.95	2.66	64.32	40.39
LV27-4-4	-360	1.63	0.99	2.75	63.92	39.21
LV27-5-3	-5	0.85	0.40	0.73	44.52	52.48
LV27-5-3	-34	1.34	0.56	2.49	77.40	57.86
LV27-5-3	-66	1.65	1.02	2.77	63.22	38.27
LV27-5-3	-95	1.55	0.87	2.74	68.22	43.94
LV27-5-3	-146	1.61	0.99	2.60	61.88	38.44
LV27-5-3	-176	1.76	1.21	2.72	55.64	31.57
LV27-5-3	-207	1.75	1.22	2.59	52.80	30.16
LV27-5-3	-236	1.71	1.14	2.66	56.98	33.26
LV27-5-3	-330	1.57	0.92	2.63	65.00	41.35
LV27-5-3	-430	1.81	1.32	2.60	49.26	27.20
LV27-5-3	-518	1.52	0.87	2.49	65.00	42.74
LV27-8-4	-8	1.15	0.23	2.95	92.22	80.07
LV27-8-4	-25	1.15	0.25	2.53	90.22	78.47
LV27-8-4	-60	1.15	0.25	2.61	90.60	78.71
LV27-8-4	-92	1.15	0.27	2.31	88.46	76.81
LV27-8-4	-130	1.18	0.28	2.80	89.90	76.10
LV27-8-4	-163	1.22	0.37	2.46	85.00	69.73
LV27-8-4	-206	1.34	0.55	2.57	78.50	58.70
LV27-8-4	-247	1.38	0.59	2.77	78.70	57.18
LV27-8-4	-319	1.35	0.54	2.79	80.52	59.72
LV27-8-4	-385	1.32	0.50	2.78	81.92	62.01
LV27-8-4	-456	1.33	0.52	2.79	81.36	60.98
LV27-8-4	-520	1.34	0.51	3.03	83.24	62.14

Table 5 A: Mechanical properties of sediments

Core number	Depth in core (cm)	Sediment density D, g/cm <sup>3</sup>	Density of mineral base Dp, g/cm <sup>3</sup>	Mineral density Dt, g/cm <sup>3</sup>	Volume humidity (porosity) Wv, %	Weight humidity Ww, %
LV27-8-4	-590	1.28	0.43	2.94	85.38	66.48
LV27-8-4	-630	1.27	0.40	3.13	87.20	68.55
LV27-8-4	-665	1.25	0.41	2.63	84.44	67.33
LV27-8-4	-698	1.27	0.43	2.69	84.16	66.40
LV27-8-4	-736	1.21	0.33	2.73	87.88	72.82
LV27-9-2	-18	1.17	0.27	2.65	89.84	76.94
LV27-9-2	-54	1.29	0.46	2.71	83.00	64.28
LV27-9-2	-92	1.35	0.56	2.65	79.04	58.69
LV27-9-2	-128	1.35	0.54	2.82	80.84	59.91
LV27-9-2	-163	1.33	0.53	2.59	79.42	59.80
LV27-9-2	-234	1.31	0.49	2.65	81.42	62.31
LV27-9-2	-304	1.29	0.46	2.67	82.60	64.01
LV27-9-2	-375	1.35	0.53	2.85	81.40	60.52
LV27-9-2	-450	1.39	0.61	2.71	77.44	55.90
LV27-9-2	-538	1.35	0.54	2.77	80.54	59.87
LV27-15	-10	1.24	0.38	2.65	85.78	69.46
LV27-15	-45	1.26	0.44	2.47	82.24	65.23
LV27-15	-80	1.41	0.64	2.78	76.84	54.40
LV27-15	-116	1.45	0.73	2.57	71.52	49.47
LV27-15	-151	1.41	0.64	2.72	76.34	54.26
LV27-15	-186	1.36	0.59	2.65	77.86	57.05
LV27-15	-220	1.43	0.68	2.69	74.52	52.13
LV27-15	-289	1.40	0.63	2.73	76.82	54.80
LV27-15	-355	1.46	0.74	2.65	72.06	49.28
LV27-15	-439	1.40	0.66	2.54	74.00	52.81
LV27-15	-538	1.43	0.68	2.73	75.02	52.36
LV27-16/1		1.38	0.60	2.74	78.18	56.63
LV27-16/2		1.43	0.75	2.37	68.44	47.82

Table 6A. Radiolarian distribution (%) in multicorer (MUC) surface sediment samples

Stations	1	2	3	4	5	6	7	8	11
<b>Radiolarians</b>									
1. <i>Acanthodesmia micropora</i>	10.8	12.1	9.4	6.4	4.0	3.9	7.0	6.3	8.1
2. ? <i>Amphumelissa setosa</i>									0.8
3. ? <i>Androcycias</i> sp.					0.3				
4. <i>Arachnocorys dubius</i>	9.7	13.2	10.9	10.6	15.6	11.0	6.6	13.4	6.8
5. <i>Artobotrys borealis</i>								0.5	
6. <i>Artostrobium aquilonaris</i>									0.4
7. <i>Astrosphaeridae</i> fam.	1.1	1.1		0.4			0.4		0.4
8. <i>Botryocampe inflata</i>	1.8	0.8	1.1	2.6	0.7	0.6	1.8	1.8	1.7
9. <i>Brobusta</i>	0.7	0.4			0.7	0.6	0.7	0.5	1.3
10. ? <i>Botryopera boreale</i>				0.4					0.4
11. <i>Cenosphaera</i> sp.	0.4	1.1	0.4	0.4	0.3	0.6	0.4		0.4
12. <i>Ceratocyrtus histicosa</i>	1.8	1.1	0.4	1.3	0.3	0.6	1.1	2.2	1.7
13. <i>Ceratocyrtis</i> sp.							0.4		
14. <i>Cladoscenum</i> sp.	0.4	1.1	1.1	0.4			0.7	1.3	0.4
15. <i>Cycladophora davisiana</i>	51.8	35.8	35.1	34.0	34.2	27.2	30.6	29.5	36.8
16. <i>C. davisiana</i> var. <i>cornutoides</i>		0.4						0.9	
17. <i>Cyrtolagena laguncula</i>	0.4								
18. <i>Cromyechinus borealis</i>		0.8				0.6	0.4	0.9	
19. <i>Cromyedrappa</i> sp.					0.3	0.6			
20. <i>Dictyophimus</i> sp.	0.4	0.4	1.1				0.7	0.5	0.4
21. <i>Enneapbormis rotula</i>	0.4	0.4	0.4						
22. <i>Echinomma delicatulum</i>				0.4		0.6			
23. <i>Eucyrtidium acuminatum</i>							0.4		
24. <i>Litharacium tentorium</i>	0.4	0.4	0.4	0.4	1.3		0.4		0.8
25. <i>Lithalius spiralis</i>	0.4	0.4	0.4		0.3		1.1		0.4
26. <i>Lithocampe platycephala</i>		0.4	0.4				0.7		
27. ? <i>Lithomelissa setosa</i>			0.4			0.6			
28. <i>Lithomitra arachnea</i>			0.4	1.7	0.3	1.3	0.4	0.9	1.3
29. <i>L. lineata</i>	0.4		0.4	0.4					
30. <i>Lophophaena</i> sp. 1								0.5	
31. <i>Lophophaena</i> sp. 2					0.3	0.6		0.5	0.4
32. <i>Peridium longispinum</i>	0.4		0.4	0.4			0.7	1.8	0.8
33. <i>Phormacantha hystrix</i>	0.4		0.4		0.3	1.3	1.5	0.5	
34. <i>Plagiocanthidae</i> fam.	0.4		0.4		0.3		0.7		
35. <i>Plectacantha oikiskos</i>	0.7		0.4				1.1		0.4
36. <i>Pylonidae</i> fam.				0.4	0.3				
37. <i>Pseudodictyophimus gracilipes</i>	6.5	9.7	7.6	2.6	1.4	9.0	7.0	5.4	7.7
38. <i>Pseudodictyophimus</i> sp.			0.4						
39. <i>Pterocanium</i> sp.	0.4								
40. <i>Pterocorys hirundo</i>	0.7	4.7	4.7	2.1	0.3	2.9	3.7	2.2	3.4
41. <i>Pterocorythium reschetnyakae</i> ?			0.4						
42. <i>Rhizoplegma boreale</i>	6.8	3.5	4.0	3.8	7.6	4.5	4.8	3.1	4.3
43. <i>Schizodiscus stylotrochoides</i>	0.4								
44. <i>Sethoconus tabularis</i>	1.4	0.8	0.7	3.4	1.1	3.2	3.7	5.4	2.1
45. <i>Spongodoscidae</i> fam.			0.7		1.1		1.1	0.5	
46. <i>Spongodiscus osculosus</i>						0.6			
47. <i>Spongotrochus glacialis</i>	0.4	0.4	0.7	11.9	2.9	5.2	2.6	3.6	1.3
48. <i>Spongurus pylomanticus borealis</i>				0.4	0.3	1.3			
49. <i>Stylatractus pyriformis</i>		0.4	1.1	0.8	0.3	0.6	3.3	2.2	3.4
50. <i>Stylochlamidium venustum</i>	1.1	0.8	1.4	2.6	12.0	7.8	4.0	9.4	3.8
51. <i>Stylodictya stellata</i>	0.4		0.4	1.7	0.7	0.6		0.5	0.8
52. <i>S. validispina</i>						0.6	0.4		
53. <i>Tholospyrus borealis</i>	5.0	5.1	10.9	6.8	9.8	8.4	7.0	5.8	6.0
54. <i>Trisulcus</i> sp.		0.4		0.8	0.3	0.6	0.7	0.9	0.4
55. <i>Tholospira</i> sp.									
56. Redeposited Tertiary rads	0.4	0.8		2.6	2.9	1.3	3.7	2.6	2.1
57. Indetermined rads	4.7	3.5	4.7	2.6	2.9	1.3	3.7	2.6	2.1
Rad content per 1 g of sediment	2,200	1,800	2,200	800	2,500	2,000	2,800	1,600	1,700



[illegible]



[illegible]

Table 8A. List of radiolarians found in sediments of core LV27-8-4.

1. *Acrosphaera lappacea*?
2. *Acrosphaera* sp.
3. *Acanthodeumia micropora*
4. *Amplimelissa setosa*
5. *Androcyclas gamphonycha*?
6. *Arachnocorys dubius*
7. *Arachnocorys* sp.
8. *Artobotrys borealis*
9. *Artostrobium aquilonaris*
10. *A. botryocytium*
11. *Artostrobium annulatus*
12. *A. joergensenii*
13. *Botryocampe inflata*
14. *B. robusta*
15. ? *Botryopera boreale*
16. ? *Carpocanium nigrinae*
17. *Cenosphaera cristata*
18. *Ceratocyrtis histricosa*
19. *Cladosoenum* sp.
20. *Clathromitridae* fam.
21. *Collosphaera huxley*?
22. *Collosphaera* sp.
23. *Comutella profunda*
24. *Cycladophora davisiana*
25. *C. davisiana* var. *comutoides*
26. *Cyrtolagena cuspidata*
27. *C. laguncula*
28. *Cromyechinus borealis*
29. *Cromyedrappa* sp.
30. *Dictyophimus* sp.
31. *Echinommina delicatulum*
32. *E. quadrisphaera*
33. *Eucyrtidium acuminatum*
34. *E. tusheri*
35. *Eucyrtidinae* fam.
36. *Lipmanella virchowii*
37. *Litharacnium tentorium*
38. *Lithelius spiralis*
39. *Lithocampe platycephala*
40. ? *Lithomelissa setosa*
41. *Lithomelissa thoracites*?
42. *Lithomelissa* sp.
43. *Lithonitra arachnea*
44. *L. lineata*

45. *L. nodosaria*
46. *Lophophaena hispida*?
47. *Lophophaena* sp.
48. *Lophophaenulæ* fam.
49. *Lophophaenoma* ? sp.
50. *Lychnocanium grande*
51. *Peridium longispinum*
52. *Peripyranis circumtexta*
53. *Phormacantha hystrix*
54. *Phorticium clevei*
55. *Plagiacanthidae* fam.
56. *Pylonidae* fam.
57. *Pseudocubus* ? sp.
58. *Pseudodictyophimus gracilipes*
59. *Pseudodictyophimus* sp.
60. *Pterocorys hirundo*
61. *Rhizoplegnia boreale*
62. *Sethocanus tabulatus*
63. *Spongodiscus osculosus*
64. *Spongotrochus glacialis*
65. *Spongurus pylonicus borealis*
66. *Spongodiscidae* fam.
67. ? *Spyrema halionuna*
68. *Stylatractus pyriformis*
69. *Stylochlanidium venustum*
70. *Stylodictya stellata*
71. *S. validispina*
72. *Tholospira* sp.
73. *Tholospyrus borealis*
74. Undetermined specimens

**Table 9 A: Dredge location and the description of dredge hauls**

Dredge	Date	Dredge Location		Depth (m)	Recovery
		Latitude, N	Longitude, E		
LV27-14	26.09.96	48°29,31´	151°02,09´	3050-2540	Rock fragments: lava and tuff of basalts, basaltic andesites, andesites, dacites unmetamorphosed and weakly metamorphosed; granites, granodiorites, diorites, gabbro; phyllites, argillites, cherts; Fe-Mn crusts. Pebbles are similar in composition as rock fragments
LV27-16	01.10.96	48°46,76´	151°56,17´	2450-2200	Rock fragments: tuff diatomaceous clays, diatomaceous oozes
LV27-17	02.10.96	48°18,39´	151°47,57´	3240-2600	Pebbles: lava and tuff of basalts, andesites, dacites; dolerites
LV27-18	02.10.96	48°19,06´	151°50,24´	2950-2600	Rock fragments: basalts pillow lava
LV27-19	03.10.96	49°39,82´	152°09,60´	1500-1300	Rock fragments: basalts; lava and tuff of basalts, andesites, dacites unmetamorphosed and weakly metamorphosed; argillites, greywakes; diorites, granodiorites, granites; metabasites and greenschist facies mafic schists; Fe-Mn crusts. Pebbles are similar in composition as rock fragments

**Table 10A: Gas composition and pH in the sediments, Okhotsk Sea**

NN	h (cm)	CH <sub>4</sub> (ml/l)	pH
LV27-1-2	-10	1	7.62
	-35	4	7.72
LV27-1-3	-516	2700	
LV27-gas	-10	70	7.49
	-40	1500	7.65
	-64	1300	7.68
	-88	900	7.78
	-120	1000	7.79
	-147	1500	7.86
	-180	6800	8.03
	-210	10200	8.04
	-245	8000	7.78
LV27-2-2	-30	30	7.72
LV27-2-4	-12	2.3	7.73
	-44	15	7.75
	-75	16.1	7.86
	-110	16.3	7.85
	-140	16.7	8.01
	-171	16.1	7.87
	-199	15.9	7.73
	-229	27	7.85
	-258	16.2	7.91
	-290	15.4	7.81
	-385	16.9	7.81
	-488	17.2	7.81
	-580	46.5	7.79
	-680	57.5	7.75
LV27-4-2	-25	1	7.68
LV27-4-4	-20	0.9	7.89
	-52	0.7	7.69
	-87	1.1	7.87
	-147	0.9	7.9
	-177	1.3	7.79
	-214	1.6	7.91
	-244	1	7.01
	-302	1.9	8.09
	-366	1.8	7.95
LV27-5-4	-5	1.3	7.68
	-34	1.1	7.92
	-66	1.3	7.77
	-95	1.3	7.8
	-146	1.4	7.9
	-176	1.5	8.03
	-207	1.6	8.03
	-236	1	7.89
	-330	1.8	8.06
	-430	1.4	7.77
	-518	1.9	7.97

Table 10A(cont.): Gas composition and pH in the sediments, Okhotsk Sea

NN	h (cm)	CH <sub>4</sub> (ml/l)	pH
LV27-8-4	-25	0.8	7.8
	-92	1.5	7.87
	-163	2	7.8
	-247	2.3	8.01
	-319	2	8.01
	-385	2.3	8.05
	-455	4.3	8.03
	-520	3.1	8.07
	-590	3.2	8.11
	-665	3.1	7.79
LV27-15	-10	0.8	7.65
	-45	0.8	7.91
	-80	1.1	7.99
	-116	1.4	7.91
	-151	1.1	7.99
	-186	1.5	7.87
	-220	1.6	8.09
	-289	1.9	8.03
	-355	2.3	7.93
	-538	3.4	7.91
LV27-9-4	-18	1.2	7.67
	-54	1.3	7.85
	-92	1.9	7.87
	-128	2.1	7.93
	-163	6.3	7.85
	-234	3.7	7.87
	-304	14.6	7.83
	-375	18.9	8.05
	-450	27.6	7.95
	-538	24.3	7.85
LV27-12-4	-18	1.2	7.79
	-61	2	7.95
	-104	2.3	7.91
	-155	4	8.07
	-205	2.9	8.31
	-277	4.7	8.4
	-349	6.6	8.33
	-420	10.1	8.03
	-526	10.3	8.01
	-654	36	8.09

Table 11A Gas composition and pH in the columns water, Okhotsk Sea

NN	h m	O <sub>2</sub> ml/l	N <sub>2</sub> ml/l	CO <sub>2</sub> ml/l	CH <sub>4</sub> n/l	pH
LV27-1-2	-1148	1.7	13.8	1.4	221	7.53
LV27-2-2	-1273				2000	7.53
LV27-3-2	-1476				50	7.58
LV27-4-2	-860	2.2	12.8	1.7	27	7.53
LV27-5-2	-50	6.8	10.2	0.5	60	
	-100	6	10.6	0.9	86	
	-200	4.5	11.2	1.1	88	
	-300				50	
LV27-5-5	-462	2.5	11.9	1.6	54	7.53
LV27-6-2	-878	1.7	12.6	1.8	20	7.63
LV27-7-2	-1172	3.8	9.5	0.6	67	7.73
LV27-8-2	-1147	2.5	13	1.74	44	7.63
LV27-11-2	-50	5.4	11.6	0.79	153	
	-100	5.2	10.7	0.8	189	
	-200	3.7	10.9	1.27	78	
	-300	3.2	11.1	1.47	53	
LV27-11-3	-1151	1.6	12.4	1.86	8	7.61
LV27-10-3	-3	5.3	9.9	0.37	69	
	-50	5.5	9.6	0.59	71	
	-100	4.1	10.1	0.93	102	
	-200	3.5	11.1	1.16	70	
	-300	3.3	11.8	1.46	51	
LV27-10-1	-1911	1.7	11.9	1.6	35	7.63
LV27-12-2b	-1296	1.8	12.6	1.8	12	7.69

## **Appendix V**

### **Sediment core description**



## Symbols used in graphical core descriptions

### Lithology



clay



silt



sand



silty clay



sandy silty clay



sandy silt



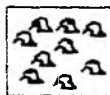
diatomaceous ooze



volcanic ash, glass



diagenetic horizon (often with authigenic clay minerals, dominantly smectite)



clay lumps (clasts)

ss

smear slide

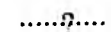
### Texture



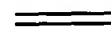
sharp boundary



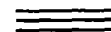
weak boundary



gradational boundary



stratification



lamination



broken disturbance



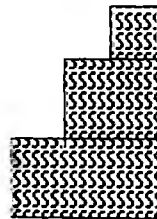
fining upwards



fining downwards



erosive surface



slight bioturbation

moderate bioturbation

strong bioturbation



vacuole (empty)



lense (filled)



dropstone



sponge spicules



wormtube



plant fragments



shell fragments



authigenic carbonaceous concretions



"ikaite" crystals



gradational color changes

LV27-1-2 MUC

Loc.: Upper slope off N-Sakhalin

KOMEX 96

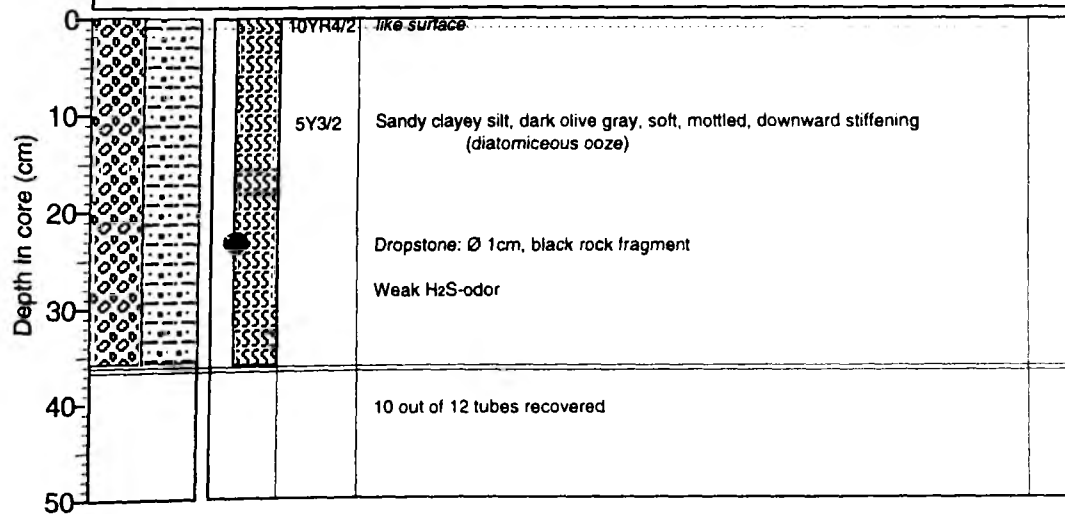
Recovery: 0.23-0.36 m

54° 34.56' N, 144° 28.36' E

Water depth: 1148 m

Lithology	Texture Color	Description	SS
-----------	---------------	-------------	----

Surface Sandy silty clay, dark brown, soft, mottled overlayn by 2 cm fluff-layer, dark brown (10YR4/2)



LV27-1-3 GC

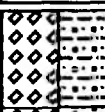

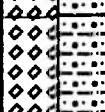


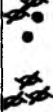
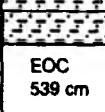
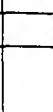
Loc.: Upper slope off N-Sakhalin

KOMEX '96

Recovery: 5.39 m

54°39.51' N 144°28.35' E

Water depth: 1141 m

(m)	Lithology	Core segment	Texture	Color	Description	SS
0.0		0-70		5Y3/2	Clayey sandy silt (diatomaceous ooze), dark olive gray, rich in diatoms and other biogenic particles (e.g. echinoderms), partly enriched in layers, black streaks and mottles, bioturbated, H <sub>2</sub> S odor	20 60
1.0		70-150		5Y3/2	Clayey sandy silt (diatomaceous ooze), as above, pebble at 103 cm, calcitic shell fragment (1 cm in length) at 130 cm	100 140
2.0		150-250		5Y3/2	Clayey sandy silt (diatomaceous ooze), as above, calcitic shell fragments at 179 cm and 204 cm, ooze reacts elastically	220 250
3.0		250-350		5Y3/2	Clayey sandy silt (diatomaceous ooze), as above, diatoms often concentrated in thick layers At 258: calcitic shell fragments At 273-277 cm: calcitic shell	270 300 340
4.0		350-450		5Y3/2	Clayey sandy silt (diatomaceous ooze), as above, but less black streaks and mottles Calcitic shell fragments at 359cm, 374 cm, 410 cm, 436 cm, 439 cm. Pebbles at 365 cm, 380 cm (0.5 cm in diameter)	360 400 440
5.0		450-491			Clayey sandy silt (diatomaceous ooze), as above, but less black streaks and mottles, few pebbles	470
		491-508		5Y4/2	Clayey silt, olive gray, black cloudy streaks, bioturbated	500
		508-539		5Y3/1	Silty clay, darker than overlying sediment (very dark gray), homogenous	520 539
	EOC 539 cm					
6.0						
7.0						
8.0						
9.0						
10.0						

LV27-1a-1 GC

Loc.: Cont. slope off N-Sakhalin

KOMEX '96

Recovery: 2.58 m

54° 26.59' N, 144° 04.58' E

Water depth: 692 m

Depth in core (m)	Lithology	Texture	Color	Description	SS
0			(5GY4/1) 5Y4/1	0-90 cm: Clayey silt, diatomaceous, dark (greenish) gray, strongly bioturbated (40%)  At 63 and 90 cm: Calcareous shell fragments  Whole core: strong H <sub>2</sub> S odor	
0.5					
1					
1.5			(5GY4/1) 5Y4/1	90-175 cm: Clayey sandy silt, diatomaceous, dark (greenish) gray  At 162 cm: Calcareous shell 150-175 cm: Small (30x10 mm) calcareous concretions, one large concretion (70x30x20 mm)	
2					
2.5					
3			(5GY4/1) 5Y4/1	175-258 cm: Clayey silt, dark (greenish) gray, disrupted sediment column on small scale (4-6 mm in the interval 175-230 cm, 1-3 mm at 230-258 cm), pores contain CH <sub>4</sub>  at 218, 236 cm: Calcareous shell fragments at 247 cm: Pebble	
3.5					
4					
4.5			(10Y4/2) 10Y4/2	--> Rock-Color Chart originally used --> transcript to Munsell Soil Color Chart	
5					

LV27-2-2 MUC

Loc.: Middle slope off N-Sakhalin

KOMEX 96

Recovery: 0.33-0.35 m

54° 30.11' N, 144° 45.33' E

Water depth: 1273 m

Lithology	Texture Color	Description	SS	
Surface	Sandy, silty, clay, dark brown, soft, mottled overlain by 2 cm fluff-layer, dark brown (10YR4/2), worm tubes			
Depth in core (cm)	0	10YR4/2	like surface Sandy clayey silt (diatomaceous ooze), dark brown, soft, mottled, gradational color change to olive	
	10	5Y3/2	Sandy clayey silt (diatomaceous ooze), dark olive gray, soft, mottled	
	20		Mollusk at 15 cm	Depth: 10-14 cm
	30	5Y3/2	Sandy silt (diatomaceous ooze), dark olive gray, stiff, bioturbated	
	40		10 out of 12 tubes recovered	
50				

LV27-2-3 GC

Loc.: Middle slope off N-Sakhalin

KOMEX '96

Recovery: 3.52 m

54°29.84' N 144°45.27' E

Water depth: 1301 m

(m)	Lithology	Core segment	Texture	Color	Description	SS
0.0				5Y3/2	Sandy silt, dark olive gray, mottled, soft, strongly disturbed	2
				5Y3/1	Clayey silt, homogenous, at 10 cm: lenses of dark olive gray sand (volcanic??), below 18 cm: increasingly black mottles and streaks	16
		0-62		5Y3/2	Sandy silt to silty sand, dark olive gray, bioturbated, rich in black grains, at 23 cm: pebble layer, well-rounded basalt and reddish quartz, at 33 cm: dropstone	27
				5Y3/1	Silty clay, very dark gray, bioturbated	40
0.5				5Y3/2	Silty clay, dark olive gray, bioturbated, with black streaks	48
				5Y3/1	Silty clay, very dark gray, bioturbated, few black streaks	57
						70
1.0		62-162		5Y3/1	Clayey silt to silty clay, very dark gray, bioturbated, few black streaks at 121-130 cm: increasingly black streaks and mottles at 94 cm: wood fragment at 132 cm: dropstone (2cm, rounded basalt)	93
						120
1.5						150
2.0		62-162		5Y3/1		180
						210
2.5					Clayey silt to silty clay, very dark gray, bioturbated, homogenous, strong H <sub>2</sub> S-odor,	230
						250
				5Y3/1	At 173 cm: dropstone (2cm, basalt), Below 234 cm: increasingly black streaks and mottles At 304-308cm: sand lense	263
3.0						287
		262-352				320
						340
3.5						352
	EOC 352 cm					
4.0						
4.5						
5.0						

LV27-2-4 GC

Loc.: Middle slope off N-Sakhalin

KOMEX '96

Recovery: 7.38 m

54°30.15' N 144°45.14' E

Water depth: 1305 m

Depth in core (m)	Lithology	Texture	Color	Description	SS
0.0			(5GY5/2) 5Y5/6?	0-170 cm: Clayey silt (diatomaceous ooze), homogenous, (dusky yellow green) olive	
0.5				At 61 cm: Gravel	
1.0				At 105 cm: Gastropod shell	
1.5			(10Y4/2) 5Y4/2	Strong H <sub>2</sub> S odor in entire core	
2.0				At 180, 265 cm: calcereous shell fragments	
2.5				At 210, 220 cm: pebbles	
3.0			(5GY3/2) 5Y3/2	170-330 cm: Clayey silt, slightly diatomaceous, olive gray, homogenous	
3.5				Clayey silt, grayish olive (green), homogenous, diatoms abundant	
4.0					
4.5			(5GY4/1) 5Y4/1	Clayey silt, (olive) gray, thinly laminated, with olive black interlayers (0.5-1 mm)	
				Silty clay, dark greenish (olive) gray, homogeneous, onset of significant authigenic pyrite abundance	
				As above, with clay lumps texture	
5.0					

LV27-2-4 GC cont.

Loc.: Middle slope off N-Sakhalin

KOMEX '96

Recovery: 7.38 m

54°30.15' N 144°45.14' E

Water depth: 1305 m

(m)	Lithology	Texture	Color	Description	SS
5.0			(5GY3/2) 5Y3/2	496-518 cm: Silty clay, dark (greenish) olive gray, stiff	
			(5Y3/2) 5Y3/2	518-553 cm: Clayey silt, dark (olive) gray, thin lamination at 518-521 cm and 538-541 cm, occasional pebbles At 536 cm: Fish bones	
5.5			(5Y3/2) 5Y3/2	At 553-585 cm: Clayey silt, dark (olive) gray, thinly laminated (0.3-1.5 mm) At 570-575 cm: Layer of calcareous concretions, hard	
6.0			(5GY3/2) 5Y3/2	Clayey silt, grayish olive (green), homogenous  At 617 and 682 cm: Vacuoles (30x40 mm), possibly contained gashydrates !  At 720 cm: Dropstone	
6.5			(10Y4/2) 10Y4/2	-> Rock-Color Chart originally used -> transcript to Munsell Soil Color Chart	
7.0					
7.5					
8.0					
8.5					
9.0					
9.5					
10.0					

Depth in core (m)

EOC  
738 cm



LV27-3-2 MUC

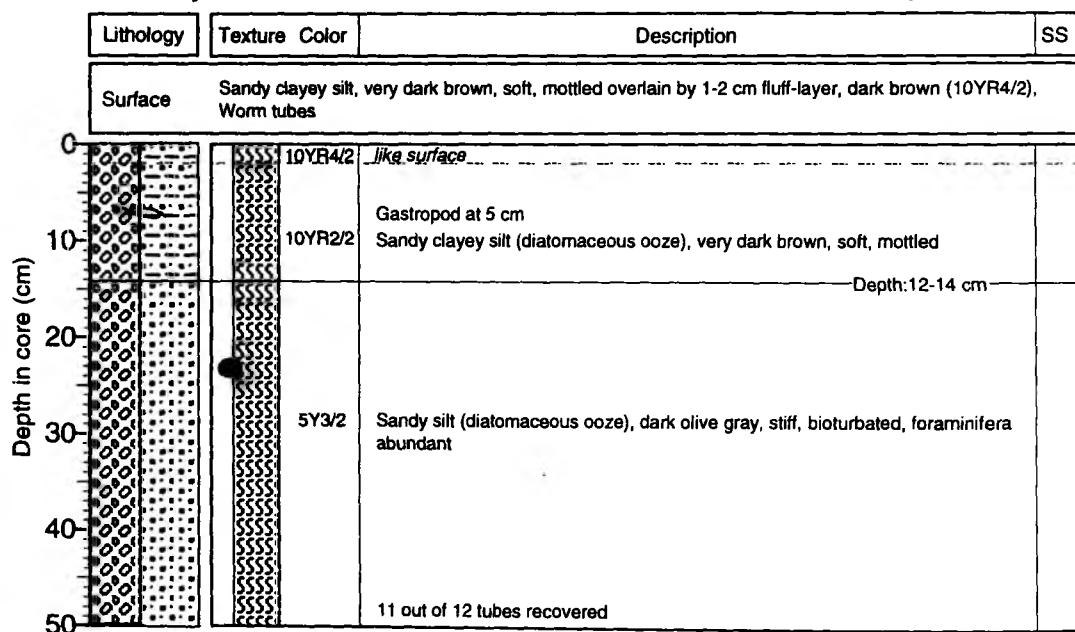
Loc.: Lower slope off N-Sakhalin

KOMEX 96

Recovery: 0.02-0.51 m

54° 24.83' N, 145° 08.41' E

Water depth: 1471 m



LV27-3-3 GC

Loc.: Lower slope of N-Sakhalin

KOMEX '96

Recovery: 5.65 m

54°24.60' N 145°07.60' E

Water depth: 1477 m

(m)	Lithology	Core segment	Texture	Color	Description	SS
0.0		0-75		5Y3/2	Sandy silt, dark olive gray, bioturbated, mottled, cloudy streaks	1
				5Y4/1	Clayey silt, homogenous, bioturbated, strong H <sub>2</sub> S-odor	15
						25
0.5		75-96		5Y3/2	Sandy silt, dark olive gray, partly laminated, uneven basal and upper contact	35
						50
				5Y3/2	Clayey silt, homogenous, bioturbated, strong H <sub>2</sub> S-odor	60
1.0		96-176				70
				5Y4/1	Clayey silt, homogenous, bioturbated, strong H <sub>2</sub> S-odor, black streaks and mottles common	110
						140
1.5		176-276				170
2.0				5Y4/1	Clayey silt, homogenous, bioturbated, strong H <sub>2</sub> S-odor, black streaks and mottles common	200
					At 195cm: dropstone (1cm in diameter) At 207-208cm: dropstone (1cm in diameter)	230
2.5		276-376		5Y3/2	Below 220cm: slightly darkening due to increasing black mottles and streaks	270
3.0						
3.5				5Y3/2	Clayey silt, homogenous, bioturbated, strong H <sub>2</sub> S-odor, black streaks and mottles common At 329-330cm: pebble layer At 344-345cm: sandy layer	
4.0		376-476				380
				5Y3/1	Clayey silt, homogenous, bioturbated, strong H <sub>2</sub> S-odor, black streaks and mottles common	420
4.5					At segment base (476cm): large ikaite crystal (ca. 10cm in length)	460
5.0					Clayey silt, homogenous, bioturbated, strong H <sub>2</sub> S-odor, black streaks and mottles common	490



LV27-3-3 GC cont. Loc.: Lower slope of N-Sakhalin

KOMEX '96

Recovery: 5.65 m

54°24.60' N 145°07.60' E

Water depth: 1477 m

(m)	Lithology	Core segment	Texture	Color	Description	SS
5.0		475-585		5Y3/1	Clayey silt, homogenous, bioturbated, strong H <sub>2</sub> S-odor, black streaks and mottles abundant	520
5.5					At 523cm: rests of ikaites At 537cm: large shell fragment (3cm)  Below 540cm: sediment becomes more stiff and more olive	550
	EOC 585cm					
6.0						
6.5						
7.0						
7.5						
8.0						
8.5						
9.0						
9.5						
10.0						

Depth in core (m)

LV27-4-2 MUC


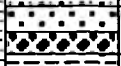


Loc.: S-slope of Kashevarov Rise

KOMEX 96

Recovery: 0.24-0.27 m

55° 03.43' N, 145° 44.08' E

Water depth: 860 m

Lithology	Texture Color	Description	SS
Surface Silty sand, brown, with mica platlets, bioturbated overlain by 0.5 cm fluff-layer, brown (10YR4/1), worm tubes, ophiolites			
Depth in core (cm)		10YR4/1	Silty sand, dark brown, with mica, bioturbated, several large dropstones (up to 2 cm Ø) at 4-6 cm: basalt with large feldspar crystals
		10YR2/2	Sand, dark brown, gradational color change to olive with pebble layer at 9-11 cm; pebbles: basalt, granite, sandstones, metamorphites Depth: 4-11 cm
		5Y3/2	Clayey silty sand dark olive gray, bioturbated  10 to 15 cm single basalt pebbles, partly well rounded
		5Y3/1	Sandy clayey silt, dark gray, stiff, bioturbated Depth: 12-23 cm
			11 out of 12 tubes recovered

LV27-4-3 GC

Loc.: S-Slope of Kashevarov Rise

KOMEX '96

Recovery: 5.52 m

55°03.22' N 145°44.19' E

Water depth: 865 m

(m)	Lithology	Core segment	Texture	Color	Description	SS
0.0		0-74		5Y3/1	Silty sand, very dark gray with large dropstone at base (3 cm in diameter), sharp lower contact	2
				5Y3/2	Sandy silt, homogeneous, dark olive gray, dark olive mottles and streaks, at 38-40 cm diatom. ooze	10 30 39 50
		74-154		5Y3/2	Sandy silt, homogeneous, dark olive gray, dark olive mottles and streaks, at 70 cm diatom. ooze, at 57 cm dropstone (1 cm in diameter)	90
1.0				5Y3/2	Sandy silt, homogeneous, dark olive gray, dark olive mottles and streaks, sand lenses at 100 cm and 138 cm, at 148-152 cm large dropstones (-5 cm in diameter), below 120 cm increasing number of pebbles.	120 138
		154-254		5Y3/2	Sandy silt, homogeneous, dark olive gray, increasing number of dark olive mottles and streaks below 2.2m, pebbles all over core, at 190-210 cm large dropstones (-5 to 10 cm in diameter)	150 170 220 230 250
2.0		254-354		5Y3/1	Sandy silt, dark olive gray, stiff, slightly layered, increasingly sandy At 263-270 cm: gravel layer (1-2 cm in diameter)	260
				5Y3/2	Below: silty sand enriched in dropstones and black sand lenses and gravel layers, coarse and stiff sediment	300
3.0		354-452		5Y3/1	Clayey silty sand, slightly finer than above, stiff, laminated, black layers, less dropstones, at 329-330 cm layer of gravel	330 350
				5Y3/2	Silty sand, homogeneous, bioturbated, rich in dropstones At 410-420 cm lenses and layers of sand (1 cm thick)	370 400 440
4.0		452-552		5Y3/2	Silty sand, homogeneous, bioturbated, rich in dropstones	470
				5Y4/2	At 533 cm: layer of gravel	500
5.0				5Y3/1		540
6.0	EOC 552 cm					
7.0						
8.0						
9.0						
10.0						

LV27-4-4 GC

Loc.: S-slope of the Kashevarov Rise

KOMEX '96

Recovery: 3.88 m

55° 03.54' N, 145° 44.16' E

Water depth: 857 m

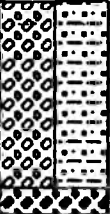
	Lithology	Texture	Color	Description	SS
0.0			(10Y4/2) 5Y4/2	0-11 cm: sandy silt (diatomaceous ooze), olive gray, abundant foraminifera and coccoliths; at 10 cm pebbles and gravel	0 10 25
			(5G4/1) 5Y4/1	11-73 cm: clayey silty sand, dark gray, abundant coccoliths, pebbles and gravel vertical worm tube filled with overlain sediment, sand lense at 50 cm	40 60
0.5			(5G4/1) 5Y4/1	73-131 cm: clayey silty sand, dark gray, homogenous, moderate hard, bioturbated horizon at 85 cm with sand lenses, various pebbles, weakly laminated around 100 cm 100-120 cm: abundance of coccoliths	80 100 120 130
1.0					
1.5			(5G4/1) 5Y4/1	131-180 cm: sandy silt, dark gray, homogenous, more stiff than overlying section, amount of pebbles, gravel and sand increases from 145 cm downward, weakly laminated between 150 and 160 cm, sand lense at 150 cm few coccoliths at 150 cm	150 170
2.0					
2.5			(5G4/1) 5Y4/1	180-212 cm: sandy silt, dark gray, homogenous, stiff, intercalated sand lenses and thin sand layer	190 205
3.0					
3.5			(5G4/1) 5Y4/1	212-262 cm: sandy silt, dark gray, homogenous, softer than above section, intercalated thin sand layer at 228, 244, 260-262 cm at 240 and 260 cm: pebbles	225 240 258
4.0					
4.5			(5G4/1) 5Y4/1	262-310 cm: silty clay, dark gray, homogenous, weakly bioturbated in the lower section, stiff at 260-270 cm: pebbles at 300 cm: layer enriched in volcanic glass	280 300
5.0					
5.5			(5G4/1) 5Y4/1	310-388 cm: sandy, silty clay, dark gray, homogenous, stiff with abundant pebbles several diagenetic horizons intercalated, greenish (like copper oxide), very stiff	320 335 350 370 380
6.0					
6.5	EOC 388 cm			(10Y4/2) --> Rock-Color Chart originally used 10Y4/2 --> transcript to Munsell Soil Color Chart	
7.0					
7.5					
8.0					
8.5					
9.0					
9.5					
10.0					

LV27-5-5 MUC

Loc.: SW-slope of North Okhotsk Rise

KOMEX 96

Recovery: 0.10-0.22 m 54° 40.56' N, 149° 32.22' E Water depth: 462 m

Lithology	Texture Color	Description	SS
Surface		Silty sand, dark brown, soft, mottled overlain by <1 cm fluff-layer, dark brown (10YR4/2)	SS
Depth in core (cm)		10YR4/2	<i>like surface</i>
		5Y3/2	Sandy silt (diatomaceous ooze), dark olive gray, soft, mottled, downward stiffening
			Gravel grading upward to sand, basalt and quartz pebbles
			11 out of 12 tubes recovered

LV27-5-4 GC

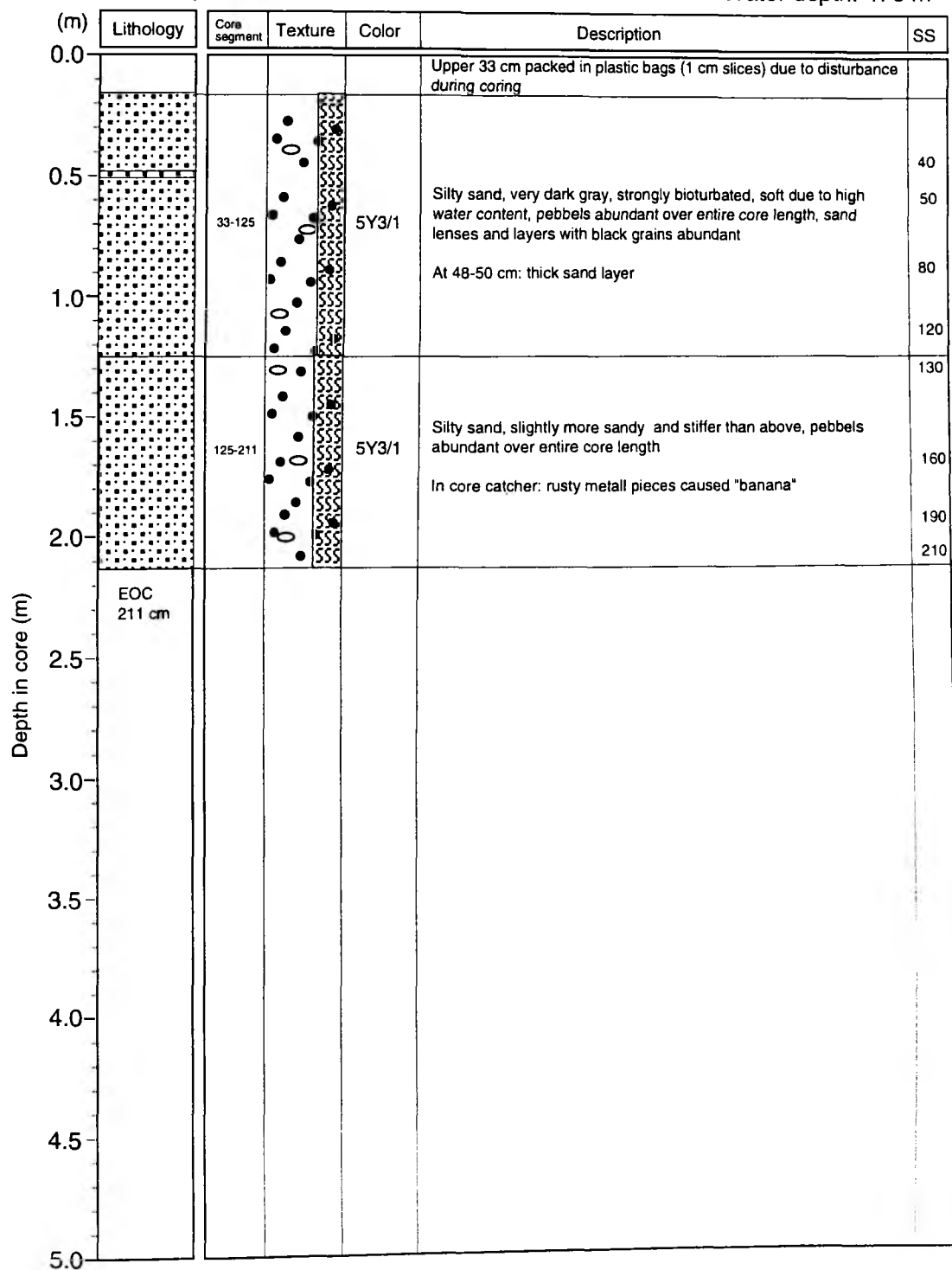
Loc.: SW-slope of North Okhotsk Rise

KOMEX '96

Recovery: 2.11 m

54°47.41' N 149°29.29' E

Water depth: 476 m





LV27-5-3 GC

Loc.: SW-Slope of North Okhosk Rise

KOMEX '96

Recovery: 5.42 m

54°44.09' N 149°29.91' E

Water depth: 482 m

(m)	Lithology	Texture	Color	Description	SS
0.0			(10Y5/4) 5Y4/4	0-35 cm: Clayey silt (diatomaceous ooze), homogenous, olive (gray), increasing sand content downward	0 10 30 35
				Below 27 cm on: sand lenses and gravel and pebbles	
0.5			(10Y5/4 to 5GY5/2)	35-58 cm: Clayey, sandy silt, mottled, gradual color change from olive to gray color at 46 cm	45 55
			(5G4/1) 5Y4/1	58-121 cm: Clayey silt, gray, homogenous, occasional sand lenses, downward increasing sand content	63 80 95 110
1.0			(5G4/1) 5Y4/1	121-228 cm: Clayey, sandy silt, gray, homogenous, stiff, occasionally sand lenses, random pebbles below 200 cm	135 145 165
1.5				At 180 cm: Up to 5 % volcanic glas	180
2.0				At 211 cm: Small lenses of silty volcanic ash (acidic composition)	200 220
			5Y3/1	228-232 cm: Silty sand, (very) dark gray, homogeneous	
2.5			(10Y4/2) 5Y4/2	232-314 cm: Clayey silt, olive gray, homogenous, stiff, occasional sand lenses and layers (up to 0.15 cm size) At 263-270 cm: occurrence of sponge spicules At 280 cm: 7 to 10 % diatom content	240 260 280 300
3.0			(10Y4/2) 5Y4/2	314-324 cm: Clayey silt, olive gray, intercalated with sand and silt layer, stiff, thin sand layer (2-3 cm thick) at 223-224 cm	310
			(5Y4/2) 5Y5/2	324-335 cm: Clayey, sandy silt (diatomaceous), olive gray, above 328 cm irregular color pattern (more olive), strongly bioturbated, stiff	325 330
3.5			(5G4/1) 5Y4/1	At 350 cm: authigenic calcite nodule (1x0.7 cm) 335-401 cm: Clayey sandy silt, gray, stiff, with gravel and pebbles of various size, occasional sand lenses At 380 cm: horizon enriched with volcanic glas (up to 5 %)	345 360 380 400
4.0			(10G4/2) 5Y4/2	Clayey silt, olive gray, homogenous, stiff, quantity of sand lenses reduced in comparison with unit above, alternating thin layers (2-3 mm) of sand/silt and fine silt below 480 cm	410 440 450 470
4.5					
5.0					490

LV27-5-3 GC cont.

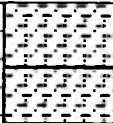
Loc.: SW-Slope of North Okhosk Rise

KOMEX '96

Recovery: 5.42 m

54°46.09' N 149°29.91' E

Water depth: 482 m

(m)	Lithology	Texture	Color	Description	SS
5.0			(10G4/2) 5Y4/2	485-532 cm: Clayey silt, olive gray, homogenous, stiff, sand content decreases to base, diatom content increases below 510 cm (to 5-7 %)	510
				Same as above but diatom content increased to 20-25 %	532
5.5	EOC 542cm				
6.0					
6.5					
7.0					
7.5					
8.0					
8.5					
9.0					
9.5					
10.0					

LV27-6-2 MUC

Loc.: SW-slope of North Okhotsk Rise

KOMEX 96

Recovery: 0.20-0.26 m

54°09.81' N, 149° 30.09' E

Water depth: 878 m

Lithology	Texture	Color	Description	SS
Surface      Silty sand, dark brown, soft, mottled overlain by <1 cm fluff-layer, dark brown (10YR4/2)				
		10YR4/2	<i>like surface</i>	
		5Y3/2	Sandy silt (diatomaceous ooze), dark olive gray, soft, mottled, downward stiffening	
			Gravel layer, basalt and quartz pebbles	
		5YR3/3	Silty sand, dark reddish brown (ash layer ?)	
			11 out of 12 tubes recovered	

LV27-6-3 GC

Loc.: SW-slope of North Okhotsk Rise

KOMEX '96

Recovery: 0.89 m

54°09.87' N 149°30.33' E

Water depth: 868 m

(m)	Lithology	Core segment	Texture	Color	Description	SS
0.0				5Y4/4	Sand rich in large dropstones (-5 cm), brownish	0
0.5		0-89		5Y3/1	Coarse sand, very dark gray, pebbles all over core At 20 cm: small rusty crust At 59 cm and 84-89 cm: gravel layer	20 49 88
1.0	EOC 89 cm					
1.5						
2.0						
2.5						
3.0						
3.5						
4.0						
4.5						
5.0						

LV27-6-4 GC

Loc.: SW-Slope of North Okhosk Rise

KOMEX '96

Recovery: 1.86 m

54°09.73' N 149°30.09' E

Water depth: 872 m

(m)	Lithology	Texture	Color	Description	SS
0.0			(10Y4/2) 5Y4/2 (5G4/1) 5Y4/1 (5G4/1) 5Y4/1 (5G4/1) 5Y4/1	0-11 cm: Sandy silt (diatomaceous), homogenous, olive (gray), soft, dropstone at 3 cm 11-29 cm: Clayey, silty sand, bioturbated, gray, stiff, few gravels incorporated, coccoliths abundant 29-48 cm: Clayey silty sand, bioturbated, gray, few intercalated sand lenses, pebbles between 32 and 48 cm 48-82 cm: Clayey silty sand, gray, intercalated sand lenses, pebbles and thin layer of sand increasing downward, very stiff between 80-82 cm, few randomly distributed pebbles 82-140 cm: Silty sand, gray, weakly bioturbated, occasional sand lenses, randomly distributed pebbles At 105 cm: Increase of volcanic glass content (up to 2 %) At 110 cm: Lense with well sorted sand 140-145 cm: Silty sand, bioturbated, gray, stiff 145-186 cm: Silty sand, gray, stiff horizon at 173-180 cm, occasional sand lenses, few pebbles at 184 cm, some coccoliths and volcanic glass content up to 5-7 %	
0.5					
1.0					
1.5					
2.0	EOC 186 cm		(10Y4/2) 10Y4/2	--> Rock-Color Chart originally used --> transcript to Munsell Soil Color Chart	

LV27-7-2 MUC

Loc.: Derugin Basin

KOMEX 96

Recovery: 0.25-0.39 m 53° 14.28' N, 149° 34.37' E Water depth: 1150 m

Lithology	Texture Color	Description	SS
Surface Sandy silty clay, dark brown, soft, mottled overlain by 1 cm fluff-layer, dark brown (10YR4/2)			
Depth in core (cm)	0		
	10	10YR4/2	Sandy clayey silt (diatomaceous ooze), dark brown, soft, mottled
	20	5Y3/2	Sandy clayey silt (diatomaceous ooze), dark olive gray, mottled, stiffening downward
	30		Black pebble, basalt, rounded
	40	10 out of 12 tubes recovered	
50			

LV27-7-3 GC

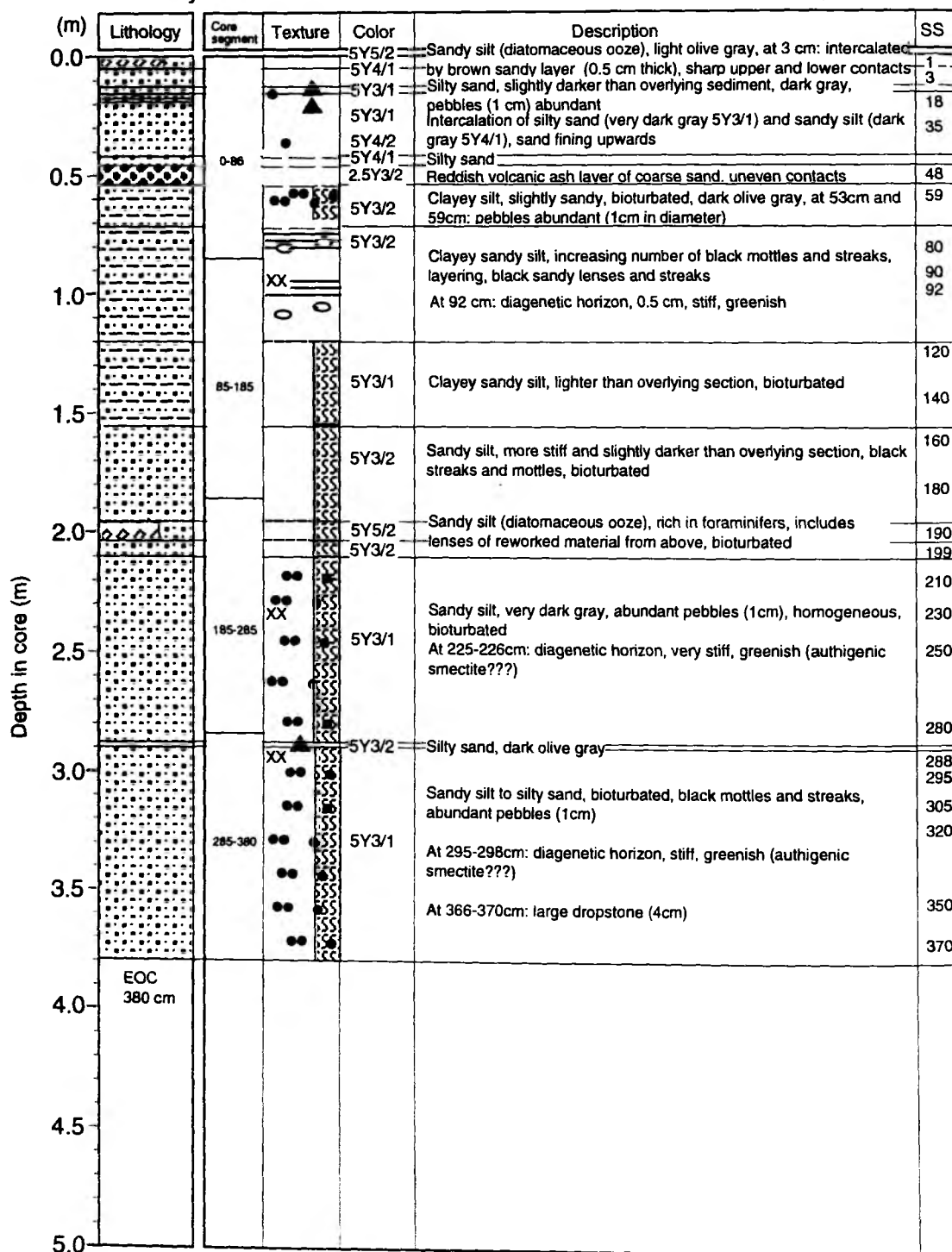
Loc.: E-Derugin Basin

KOMEX '96

Recovery: 3.80 m

53°15.27' N 149°35.73' E

Water depth: 1140 m



LV27-8-2 MUC



Loc.: Makarov Trough

KOMEX 96

Recovery: 0.26-0.31 m

51° 29.82' N, 150° 30.73' E

Water depth: 1147 m

Lithology	Texture	Color	Description	SS
Surface      Sandy silty clay, dark brown,soft, mottled overlain by 1 cm fluff-layer, dark brown (10YR4/2)				
0  10  20  30  40  50 Depth in core (cm)			10YR4/2      Sandy, clayey silt (diatomaceous ooze), dark brown,soft, mottled at 3 cm: benthic foraminifera Pyrgo sp.	
			5Y3/2      Sandy clayey silt (diatomaceous ooze), dark olive gray, mottled, stiffening downward	
			9 out of 12 tubes recovered	



LV27-8-3 GC

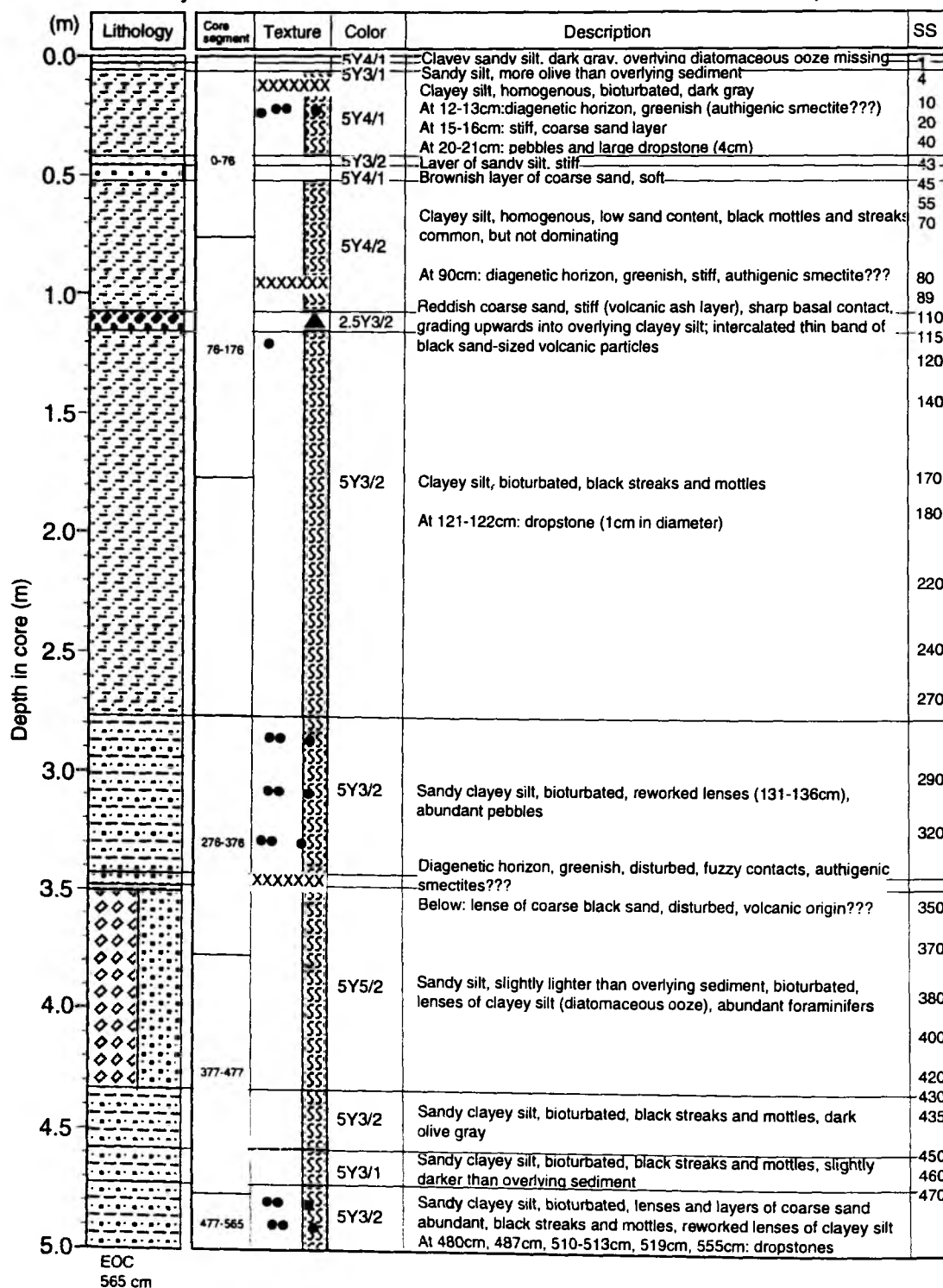
Loc.: Makarov Trough

KOMEX '96

Recovery: 5.65 m

51°29.88' N 150°32.46' E

Water depth: 1160 m



LV27-8-4 GC

Loc.: Makarov Trough Basin

KOMEX '96

Recovery: 7.60 m

51°30.20' N 150°34.29' E

Water depth: 1144 m

(m)	Lithology	Texture	Color	Description	SS
0.0			(10Y5/4) 5Y4/4	0-14 cm: Clayey silt (diatomaceous ooze), homogenous, olive brown, oxidation layer, soft in the upper 5 cm (high water content)	
0.5			(5GY5/2) 5Y5/6?	14-96 cm: Clayey silt (diatomaceous ooze), homogenous, (dusky yellow green) olive, rare foraminifera tests	
1.0			(5Y5/2) 5Y5/2	96-140 cm: Silty clay, diatomaceous, homogenous, (light) olive gray	
1.5			(5GY5/2) 5Y5/6?	140-154 cm: Clayey silt, diatomaceous, homogenous, (dusky yellow green) olive, rare foraminifera tests	
			5Y7/1?	154-157 cm: Coarse silt to fine sand, volcanic ash, light gray	
				154-180 cm: similar to 140-154 cm	
				At 182 cm: Lense of greenish authigenic lumps	
2.0			(5GY4/1) 5Y4/1	180-207 cm: Clayey silt, homogenous, gray, mottled 191-200 cm: Lenses filled with diatomaceous ooze mottled from above	
2.5			5Y3/2	207-360 cm: Silty clayey sand, olive gray with lenses and intercalated layers of sandy silt and silty sand  At 290-293, 302-303, 308-310, 337-339, 345-347 cm: Lenses and layer of dense greyish green authigenic clays	
3.0				At 310-315 cm: Gravel abundant	
3.5				321-327 cm: Lense of light gray volcanic ash	
			5Y4/1	360-376 cm: Clayey sandy silt, dark (olive) gray, homogeneous	
4.0			(5GY5/2) 5Y5/6?	At 372 and 394 cm: Dropstones 393-412 cm: Small grayish green clay lumps 376-462 cm: Silty clay, (dusky yellow green) olive, homogenous, occasional sand admixtures	
4.5			5Y4/1	462-505 cm: Clayey silt, dark (olive) gray, homogeneous, with occasional sand admixtures, pebbles at 471, 480, and 500 cm	
5.0					

LV27-8-4 GC cont.

Loc.: Makarov Trough

KOMEX '96

Recovery: 7.60 m

51°30.20' N 150°34.29' E

Water depth: 1144 m

(m)	Lithology	Texture	Color	Description	SS
5.0			(5G4/1) 5Y4/1	505-595 cm: Clayey silt, dark (olive) gray, homogenous, diatom abundant, increasing in abundance at 575-590 cm	
5.5				At 591 cm: Dropstone	
6.0			(5GY3/2) 5Y3/2	At 610 cm: Calcareous shell fragment	
6.5				At 628- 632 cm: Dropstones	
7.0			(5GY3/2) 5Y3/2	595-710 cm: Sandy silty clay, dark (greenish) olive gray, homogenous	
7.5				At 650,655 cm: dropstone	
7.0			(5GY3/2) 5Y3/2	700-710 cm: Significant increase in sand content	
7.5				700-732 cm: Sandy silt (diatomaceous ooze), (light) olive gray (brown), gravity turbation from overlaying unit (boundary disturbance)	
7.5			(5Y5/6) 2.5Y5/6	732-760 cm: Sandy silt (diatomaceous ooze), some gradational color changes to light olive brown, occurrence of foraminifera (up to 20 %), lenses of light ooze (2.5Y5/6)	
8.0			(10Y4/2) 10Y4/2	→ Rock-Color Chart originally used → transcript to Munsell Soil Color Chart	
8.0	EOC 760 cm				
8.5					
9.0					
9.5					
10.0					

LV27-9-4 GC

Recovery: 5.40 m

Loc.: E-slope of Academy of  
Sciences Rise

50°00.76' N 152°28.43' E

KOMEX '96

Water depth: 1400 m

(m)	Lithology	Core segment	Texture	Color	Description	SS
0.0				5Y4/2	Sandy silt, dark olive gray, homogenous (diatomaceous ooze)	0
		0-50		5Y4/1	At 10 cm: dropstone (0.5 cm in diameter), at base slightly darker	15
				5Y7/1	Clayey sandy silt, weak diatomaceous, includes patches of sand from below, bioturbation	30
0.5				5Y4/1	At 34-38 cm: white grayish sand layer (volcanic???), sharp base, upwards strongly bioturbated	38
					Clayey sandy silt as above, rich in diatoms and foraminifers	45
		50-152		5Y3/1	Clayey silt, homogenous, bioturbated, with reworked lenses of diatom-rich clayey sandy silt, very dark gray, downward increasingly black streaks and mottles	55
1.0					At 78-79 cm: traces of calcareous shell fragments	65
					At 96-97 cm: traces of calcareous shell fragments	80
1.5						120
		152-252		5Y3/1	Clayey silt, homogenous, bioturbated, black streaks and mottles, no more diatomaceous lenses, pebbles all over segment	150
2.0					At 173 cm, 185 cm, 188 cm, 220 cm: dropstones	
					At 167 cm: calcareous shell fragment	
2.5						
		252-352		5Y3/1	Clayey silt, homogenous, bioturbated, black streaks and mottles, pebbles all over segment	
3.0					At 252-263 cm: reworked volcanic ash, sand lenses	
3.5						
		352-451			Clayey silt, homogenous, bioturbated, black streaks and mottles, pebbles all over segment	360
4.0					At 376 cm: sand lense	400
					Below 383 cm: slightly darker than above	440
4.5		451-540		3Y3/2	Clayey silt, homogenous, bioturbated, black streaks and mottles	460
					At 477-503 cm: strongly mottled area, bioturbation	490
5.0						

LV27-9-4 GC cont.

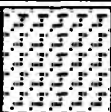
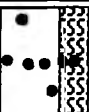
Loc.: E-slope of Academy of  
Sciences Rise

KOMEX '96

Recovery: 5.40 m

50°00.76' N 152°28.43' E

Water depth: 1400 m

(m)	Lithology	Core segment	Texture	Color	Description	SS
5.0		451-540		5Y3/1	Clayey silt, homogenous, bioturbated, black streaks and mottles In core catcher: diatomaceous ooze	520 539
5.5	EOC 540 cm					
6.0						
6.5						
7.0						
7.5						
8.0						
8.5						
9.0						
9.5						
10.0						

LV27-10-1 MUC

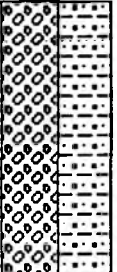
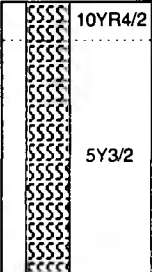
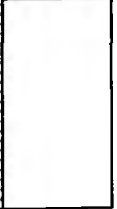

Loc.: Atlasov Trough

KOMEX 96

Recovery: 0.18-0.28 m

48° 57.74' N, 152° 09.34' E

Water depth: 1911 m

Lithology	Texture Color	Description	Age
Surface	Sandy silty clay, dark brown, soft, mottled overlain by 1 cm fluff-layer, dark brown (10YR4/2)		
Depth in core (cm)			10YR4/2 Sandy clayey silt, (diatomaceous ooze) dark brown, soft, mottled
			5Y3/2 Sandy clayey silt, (diatomaceous ooze), dark olive gray, mottled, stiffening downward
			10 out of 12 tubes recovered

LV27-10-5 GC

Loc.: Atlasov Trough

KOMEX '96

Recovery: 5.79 m

48°57.36' N 152°08.29' E

Water depth: 1906 m

(m)	Lithology	Core segment	Texture	Color	Description	SS
0.0		0-18		5Y4/2	Sandy silt, dark olive gray, homogenous (diatomaceous ooze), upper 18 cm were found in corer weight, slightly disturbed, packed in 1cm slices in plastic bags	20
0.5		18-94		5Y4/2	Sandy silt, dark olive gray, homogenous (diatomaceous ooze)	60
1.0				5Y3/2	Below 65 cm: gradual color change to darker ooze, lenses of lighter diatomaceous ooze included (at 76 cm, 80 cm) At 87 cm: dropstone (0.5 cm in diameter)	90 100
1.5		94-194		3Y3/1	Clayey sandy silt, homogenous, abundant black streaks and mottles	140
				2.5Y3/2	Sand (volcanic ash), uneven contacts	159
2.0				3Y3/1	Clayey sandy silt, homogenous, bioturbated, black streaks and mottles	170 190
2.5		194-294		3Y3/2	At 210 cm: dropstone (1 cm in diameter)	210
				2.5Y3/2	At 255-258 cm: sand lense, 3 cm in diameter (volc. ash)	250 257
3.0				3Y3/2	Clayey sandy silt, homogenous, bioturbated, black streaks and mottles, small calc. shell fragments common	290 310
3.5		294-394		3Y3/2	At 340 cm: dropstone (0.5 cm in diameter) At 358 cm: dropstone (0.5 cm in diameter)	350
4.0					At 394-402 cm: greenish diagenet. horizons (authig. smectite???)	390 410
4.5		294-394			Sand, white, sharp base, grading from 427-420 cm upward (volcanic ash)	428
5.0				3Y3/2	Clayey sandy silt, homogenous, bioturbated, black streaks and mottles, small calc. shell fragments common At 464 cm: sand lense	460 464 490

LV27-10-5 GC cont.

Loc.: Atlasov Trough

KOMEX '96

Recovery: 5.79 m

48°57.36' N 152°08.29' E

Water depth: 1906 m

(m)	Lithology	Core segment	Texture	Color	Description	SS
5.0		494-579		3Y3/2	Clayey sandy silt, homogenous, bioturbated, black streaks and mottles, calc. shell fragments common, pebbles all over the segment	500
					At 514-515 cm: greenish diagenet. horizon (authigenic smectite???)	530
5.5					At 546 cm: lenses	
					Below 550 cm: increasing amount of sandy layers	560 579
6.0	EOC 579 cm					
6.5						
7.0						
7.5						
8.0						
8.5						
9.0						
9.5						
10.0						





LV27-11-3 MUC

Loc.: Academy of Sciences Rise

KOMEX 96

Recovery: 0.33-0.38 m 49° 51.06' N, 150° 19.07' E Water depth: 1151 m

Lithology		Texture	Color	Description	SS
Surface		Sandy clayey silt, dark brown, soft, mottled overlain by 1-2 cm fluff-layer, dark brown (10YR4/2)			
Depth in core (cm)	0		10YR4/2	Sandy clayey silt (diatomaceous ooze), dark brown, soft, mottled	
	10				
	20		5Y3/2	Sandy clayey silt (diatomaceous ooze), dark olive gray, mottled, stiffening downward	
	30				
	40			12 out of 12 tubes recovered	
	50				

LV27-11-4 GC

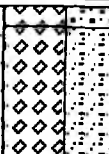

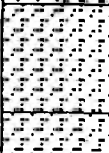

Loc.: Academy of Sciences Rise

KOMEX '96

Recovery: 1.63 m

49°51.10' N 150°19.59' E

Water depth: 1153 m

(m)	Lithology	Core segment	Texture	Color	Description	SS
0.0				5Y3/2	Sandy silt, dark olive gray, homogenous (diatomaceous ooze)	5
				5Y3/2	Sandy silty clay, dark olive gray, homogenous (diatomaceous ooze), at 19-29cm: bioturbation	16 21
0.5				5Y3/2	Sandy silty clay, dark olive gray, homogenous, increasing black streaks and mottles	60 80
1.0				5Y4/1	Sandy silty clay, dark gray, homogenous, increasing black streaks and mottles	110
1.5					At 116-132cm: gradational change to clayey sandy silt	150
2.0	EOC 163cm					
2.5						
3.0						
3.5						
4.0						
4.5						
5.0						

Depth in core (m)

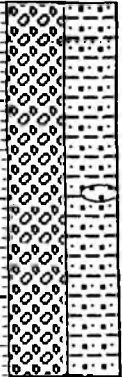

LV27-12-2 MUC

Loc.: Kurile Basin

KOMEX 96

Recovery: 0.15-0.38 m 48° 43.49' N, 148° 14.77' E

Water depth: 1301 m

Lithology	Texture Color	Description	Age
Surface		Sandy, silty clay, dark brown, soft, mottled overlain by 1 cm fluff-layer, dark brown (10YR4/2)	
Depth in core (cm)		10YR4/2 Sandy, clayey silt (diatomaceous ooze), dark brown, soft, mottled	
		5Y3/2 Sandy, clayey silt (diatomaceous ooze), dark olive gray, mottled, stiffening downward At 13-14 cm sponge spicules, arenaceous benthic foraminifers between 6 and 10 cm, calcareous benthic foraminifers abundant below 13 cm At 19-20 cm sand lense	
		11 out of 12 tubes recovered	

LV27-12-3 GC

Loc.: Kurile Basin

KOMEX '96

Recovery: 5.85 m

48°43.49' N 148°14.77' E

Water depth: 1301 m

(m)	Lithology	Core segment	Texture	Color	Description	SS
0.0		0-25		5Y5/2	Clayey sandy silt (diatomaceous ooze), upper 25 cm disturbed, packed in plastic bag	25
0.5		25-100		5Y4/1	Clayey sandy silt (weak diatomaceous), reworked lenses of diatomaceous ooze	60
1.0				5Y3/1	Clayey sandy silt, homogenous, bioturbated, downward increasingly black streaks and mottles	90
				5Y7/1	At 87-91: light grayish sand layer (volcanic ash???), sharp basal contact	100
					Silty sand	
1.5		100-200		5Y3/1	Clayey sandy silt, homogenous, bioturbated, black streaks and mottles	120
				5Y5/1	Sandy silt, gray, very stiff	133
				5Y3/1	Clayey sandy silt, homogenous, bioturbated, black streaks and mottles	150
2.0				5Y5/1	Sandy silt, gray, very stiff, pebbles abundant	170
						190
2.5		200-300		5Y6/1	Coarse sand (volcanic ash), black to white components, up to 1 cm large fragments, sharp basal contact, upper contact wavy due to bioturbation	210
				5Y3/1	Clayey sandy silt, diagenetic greenish mottles (authigenic smectite?)	232
				5Y6/1	Sandy horizon (volcanic ash), light grayish, at base sand lense (3 cm), sharp basal contact, upper contact wavy due to bioturbation, grading upwards, 1 cm below: diagenetic greenish horizon	255
				5Y3/1	Clayey sandy silt, homogenous, black streaks and mottles	290
3.0				5Y3/1	Silty sand, black streaks, stiff	310
		300-400		5Y3/1	Clayey silty sand, pebbles abundant	340
					At 303-304 cm and 308-310 cm: Large dropstones (2 cm)	
					At 350-351 cm: Greenish diagenetic horizon (authigenic clays)	380
4.0						410
4.5		400-500		5Y3/1	Clayey sandy silt, large dropstones abundant, increasingly pebbles	450
					At 404-405 cm: Greenish diagenetic horizon	
5.0						490

LV27-12-3 GC cont.

Loc.: Kurile Basin

KOMEX '96

Recovery: 5.85 m

48°43.49' N 148°14.77' E

Water depth: 1301 m

(m)	Lithology	Core segment	Texture	Color	Description	SS
5.0			• • • • •	5Y3/1	Clayey sandy silt, large dropstones abundant, increasingly pebbles	510
5.5			• • • • •			540
			• • • • •			580
6.0	EOC 585 cm					
6.5						
7.0						
7.5						
8.0						
8.5						
9.0						
9.5						
10.0						

LV27-15-1 GC

Loc.: Atlasov Trough

KOMEX '96

Recovery: 5.77 m

49°00.01' N 152°11.63' E

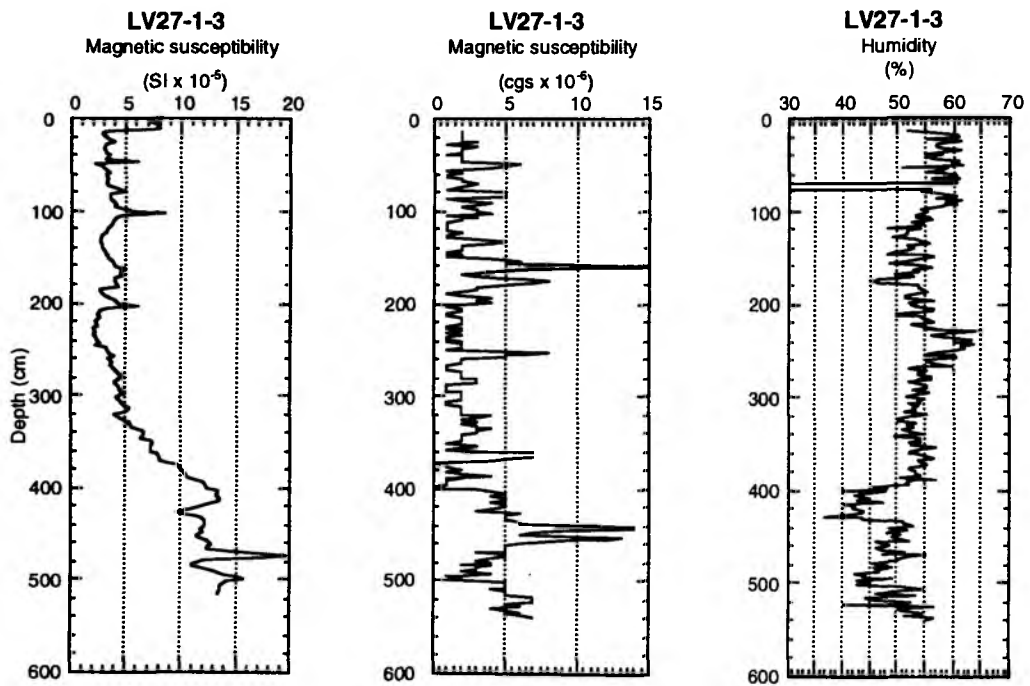
Water depth: 1991 m

(m)	Lithology	Texture	Color	Description	SS
0.0			(10Y4/2) 5Y4/2	0-68 cm: Clayey silt (diatomaceous), homogenous, (grayish) olive gray	0 35
0.5					60
1.0			(5GY3/2) 5Y3/2	68-80 cm: Burrow filled with sediment from above  114-118 cm: Lense of dark grey volcanic ash (5Y5/1) 68-174 cm: Silty clay, diatomaceous, homogenous, grayish olive (green), some admixture of sand	85 110 130
1.5					170
2.0			(5GY3/2) 5Y3/2	174-220 cm: Clayey, sandy silt, grayish olive (green) with lenses of black coarse sand at 181 and 202 cm 210 cm: gravel	210
2.5			(5GY5/2) 5Y5/6?	240-250 cm: Some gravel 258 cm: Pumice fragments 220-295 cm: Clayey silt, (dusky yellow green) olive, homogenous, abundance of diatoms	250 280 300
3.0			(5GY3/2) 5Y3/2	174-220 cm: Clayey silt, slightly sandy, grayish olive (green) with intercalated coarse sand and gravel lenses at 303-306, 334-335, 345-347 cm	320 340
3.5			(5GY4/1) 5Y4/1	350-403 cm: Clayey silty sand, dark (greenish)olive gray, with sand and volcanic ash contents 362-367 cm: Some small pumice fragments 367-368 cm: Lense of volcanic glas 369-373 cm: Many pumice fragments 390 cm: Lense of coarse sand	365 400
4.0			(10Y4/2) 5Y4/2	403-493 cm: Clayey silt, dark (grayish) olive (gray), with occasional sand and volcanic ash contents  410-412 cm: Layer with authigenic green clay occurrence At 433, 437, 445, 449, 458, 462, and 470 cm ; lenses of dark gray sand At 430 cm: Layer of sand (5 mm) At 487 cm: Gravel	410 440 480
4.5					
5.0			(5GY4/1) 5Y4/1	493-530 cm: Clayey silt, dark (greenish)olive gray,  528-530 cm: Lense of volcanic ash	520
5.5			(5GY3/2) 5Y3/2	530-577 cm: silty clay, grayish olive (green), mottled	560
6.0	EOC 577 cm		(10Y4/2) 10Y4/2	--> Rock-Color Chart originally used --> transcript to Munsell Soil Color Chart	

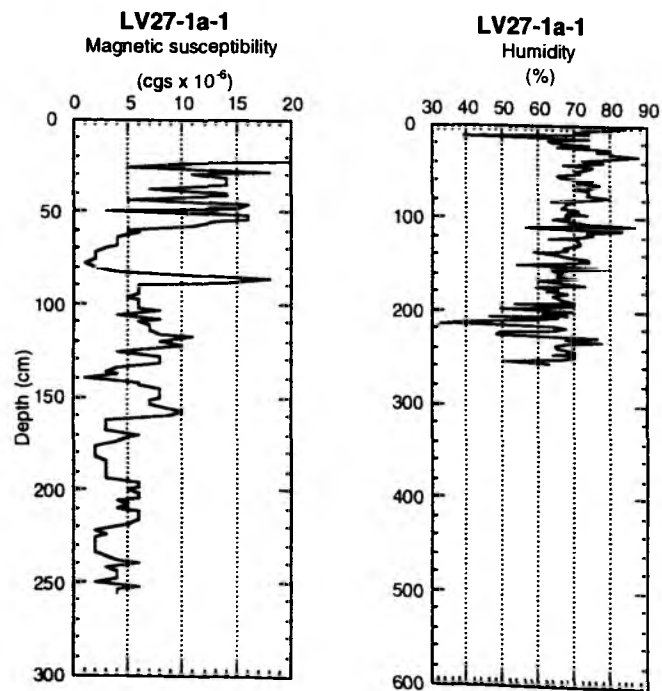
**Appendix VI**  
**Magnetic susceptibility and humidity**  
**records of all sites**

## Magnetic susceptibility and humidity records of all sites

### Station 1



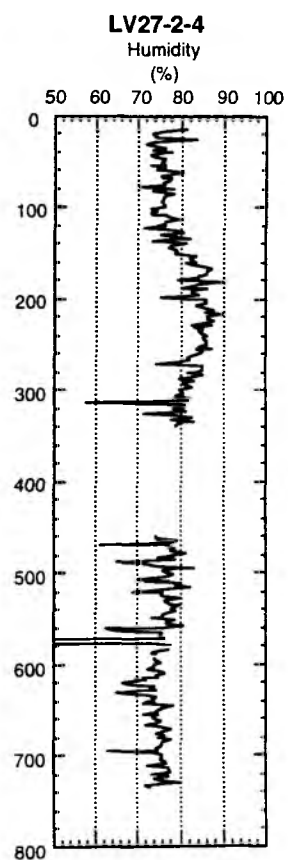
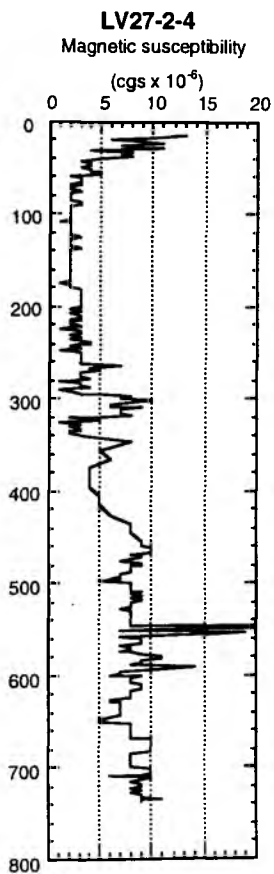
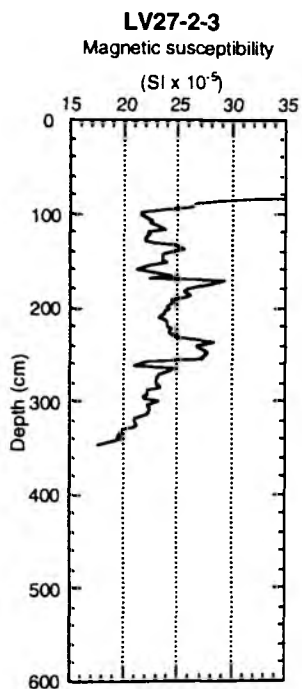
### Station 1a



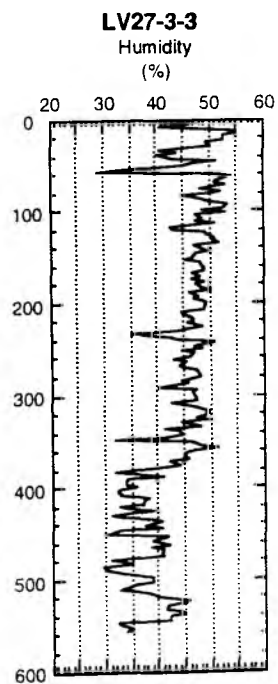
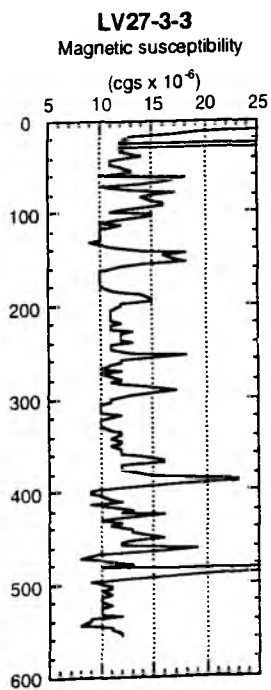
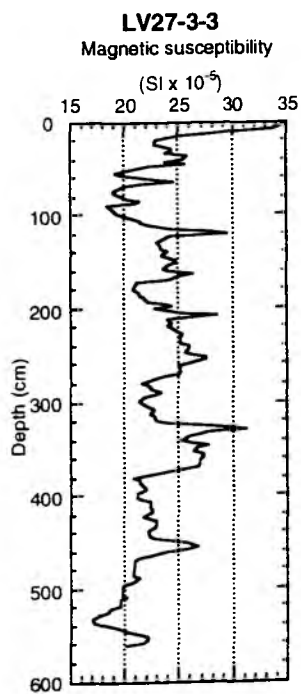


## Magnetic susceptibility and humidity records of all sites

### Station 2

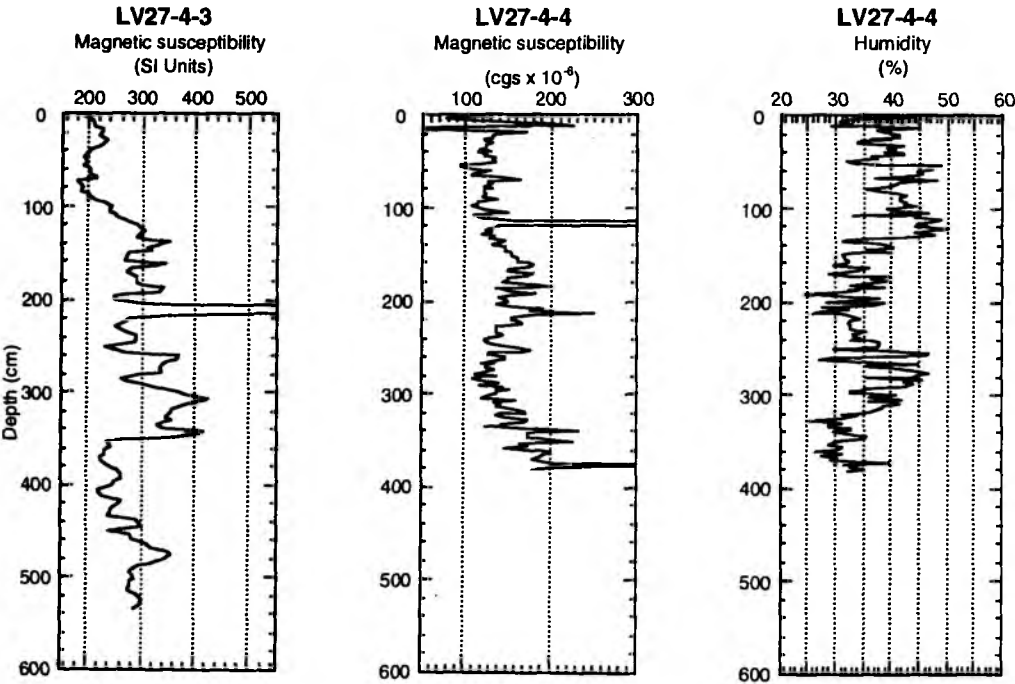


### Station 3

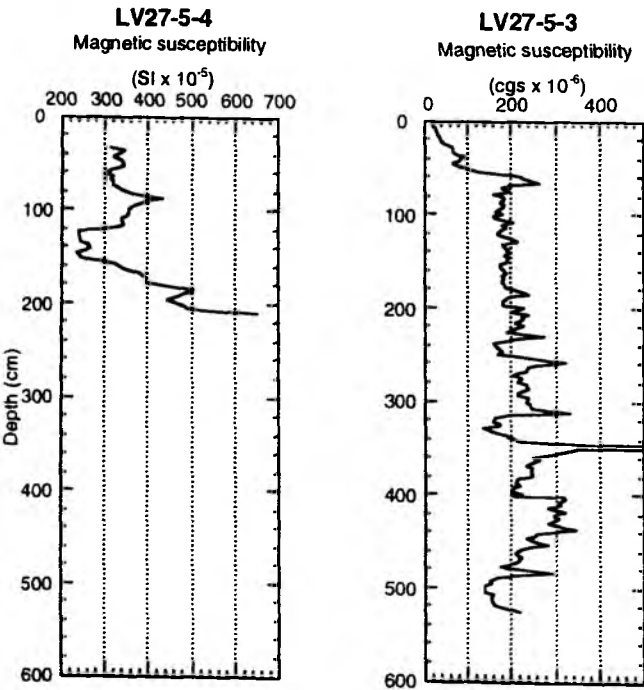


Magnetic susceptibility and humidity records of all sites

Station 4

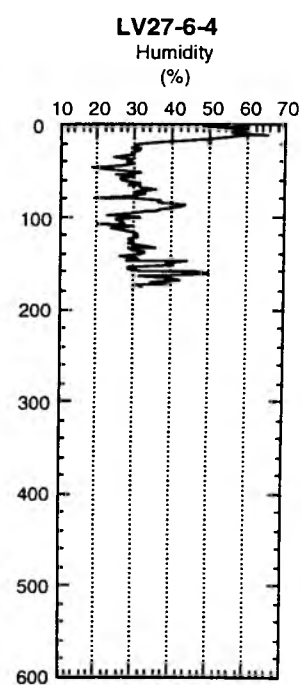
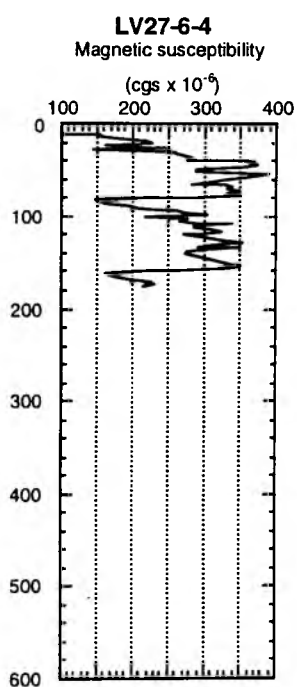
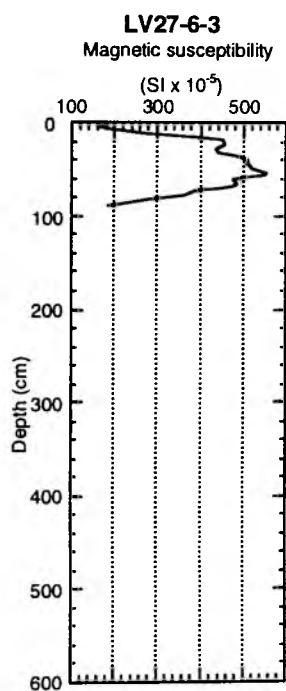


Station 5

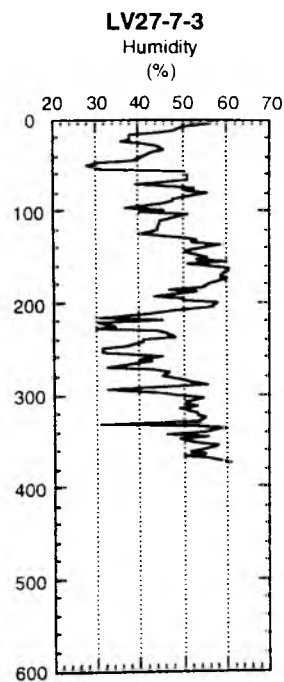
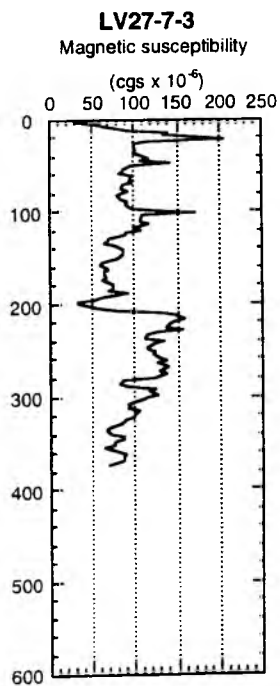
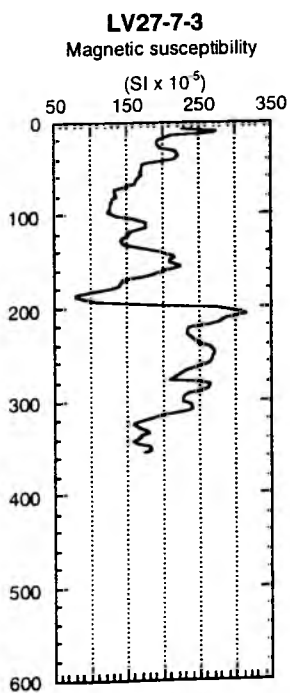


## Magnetic susceptibility and humidity records of all sites

### Station 6

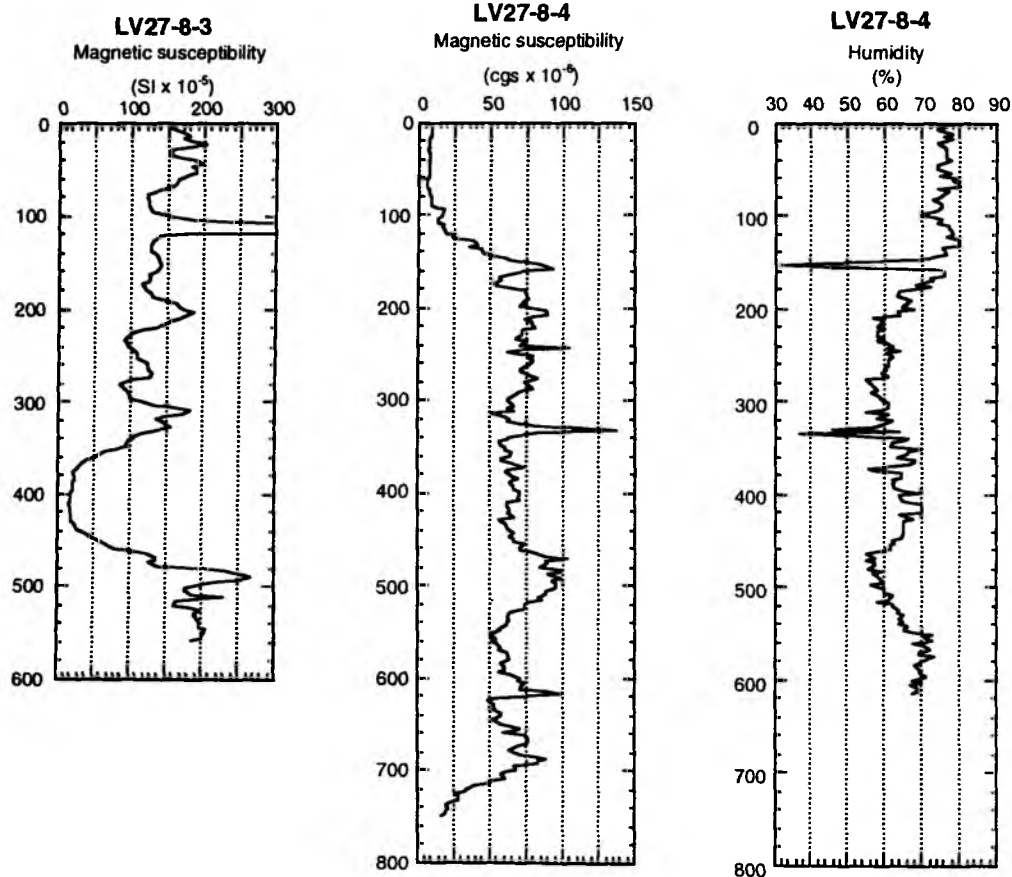


### Station 7

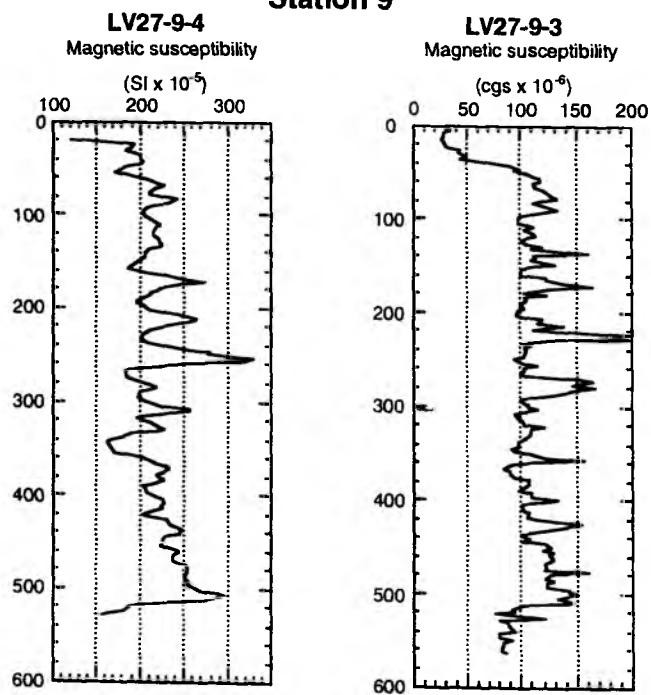


Magnetic susceptibility and humidity records of all sites

Station 8

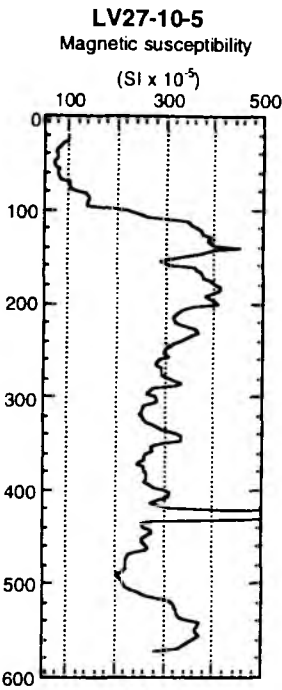


Station 9

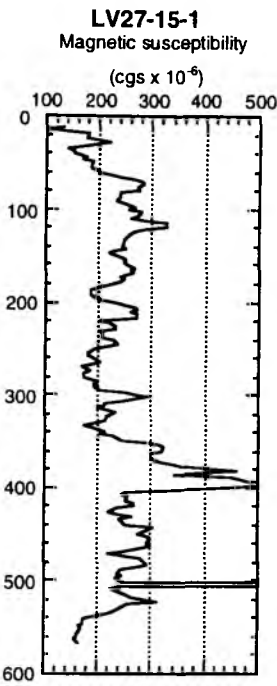


Magnetic susceptibility and humidity records of all sites

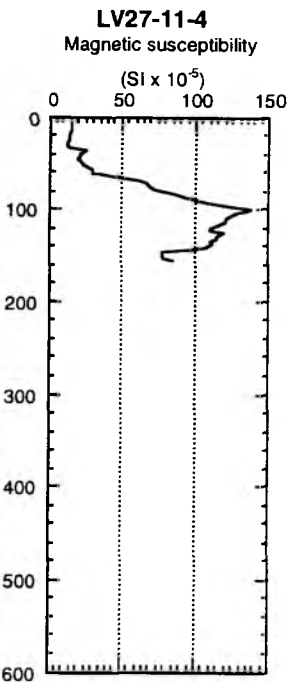
Station 10



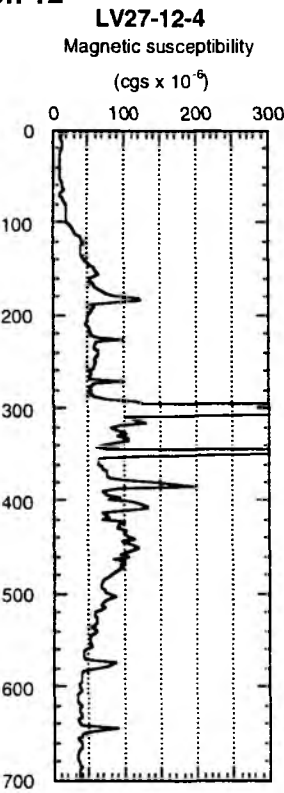
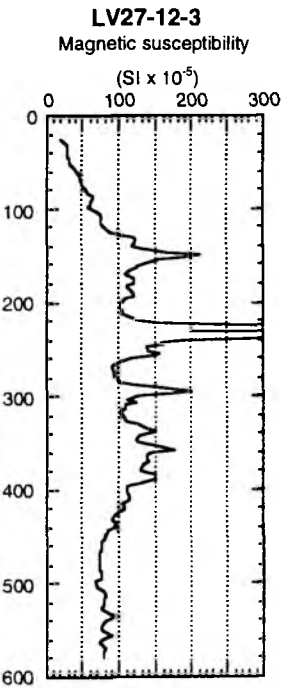
Station 15



Station 11



Station 12





## GEOMAR REPORTS

- 1 GEOMAR FORSCHUNGSZENTRUM FÜR MARINE GEOWISSENSCHAFTEN DER CHRISTIAN-ALBRECHTS-UNIVERSITÄT ZU KIEL  
BERICHT FÜR DIE JAHRE 1987 UND 1988. 1989. 71 + 6 pp.  
In German
- 2 GEOMAR FORSCHUNGSZENTRUM FÜR MARINE GEOWISSENSCHAFTEN DER CHRISTIAN-ALBRECHTS-UNIVERSITÄT ZU KIEL  
JAHRESBERICHT / ANNUAL REPORT 1989. 1990. 96 pp.  
In German and English
- 3 GEOMAR FORSCHUNGSZENTRUM FÜR MARINE GEOWISSENSCHAFTEN DER CHRISTIAN-ALBRECHTS-UNIVERSITÄT ZU KIEL  
JAHRESBERICHT / ANNUAL REPORT 1990. 1991. 212 pp.  
In German and English
- 4 ROBERT F. SPIELHAGEN  
DIE EISDRIFT IN DER FRAMSTRASSE WÄHREND DER LETZTEN 200.000 JAHRE. 1991. 133 pp.  
In German with English summary
- 5 THOMAS C. W. WOLF  
PALÄO-OZEANOGRAPHISCHE KLIMATISCHE ENTWICKLUNG DES NÖRDLICHEN NORDATLANTIKS SEIT DEM SPÄTEN NEOGEN  
(ODP LEGS 105 UND 104, DSDP LEG 81). 1991. 92 pp.  
In German with English summary
- 6 SEISMIC STUDIES OF LATERALLY HETEROGENEOUS STRUCTURES - INTERPRETATION AND MODELLING OF SEISMIC DATA  
Edited by ERNST R. FLUEH  
Commission on Controlled Source Seismology (CCSS), Proceedings of the 8th Workshop Meeting, held at  
Kiel - Fellhorst (Germany), August 27-31, 1990. 1991. 359 pp.  
In English
- 7 JENS MATTHIESSEN  
DINOFLAGELLATEN-ZYSTEN IM SPÄTQUARTÄR DES EUROPÄISCHEN NORDMEERES: PALÖKOLOGIE UND PALÄO-OZEANOGRAPHIE. 1991. 104 pp.  
In German with English summary
- 8 DIRK NÜRNBERG  
HAUPT- UND SPURENELEMENTE IN FORAMINIFERENGHÄUSEN - HINWEISE AUF KLIMATISCHE UND OZEANOGRAPHISCHE ÄNDERUNGEN  
IM NÖRDLICHEN NORDATLANTIK WÄHREND DES SPÄTQUARTÄRS. 1991. 117 pp.  
In German with English summary
- 9 KLAS S. LACKSCHEWITZ  
SEDIMENTATIONSPROZESSE AM AKTIVEN MITTELOZEANISCHEN KOLBEINSEY RÜCKEN (NÖRDLICH VON ISLAND). 1991. 133 pp.  
In German with English summary
- 10 UWE PAGELS  
SEDIMENTOLOGISCHE UNTERSUCHUNGEN UND BESTIMMUNG DER KARBONATLÖSUNG IN SPÄTQUARTÄREN SEDIMENTEN DES ÖSTLICHEN  
ARKTISCHEN OZEANS. 1991. 106 pp.  
In German with English summary
- 11 FS POSEIDON - EXPEDITION 175 (9.10.-1.11.1990)  
175/1: OSTGRÖNLÄNDISCHER KONTINENTALRAND (65° N)  
175/2: SEDIMENTATION AM KOLBEINSEYRÜCKEN (NÖRDLICH VON ISLAND)  
Hrsg. von J. MIENERT und H.-J. WALLRABE-ADAMS. 1992. 56 pp. + app.  
In German with some English chapters
- 12 GEOMAR FORSCHUNGSZENTRUM FÜR MARINE GEOWISSENSCHAFTEN DER CHRISTIAN-ALBRECHTS-UNIVERSITÄT ZU KIEL  
JAHRESBERICHT / ANNUAL REPORT 1991. 1992. 152 pp.  
In German and English
- 13 SABINE E. I. KÖHLER  
SPÄTQUARTÄRE PALÄO-OZEANOGRAPHISCHE ENTWICKLUNG DES NORDPOLARMEERES UND EUROPÄISCHEN NORDMEERES ANHAND VON  
SAUERSTOFF- UND KOHLENSTOFF- ISOTOPENVERHÄLTNISSEN DER PLANKTISCHEN FORAMINIFERE  
*Neogloboquadrina pachyderma* (sin.). 1992. 104 pp.  
In German with English summary
- 14 FS SONNE - FAHRTBERICHT SO 78 PERUVENT: BALBOA, PANAMA - BALBOA, PANAMA. 28.2.1992-16.4.1992  
Hrsg. von ERWIN SUESS. 1992. 120 pp.  
In German with some English chapters
- 15 FOURTH INTERNATIONAL CONFERENCE ON PALEOCEANOGRAPHY (ICP IV): SHORT- AND LONG-TERM GLOBAL CHANGE  
RECORDS AND MODELLING 21-25 SEPTEMBER 1992, KIEL/GERMANY  
PROGRAM & ABSTRACTS. 1992. 351 pp.  
In English
- 16 MICHAELA KUBISCH  
DIE EISDRIFT IM ARKTISCHEN OZEAN WÄHREND DER LETZTEN 250.000 JAHRE. 1992. 100 pp.  
In German with English summary
- 17 PERSISCHER GOLF: UMWELTGEFAHRDUNG, SCHADENSERKENNUNG, SCHADENSBEWERTUNG AM BEISPIEL DES MEERESBODENS. ERKENNEN  
EINER ÖKOSYSTEMVERÄNDERUNG NACH ÖLEINTRÄGEN. Schlußbericht zu den beiden BMFT-Forschungsvorhaben 03F0055 A+B. 1993. 108 pp.  
In German with English summary
- 18 TEKTONISCHE ENTWÄSSERUNG AN KONVERGENTEN PLATTENRÄNDERN / DEWATERING AT CONTINENTAL MARGINS  
Hrsg. von / ed. by ERWIN SUESS. 1993. 106 + 32 + 68 + 16 + 22 + 38 + 4 + 19 pp.  
Some chapters in English, some in German

- 19 THOMAS DICKMANN  
DAS KONZEPT DER POLARISATIONSMETHODE UND SEINE ANWENDUNGEN AUF DAS SEISMISCHE VEKTORWELLENFELD  
IM WEITWINKELBEREICH. 1993. 121 pp.  
In German with English summary
- 20 GEOMAR FORSCHUNGSZENTRUM FÜR MARINE GEOWISSENSCHAFTEN DER CHRISTIAN-ALBRECHTS-UNIVERSITÄT ZU KIEL  
JAHRESBERICHT / ANNUAL REPORT 1992. 1993. 139 pp.  
In German and English
- 21 KAI UWE SCHMIDT  
PALYNO MORPHE IM NEOGENEN NORDATLANTIK - HINWEISE ZUR PALÄO-OZEANOGRAPHIE UND PALÄOKLIMATOLOGIE. 1993. 104 + 7 + 41 pp.  
In German with English summary
- 22 UWE JÜRGEN GRÜTZMACHER  
DIE VERÄNDERUNGEN DER PALÄO GEOGRAPHISCHEN VERBREITUNG VON *BOLBOFORMA* - EIN BEITRAG ZUR REKONSTRUKTION UND  
DEFINITION VON WASSERMASSEN IM TERTIÄR. 1993. 104 pp.  
In German with English summary
- 23 RV PROFESSOR LOGACHEV - Research Cruise 09 (August 30 - September 17, 1993): SEDIMENT DISTRIBUTION ON THE REYKJANES RIDGE NEAR 59°N  
Edited by H.-J. WALLRABE-ADAMS & K.S. LACKSCHEWITZ. 1993. 66 + 30 pp.  
In English
- 24 ANDREAS DETTMER  
DIATOMEEN-TAPHOZÖNOSEN ALS ANZEIGER PALÄO-OZEANOGRAPHISCHER ENTWICKLUNGEN IM PLIOZÄN UND QUARTÄREN  
NORDATLANTIK. 1993. 113 + 10 + 25 pp.  
In German with English summary
- 25 GEOMAR FORSCHUNGSZENTRUM FÜR MARINE GEOWISSENSCHAFTEN DER CHRISTIAN-ALBRECHTS-UNIVERSITÄT ZU KIEL  
JAHRESBERICHT / ANNUAL REPORT 1993. 1994. 69 pp.  
In German and English
- 26 JÖRG BIALAS  
SEISMISCHE MESSUNGEN UND WEITERE GEOPHYSIKALISCHE UNTERSUCHUNGEN AM SÜD-SHETLAND TRENCH  
UND IN DER BRANSFIELD STRASSE - ANTARKTISCHE HALBINSEL. 1994. 113 pp.  
In German with English summary
- 27 JANET MARGARET SUMNER  
THE TRANSPORT AND DEPOSITIONAL MECHANISM OF HIGH GRADE MIXED-MAGMA IGIMBRITE TL, GRAN CANARIA:  
THE MORPHOLOGY OF A LAVA-LIKE FLOW. 1994. 224 pp.  
In English with German summary
- 28 GEOMAR LITHOTHEK. Edited by JÜRGEN MIENERT. 1994. 12 pp + app.  
In English
- 29 FS SONNE - FAHRTBERICHT SO 97 KODIAK-VENT: KODIAK - DUTCH HARBOR - TOKYO - SINGAPUR, 27.7. - 19.9.1994  
Hrsg. von ERWIN SUESS. 1994.  
Some chapters in German, some in English
- 30 CRUISE REPORTS:  
RV LIVONIA CRUISE 92, KIEL-KIEL, 21.8.-17.9.1992: GLORIA STUDIES OF THE EAST GREENLAND CONTINENTAL MARGIN BETWEEN 70° AND 80°N  
RV POSEIDON PO200/10, LISBON-BREST-BREMERHAVEN, 7.-23.8.1993: EUROPEAN NORTH ATLANTIC MARGIN: SEDIMENT PATHWAYS,  
PROCESSES AND FLUXES  
RV AKADEMIK ALEKSANDR KARPINSKIY, KIEL-TROMSØ, 5.-25.7.1994: GAS HYDRATES ON THE NORTHERN EUROPEAN CONTINENTAL MARGIN  
Edited by JÜRGEN MIENERT. 1994.  
In English; report of RV AKADEMIK ALEKSANDR KARPINSKIY cruise in English and Russian
- 31 MARTIN WEINELT  
BECKENENTWICKLUNG DES NÖRDLICHEN WIKING-GRABENS IM KÄNOZOIKUM - VERSENKUNGSGESCHICHTE, SEQUENZSTRATIGRAPHIE,  
SEDIMENTZUSAMMENSETZUNG. 1994. 85 pp.  
In German with English summary
- 32 GEORG A. HEISS  
CORAL REEFS IN THE RED SEA: GROWTH, PRODUCTION AND STABLE ISOTOPES. 1994. 141 pp.  
In English with German summary
- 33 JENS A. HÖLEMANN  
AKKUMULATION VON AUTOCHTHONEM UND ALLOCHTHONEM ORGANISCHEM MATERIAL IN DEN KÄNOZOISCHEN SEDIMENTEN  
DER NORWEGISCHEN SEE (ODP LEG 104). 1994. 78 pp.  
In German with English summary
- 34 CHRISTIAN HASS  
SEDIMENTOLOGISCHE UND MIKROPALAONTOLOGISCHE UNTERSUCHUNGEN ZUR ENTWICKLUNG DES SKAGERRAKS (NE NORDSEE)  
IM SPÄTHOLOZÄN. 1994.  
In German with English summary
- 35 BRITTA JÜNGER  
TIEFENWASSERERNEUERUNG IN DER GRÖNLANDSEE WÄHREND DER LETZTEN 340.000 JAHRE.  
DEEP WATER RENEWAL IN THE GREENLAND SEA DURING THE PAST 340,000 YEARS. 1994. 6 + 109 pp.  
In German with English summary
- 36 JÖRG KUNERT  
UNTERSUCHUNGEN ZU MASSEN- UND FLUIDTRANSPORT ANHAND DER BEARBEITUNG REFLEXIONSSEISMISCHER DATEN AUS DER  
KODIAK-SUBDUKTIONSZONE, ALASKA. 1995. 129 pp.  
In German with English summary
- 37 CHARLOTTE M. KRAWCZYK  
DETACHMENT TECTONICS DURING CONTINENTAL RIFTING OFF THE WEST IBERIA MARGIN: SEISMIC REFLECTION AND  
DRILLING CONSTRAINTS. 1995. 133 pp.  
In English with German summary
- 38 CHRISTINE CAROLINE NÜRNBERG  
BARIUMFLUSS UND SEDIMENTATION IM SÜDLICHEN SÜDATLANTIK - HINWEISE AUF PRODUKTIVITÄTSÄNDERUNGEN IM QUARTÄR. 1995. 6 + 108pp  
In German with English summary
- 39 JÜRGEN FRÜHN  
TEKTONIK UND ENTWÄSSERUNG DES AKTIVEN KONTINENTALRANDES SÜDÖSTLICH DER KENAI-HALBINSEL, ALASKA. 1995. 93 pp.  
In German with English summary

- 40 GEOMAR FORSCHUNGSZENTRUM FÜR MARINE GEOWISSENSCHAFTEN DER CHRISTIAN-ALBRECHTS-UNIVERSITÄT ZU KIEL  
JAHRESBERICHT / ANNUAL REPORT 1994. 1995.  
In German and English
- 41 FS SONNE - FAHRTBERICHT / CRUISE REPORT SO 103 CONDOR 1 B: VALPARAISO-VALPARAISO, 2.-21.7.1995.  
Hrsg. von ERNST R. FLUEH. 1995. 140 pp.  
Some chapters in German, some in English
- 42 R/V PROFESSOR BOGOROV CRUISE 37: CRUISE REPORT "POSETIV": Vladivostok - Vladivostok, September 23 - October 22, 1994  
Edited by CHRISTOPH GAEDICKE, BORIS BARANOV and EVGENYI LELIKOV. 1995. 48 + 33 pp.  
In English
- 43 CHRISTOPH GAEDICKE  
DEFORMATION VON SEDIMENTEN IM NANKAI-AKKRETIONSKEIL, JAPAN. BILANZIERUNG TEKTONISCHER VORGÄNGE ANHAND VON SEISMISCHEN  
PROFILIEN UND ERGEBNISSEN DER ODP-BOHRUNG 808. II + 89 pp.  
In German with English summary
- 44 MARTIN ANTONOW  
SEDIMENTATIONSMUSTER UM DEN VESTERIS SEAMOUNT (ZENTRALE GRÖNLANDSEE) IN DEN LETZTEN 250.000 JAHREN. 1995.  
In German with English summary
- 45 INTERNATIONAL CONGRESS: CORING FOR GLOBAL CHANGE - ICGC '95. KIEL, 28 - 30 June, 1995.  
Edited by JÜRGEN MIENERT and GEROLD WEFER. 1996.  
In English
- 46 JENS GRÜTZNER  
ZUR PHYSIKALISCHEN ENTWICKLUNG VON DIAGENETISCHEN HORIZONTEN IN DEN SEDIMENTBECKEN DES ATLANTIKS. 1995. 96 pp.  
In German with English summary
- 47 INGO A. PECHER  
SEISMIC STUDIES OF BOTTOM SIMULATING REFLECTORS AT THE CONVERGENT MARGINS OFFSHORE PERU AND COSTA RICA. 1996. 159 pp.  
In English with German summary
- 48 XIN SU  
DEVELOPMENT OF LATE TERTIARY AND QUATERNARY COCCOLITH ASSEMBLAGES IN THE NORTHEAST ATLANTIC. 1996. 120 pp. + 7 pl.  
In English with German summary
- 49 FS SONNE - FAHRTBERICHT / CRUISE REPORT SO 108 ORWELL: SAN FRANCISCO - ASTORIA, 14.4. - 23.5.1996  
Edited by ERNST R. FLUEH and MICHAEL A. FISHER. 1996.
- 50 GEOMAR FORSCHUNGSZENTRUM FÜR MARINE GEOWISSENSCHAFTEN DER CHRISTIAN-ALBRECHTS-UNIVERSITÄT ZU KIEL  
JAHRESBERICHT / ANNUAL REPORT 1995. 1996. 93 pp.  
In German and English
- 51 THOMAS FUNCK  
STRUCTURE OF THE VOLCANIC APRON NORTH OF GRAN CANARIA DEDUCED FROM REFLECTION SEISMIC, BATHYMETRIC  
AND BOREHOLE DATA. 1996. VI, 144 pp.  
In English with German summary
- 52 PETER BRUNS  
GEOCHEMISCHE UND SEDIMENTOLOGISCHE UNTERSUCHUNGEN ÜBER DAS SEDIMENTATIONSVERHALTEN IM BEREICH  
BIOSTRATIGRAPHISCHER DISKONTINUITÄTEN IM NEOGEN DES NORDATLANTIK, ODP LEG 104, SITES 642B UND 643A. 1993. V, 73 pp.  
In German with English summary
- 53 CHRISTIANE C. WAGNER  
COLD SEEPS AN KONVERGENTEN PLATTENRÄNDERN VOR OREGON UND PERU: BIOGEOCHEMISCHE BESTANDSAUFNAHME. 1996. 108, XXXVI pp.  
In German with English summary
- 54 FRAUKE KLINGELHÖFER  
MODEL CALCULATIONS ON THE SPREADING OF SUBMARINE LAVA FLOWS. 1996. 98 pp.  
In English with German summary
- 55 HANS-JÜRGEN HOFFMANN  
OBJEKTORIENTIERTE ANALYSE UND MIGRATION DIFFRAKTIERTER WELLENFELDER UNTER VERWENDUNG DER STRAHLENMETHODE UND  
DER EDGE-WAVE-THEORIE. 1996. XXI, 153 pp.  
In German with English summary
- 56 DIRK KLÄSCHEN  
STRAHLENSEISMISCHE MODELLIERUNG UNTER BERÜCKSICHTIGUNG VON MEHRFACHDIFFRAKTIONEN MIT HILFE DER EDGE-WAVES:  
THEORIE UND ANWENDUNGSBEISPIELE. 1996. X, 159 pp.  
In German with English summary
- 57 NICOLE BIEBOW  
DINOFLAGELLATENZYSTEN ALS INDIKATOREN DER SPÄT- UND POSTGLAZIALEN ENTWICKLUNG DES AUFTRIEBSGESCHEHENS VOR PERU  
1996. IV, 100, 17, 14 (7 pl.) pp.  
In German with English summary
- 58 RV SONNE - CRUISE REPORT SO109: HYDROTRACE. ASTORIA-VICTORIA-ASTORIA-VICTORIA. MAY 23 - JULY 8, 1996.  
Ed. by PETER HERZIG, ERWIN SUESS, and PETER LINKE. 1997  
In English
- 59 RV SONNE - CRUISE REPORT SO110: SO - RO (SONNE - ROPOS). VICTORIA-KODIAK-VICTORIA. JULY 9 - AUGUST 19, 1996.  
Ed. by ERWIN SUESS and GERHARD BOHRMANN. 1997.  
In English
- 60 RV AKADEMIK M. A. LAVRENTYEV CRUISE 27. CRUISE REPORT GREGORY. VLADIVOSTOK-PUSAN-OKHOTSK SEA-PUSAN-VLADIVOSTOK  
SEPTEMBER 7 - OCTOBER 12, 1996. Ed. by DIRK NÜRNBERG, BORIS BARANOV, and BORIS KARP. 1997. 143 pp.  
In English